DISSERTATION

THE ROLE OF ORGANIC MATTER CHEMISTRY IN IRON REDOX TRANSFORMATIONS, SORPTION TO IRON OXIDES, AND WETLAND CARBON STORAGE

Submitted by

Ellen E. Daugherty

Department of Chemistry

In partial fulfillment of the requirements

For the Degree of Doctor of Philosophy

Colorado State University

Fort Collins, Colorado

Summer 2018

Doctoral Committee:

Advisor: Thomas Borch

George Barisas
Richard Conant
James Neilson

ABSTRACT

THE ROLE OF ORGANIC MATTER CHEMISTRY IN IRON REDOX TRANSFORMATIONS, SORPTION TO IRON OXIDES, AND WETLAND CARBON STORAGE

Organic carbon comprises a versatile and complex class of compounds that influence water quality, soil health, fate and transport of environmental contaminants, biogeochemical cycles, and climate change. Key to predicting the responses of these systems and processes to environmental change is a molecular-level understanding of how organic carbon reacts with other components of soil and water. Yet due to its complexity and that of the systems in which it is found, organic carbon dynamics remain poorly understood.

In both terrestrial and aquatic environments, the reactivity and biological necessity of iron and carbon link the biogeochemical cycling of these elements. Complexation of iron by dissolved organic carbon molecules alters its solubility and oxidation-reduction behavior and may explain the persistence of reduced iron (Fe(II)) in oxic aquatic environments. By examining the coordination environment of Fe(II) complexed by dissolved organic matter (DOM) and evaluating the effects of complexation on Fe(II) oxidation, I determined that the majority of Fe(II)–DOM complexes were characterized by coordination with citrate-like ligands, which were unlikely to inhibit oxidation by molecular oxygen. Nonetheless, association with reduced organic matter could extend the lifetime of Fe(II) in oxic environments by several hours.

In soils and sediments, iron minerals act as effective sorbents of organic matter, preserving substantial amounts of carbon from microbial decomposition. These interactions have increasingly been recognized as important components of carbon sequestration, yet the effects of temperature on

sorption behavior remain unknown. Through several batch and continuous flow experiments, I demonstrated a positive relationship between temperature and sorption of DOM on iron oxide surfaces. The temperature sensitivity of sorption behavior varied among riverine, peat, and soil DOM types, with riverine natural organic matter sorbing and desorbing the most at all temperatures. Analyses of effluents also revealed preferential sorption of aromatic compounds during the initial stages of sorption.

In soils, organic matter quantity and composition are determined primarily by the balance between plant productivity and microbial decomposition, which are in turn dependent upon climate, temperature, hydrology, nutrient availability, and soil composition. Wetlands store disproportionately large amounts of carbon, yet the processes controlling storage are poorly understood. I investigated how different environments created by the hydrology and geomorphic setting of two wetland types, depressional and slope, impacted soil organic carbon storage and composition. Results showed a prevalence of aliphatic structures in depressional wetlands, especially in deeper soils, suggestive of anaerobic decomposition processes. By comparison, carbon in slope wetlands was dominated by labile plant carbohydrates in surface soils and aromatic compounds at depth, a likely indication of less anaerobic conditions. These results demonstrate divergent pathways of organic matter processing in different hydrogeomorphic environments.

In total, this work contributes to more mechanistic understandings of important carbon dynamics that influence carbon and iron cycling, climate change, and environmental health.

ACKNOWLEDGEMENTS

I am grateful to my advisor, Thomas Borch, who has supported my research, my growth as a scientist, and my extracurricular endeavors. Without doubt, graduate school has been an intellectually and emotionally challenging experience. I am incredibly grateful to those who have supported me, especially my partner, Dan Scott. Thank you for holding out the hand that helps me get back on my feet again when serendipity or foolishness has knocked me down. By setting examples of thoughtful and curious scientists and encouraging my inquisitiveness, my parents, Leslie and Byron Daugherty, raised me with an appreciation for the natural world and a penchant for science. They also supported my education such that obtaining a doctorate degree was a realistic goal, for which I cannot thank them enough.

I would also like to thank the other critical members of my intellectual and emotional support network, including Laurel Lynch, whose lunches and adventures made research a less lonely pursuit; Elise Daugherty, who sometimes knows me better than I know myself; Robert Young, who is the best brainstorming buddy a scientist could ask for; and the community of women in the Northern Colorado Chapter of Graduate Women in Science. I feel lucky to have worked in the supportive and constructively critical environment of the Borch group: thanks to all of you who have improved my way of thinking about science and how I present my work to others, as well as those who have contributed to and assisted me with laboratory and field work, including Vincenzo Leone, Yuheng Qiu, Merritt Logan, Margaret Phillips, Adam Fitzsimmons, Rob Hubbard, and Robert Bergstrom. I also thank my collaborators, Benjamin Gilbert, Charles Rhoades, and Gina McKee, for their contributions to this work as well as their insight and guidance. I would like to thank my committee members for their feedback on this dissertation and the publications developing from it.

A portion of this research was performed using EMSL, a DOE Office of Science User Facility sponsored by the Office of Biological and Environmental Research and located at Pacific Northwest National Laboratory. Use of the Stanford Synchrotron Radiation Lightsource (SSRL), SLAC National Accelerator Laboratory, is supported by the U.S. Department of Energy, Office of Science, Office of Basic Energy Sciences under Contract No. DE-AC02-76SF00515. Part of this research was conducted at the National High Magnetic Field Laboratory (NHMFL), which is supported by the National Science Foundation Division of Materials Research through DMR-1157490, Florida State University and the State of Florida. Thank you to the staff scientists at these instrument facilities who helped my collaborators and me perform analyses: Ryan Davis (SSRL), Sarah Burton (EMSL), Eric Walter (EMSL), Amy McKenna (NHMFL), and Huan Chen (NHMFL). This material is based upon work that is supported by the National Institute of Food and Agriculture, U.S. Department of Agriculture, under award number 2013-67019-21359, a Colorado Mountain Club Foundation Fellowship, and the Borch-Hoppess Fund for Environmental Contaminant Research.

This dissertation often uses "I" and "my" to describe this work. This is solely a formality, and the credit for this work is rightfully shared amongst myself, Thomas Borch, and the collaborators listed above.

DEDICATION

This work is dedicated to the community that has supported my development and well-being throughout my dissertation.

TABLE OF CONTENTS

CHAPTER 1: INTRODUCTION

1.1 General background

Carbon (C) stored on the earth's surface—in soils and oceans—represents the largest group of dynamic C reservoirs (Jobbágy and Jackson, 2000; IPCC, 2007). Aside from human disturbances, the amount of C stored in these pools depends on the balance among inputs directly from the atmosphere and from photosynthetic organisms and outputs from respiration. All of these processes depend on the intimate interactions among C, other nutrients, minerals, and environmental conditions such as pH, temperature, and oxidation-reduction potential. Natural organic matter, the major form of carbon in soils (Scharlemann et al., 2014), comprises the organic material, in various states of decomposition, derived from living organisms. Soil organic matter (SOM) confers numerous benefits to soil productivity and stability, such as increasing moisture retention (Hudson, 1994), forming aggregates to stabilize soil structure (Tisdall and Oades, 1982), and regulating nutrient supply (Tiessen et al., 1994). SOM also impacts cycling of important elements such as nitrogen (N) and iron (Fe) (Van Cappellen and Wang, 1996) that are essential to biological productivity, and it regulates the fate and transport of heavy metals and anthropogenic compounds (Huang et al., 2003; McBride et al., 2005).

Understanding the chemical composition of organic matter and its molecular interactions with other components of soil and water is essential for accurate carbon cycle modeling and soil health management. The formation, structure, and reactivity of natural organic matter are incredibly complex, presenting a fascinating analytical challenge in the study of this material. Molecules range from identifiable biomolecules to complex degradation products, from small organic acids to large biopolymers weighing kilodaltons (Knicker, 2000; Kramer et al., 2001; Kiem and Kögel-Knabner, 2003; Kallenbach et al., 2016). A large variety of functional groups contribute to variable acidity and basicity, hydrophobicity and hydrophilicity, and reduction potentials (Aeschbacher et al., 2011;

Brezonik et al., 2015). Analysis of NOM requires careful experimental design and often a variety of high resolution instrumental techniques.

Nuclear magnetic resonance (NMR) experiments such as cross-polarization magic angle spinning (CP-MAS), numerous two-dimensional techniques, and traditional ^{1}H, ^{13}C, and ^{15}N NMR provide useful bulk chemistry information that can identify relative proportions of functional groups, and in some instances, more precise identification of specific compounds (Knicker, 2000; Simpson, 2002; Simpson and Simpson, 2014). Synchrotron radiation-based X-ray absorption spectroscopy analyses of C, N, S, and other elements can also yield clues to functional group distributions as well as interactions amongst elements, such as organo-metallic complexes (Karlsson et al., 2006; Prietzel et al., 2007; Wan et al., 2007; Karlsson and Persson, 2010). Fourier transform ion cyclotron resonance mass spectrometry (FT-ICR-MS) has become an increasingly popular technique for identifying mass distributions and general elemental and chemical characteristics of individual molecules (Koch and Dittmar, 2006; Sleighter and Hatcher, 2007; Hertkorn et al., 2008). Continual advances in sample preparation and data analysis are also improving data quality and expanding the usefulness of these methods (Grinhut et al., 2010; Hao et al., 2016; Tfaily et al., 2017).

The work presented in this dissertation examines the role of natural organic matter chemistry in Fe binding and redox behavior (Chapter 2), temperature controls on dissolved organic carbon (DOC) sorption to the iron oxide ferrihydrite (Chapter 3), and carbon storage and processing in two hydrologically different subalpine wetlands (Chapter 4).

1.2 Iron-organic matter complexation and iron redox cycling

The biogeochemical cycles of C and Fe are closely linked: both are essential for all organisms (or nearly all, in the case of Fe), they are frequently co-located in soils, sediments, and waters (Kaiser and Guggenberger, 2000; Lalonde et al., 2012; Rasmussen et al., 2018), and each can have profound

influence on the activity and solubility of the other. For example, bioavailability of Fe in aquatic environments depends on redox reactions that interconvert oxidized Fe(III) and reduced Fe(II) as well as complexation of Fe. At pH >5, Fe(II) is several orders of magnitude more soluble than Fe(III) (Gayer and Woontner, 1956), but it rapidly oxidizes in the presence of oxygen ($k = 3.1 \times 10^{-3}$ s) to the relatively insoluble ferric hydroxide (Rose and Waite, 2003). Generally, Fe(II) is more soluble than Fe(III), and both can form complexes with organic matter that increase solubility and therefore Fe bioavailability (Gledhill and Buck, 2012; Karlsson and Persson, 2012).

Several studies have noted the presence of Fe(II) associated with natural organic matter (NOM) under conditions favorable for Fe oxidation (Toner et al., 2009; von der Heyden et al., 2012; von der Heyden et al., 2014; Sundman et al., 2014), leading to speculation that complexation with NOM stabilizes Fe(II) against oxidation. These are significant findings with implications for several environmental systems. In the equatorial Pacific, the subarctic Pacific, and the Southern Ocean, Fe is the limiting nutrient for primary production and therefore restricts regional carbon sequestration (Falkowski, 2005). Primary inputs of dissolved Fe to oceans include DOM-complexed Fe from rivers and coastal sediments (Krachler et al., 2005), most of which precipitates upon mixing with saline ocean water. Recently, concerning increases in DOC concentrations in streams and rivers have been correlated with dissolved Fe concentrations, suggesting an Fe reduction-based mechanism of DOC release from soils (Knorr, 2013).

Despite their importance to C and Fe cycling in rivers and oceans, the thermodynamic impacts of Fe(II)-NOM complexation remain relatively uncharacterized, while results from kinetics experiments demonstrate variable effects of NOM on Fe oxidation rates (Jobin and Ghosh, 1972; Emmenegger et al., 1998; Rose and Waite, 2002; Pullin and Cabaniss, 2003; Rose and Waite, 2003; Craig et al., 2009; Bligh and Waite, 2010). Furthermore, few studies have examined the complexation of Fe(II) by NOM, and none have directly probed Fe(II)-NOM bonds. These complexes present an

analytical challenge due to their weak interactions and the rapid oxidation of Fe(II) under most ambient conditions. In collaboration with Dr. Benjamin Gilbert at Lawrence Berkeley National Laboratory, I characterized Fe(II)-NOM binding using X-ray absorption spectroscopy and evaluated the impacts of Fe(II) complexation with reduced NOM on Fe(II) oxidation. The work from these studies is presented in Chapter 2.

1.3 Sorption of organic matter to iron minerals

Globally, soils store an estimated 3000 Pg of C, which is more than the amount stored in the atmosphere and vegetation combined (Köchy et al., 2015). The quantity of soil organic carbon (SOC) stocks depends on the intricate balance among plant inputs, microbial mineralization, and export of dissolved organic carbon, and is sensitive to changes in climate. An important constraint on microbial respiration is the interaction between organic substrates and mineral surfaces such as those of clays and Fe and Al oxides (Chorover and Amistadi, 2001; Mikutta et al., 2006; Saidy et al., 2013). Strong physical associations between these groups can sequester as much as 82% of organic carbon (OC) in organo-mineral complexes (Kaiser and Guggenberger, 2000; Eusterhues et al., 2003; Basile-Doelsch et al., 2007; Lalonde et al., 2012). The presence of short-range order mineral phases correlates with higher OC and organic nitrogen content in soils (Wagai and Mayer, 2007; Rasmussen et al., 2018), older C (Torn et al., 1997), and lower C mineralization rates (Mikutta and Kaiser, 2011; Eusterhues et al., 2014).

Despite this apparent protection, mineral-bound OC is vulnerable to environmental changes and inputs that disrupt organo-mineral interactions. For example, organic acids from root exudates and seasonally reducing conditions may solubilize amorphous Fe oxides, releasing associated organic matter (Koretsky et al., 2006; Riedel et al., 2013; Keiluweit et al., 2015). With increasing global temperatures, the outstanding question of how temperature affects sorption of organic matter to iron

oxides has become a rather important and urgent one. Extensive research efforts have been dedicated to understanding the effects of temperature on microbial respiration rates, with results indicating an overall increase in respiration with temperatures up to 25 °C (Carey et al., 2016). Yet the role of mineral protection in controlling substrate availability as a function of temperature remains poorly characterized.

Sorption of organic matter on mineral surfaces at room temperature has been studied extensively, but the difficulty of detangling the chemical complexity of organic matter has led to diverse results. While most studies have demonstrated preferential sorption of aromatic and carboxylic moieties to clay, Fe, and Al minerals (McKnight et al., 1992; Gu et al., 1994; Gu et al., 1995; Meier et al., 1999; Kaiser, 2003; Eusterhues et al., 2011; Galindo and Del Nero, 2014; Chassé et al., 2015; Avneri-Katz et al., 2016; Lv et al., 2016; Coward et al., 2018), a few have shown preferential interactions between minerals and polysaccharides (Eusterhues et al., 2011; Avneri-Katz et al., 2016) and amino acids (McKnight et al., 1992; Chassé et al., 2015). While these results seem somewhat contradictory, they may be accounted for in zonal conceptual models of sorption, such as those proposed by Kleber et al. (2007) and Wershaw et al. (1996) (Figure 1.1). In these models, polar organic groups interact electrostatically or via inner-sphere complexation with the mineral surface in a contact zone and attached aliphatic and aromatic groups and other hydrophobic compounds associate more loosely in a hydrophobic zone. Hydrophilic groups at the outer edge of this zone come into contact with the bulk solution. Kleber also proposes a third "kinetic zone" in which various types of organic compounds and cations interact briefly with the mineral-associated compounds. Results from depth-probing ^{1}H high resolution-magic angle spinning nuclear magnetic resonance (^{1}H HR-MAS NMR) experiments with clay-bound organic matter have supported the multi-layer model, identifying aliphatic, carbohydrate, and amino acid groups at the solution interface and aromatic groups located closer to the clay surface (Genest et al., 2014).

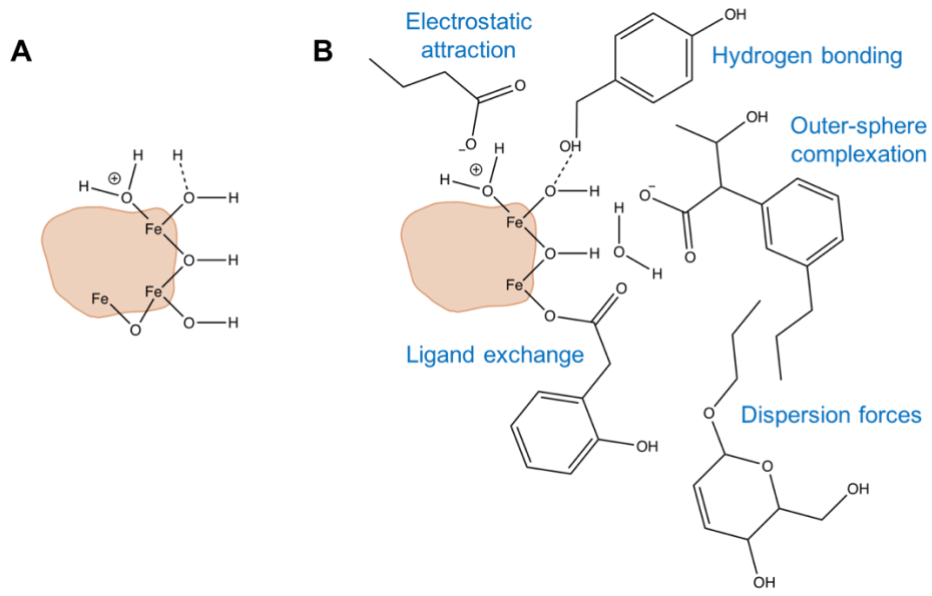

Figure 1.1. Types of surface hydroxyl groups on goethite (α-FeOOH) (A) and different types of sorption interactions between organic molecules and goethite (B).

While there have been some similarities in sorptive fractionation among different minerals and DOM types, mineral surfaces vary sufficiently to participate in different chemical interactions. Iron and aluminum oxides have pH-dependent surface charges, while clays can have permanent or pH-dependent charges, depending on their structure (Essington, 2004). Whether a mineral surface is positive, negative or neutral at the soil solution pH can have a profound effect on the dominant sorption interactions. For example, at neutral pH, a carboxylate group in DOM may interact with a negatively charged clay surface via cation-bridging, but would be more likely to be electrostatically attracted to a positively charged hydrous Fe oxide. At low pH, carboxylic groups are more likely to participate in direct interactions with Fe oxide surfaces through ligand exchange. These differences in sorption interactions among minerals may be expected to result in different responses of sorption behavior to temperature changes.

Very few studies have investigated the effect of temperature on sorption of DOM to soil minerals. Baham and Sposito (1994) and Arnarson and Keil (2000) examined the effect of temperature on DOM sorption to montmorillonite and kaolinite clays, reporting no dependence on temperature

and decreasing sorption with temperature, respectively. Due to the differences in surface reactivity between these clays and other soil minerals such as Fe and Al oxides, it is not clear whether the same effects of temperature could be expected in those systems.

Iron oxides are prevalent and important sorbents of DOM in many soils. Ferrihydrite is a poorly crystalline hydrous Fe oxide with high surface area relative to other iron oxides (Borggaard, 1983) and can adsorb large quantities of organic carbon (Kaiser et al., 1997). It has been shown to induce more pronounced fractionation of DOM than other, more ordered Fe oxides (Lv et al., 2016), and may therefore exhibit more sensitivity in sorption response to temperature. To determine the influence of temperature on sorption and desorption of organic matter on ferrihydrite, I performed continuous flow and batch sorption experiments with various types of dissolved organic matter at 7, 25, and 45°C. The results from this work are presented and discussed in Chapter 3.

1.4 Carbon cycling in wetlands

The high moisture content of wetland soils leads to anaerobic conditions that slow the processing of organic litter inputs, leading to extensive accumulation of organic material. Saturated soil conditions and fine sediment limit oxygen diffusion into wetland soils. With limited or no oxygen available, decomposing microorganism communities turn to alternative decomposition and respiration pathways. The first step in decomposition, depolymerization, can be rate-limiting in either aerobic or anaerobic environments, but occurs more quickly in the presence of oxygen (Freeman et al., 2001; Reineke, 2001). It is thought that the reliance of anaerobic depolymerization on mostly hydrolytic enzymes results in the accumulation of hydrolysis-resistant compounds such as lipids and lignin (Hedges and Keil, 1995). The second step in decomposition involves coupling the oxidation of low molecular weight organic molecules with the reduction of a terminal electron acceptor (TEA). Oxygen reduction provides the most energy, followed by NO_3^-, Mn(III/IV), Fe(III), SO_4^{2-}, and finally CO_2.

Recent research has demonstrated that the oxidation rate of the organic substrate depends not only on the Gibbs free energy of the reduction of the TEA, but also on the free energy of the oxidation of the organic substrate (Keiluweit et al., 2016; Boye et al., 2017; Noël et al., 2017). Depending on the reduction potential of available TEAs, microbes may be unable to oxidize very reduced compounds, such as aliphatic waxes and lipids, quickly. The exact reducing conditions and their impact on organic matter chemistry and decomposition rates depends on the availability of NO_3^-, SO_4^{2-}, Fe, and Mn in the soil and porewater (Keiluweit et al., 2015; Noël et al., 2017).

Overall, the anaerobic decomposition pathways occur at slower rates than aerobic ones. This promotes C stabilization in saturated soils relative to unsaturated soils—wetlands make up 5-8% of the land surface but store 20-30% of soil organic carbon (Mitsch and Gosselink, 2007; Lal, 2008). Diverging decomposition pathways can also lead to different forms of organic matter: relatively reduced aliphatic compounds tend to accumulate more in anaerobic soils (Keiluweit et al., 2015; Keiluweit et al., 2016; Boye et al., 2017).

Hydrologic flow paths linking wetlands with upland landscapes govern their water table fluctuations and biogeochemical processes. Differences in hydraulic residence time and flow paths may influence the inputs and outputs of C and other nutrients, ultimately regulating the amount and type of C stored. With predicted changes in precipitation and snowmelt patterns that could dramatically alter wetland hydrology and chemistry (Williams et al., 1996; Lukas et al., 2014), accurate carbon accounting and a detailed understanding of the carbon dynamics in these crucial systems is vital for effective management of wetlands that store disproportionate amounts of carbon. In the Rocky Mountains, subalpine wetlands also serve as headwaters for drinking water consumed by millions of people, and biogeochemical processes in these watersheds can affect downstream water quality, including the formation of hazardous disinfection byproducts during water treatment (Singer, 1999; MacDonald and Coe, 2007). To evaluate the effect of hydrogeomorphic conditions on the

storage and biogeochemical cycling of carbon in subalpine wetlands, I quantified and characterized the soil organic carbon composition in wetlands with short and long hydraulic residence times using total organic carbon measurements and solid-state ^{13}C NMR spectroscopy. The findings from this work are presented and discussed in Chapter 4.

1.5 Publications

Most of this dissertation work is either planned for submission to or already published in peer-reviewed journals. Chapter 2 (Daugherty et al., 2017a) was recently published in *Environmental Science & Technology*. Chapter 3 (Daugherty and Borch) will be submitted for publication in *Organic Geochemistry* this summer. Chapter 4 (Daugherty et al.) will be submitted for review later this summer. Parts of the dissertation have also been presented at several national and international conferences including the American Geophysical Union Fall Meeting in December, 2017 (Daugherty et al., 2017b), at the American Chemical Society Meeting in March, 2015 (Daugherty and Borch, 2015), and at Goldschmidt in June, 2014 (Daugherty et al., 2014).

REFERENCES

Aeschbacher M., Vergari D., Schwarzenbach R. P. and Sander M. (2011) Electrochemical analysis of proton and electron transfer equilibria of the reducible moieties in humic acids. *Environ. Sci. Technol.* **45**, 8385–8394.

Arnarson T. S. and Keil R. G. (2000) Mechanisms of pore water organic matter adsorption to montmorillonite. *Mar. Chem.* **71**, 309–320.

Avneri-Katz S., Young R. B., McKenna A. M., Chen H., Corilo Y. E., Polubesova T., Borch T. and Chefetz B. (2016) Adsorptive fractionation of dissolved organic matter (DOM) by mineral soil: Macroscale approach and molecular insight. *Org. Geochem.* Available at: http://dx.doi.org/10.1016/j.orggeochem.2016.11.004.

Baham J. and Sposito G. (1994) Adsorption of Dissolved Organic Carbon Extracted from Sewage Sludge on Montmorillonite and Kaolinite in the Presence of Metal Ions. *J. Environ. Qual.* **23**, 147.

Basile-Doelsch I., Amundson R., Stone W. E. E., Borschneck D., Bottero J. Y., Moustier S., Masin F. and Colin F. (2007) Mineral control of carbon pools in a volcanic soil horizon. *Geoderma* **137**, 477–489.

Bligh M. W. and Waite T. D. (2010) Role of heterogeneous precipitation in determining the nature of products formed on oxidation of Fe(II) in seawater containing natural organic matter. *Environ. Sci. Technol.* **44**, 6667–6673.

Borggaard O. K. (1983) Effect of Surface Area and Mineralogy of Iron Oxides on Their Surface Charge and Anion-Adsorption Properties. *Clays Clay Miner.* **31**, 230–232.

Boye K., Noël V., Tfaily M. M., Bone S. E., Williams K. H., Bargar J. R. and Fendorf S. (2017) Thermodynamically controlled preservation of organic carbon in floodplains. *Nat. Geosci.* **10**, 415–419.

Brezonik P. L., Bloom P. R., Sleighter R. L., Cory R. M., Khwaja A. R. and Hatcher P. G. (2015) Chemical differences of aquatic humic substances extracted by XAD-8 and DEAE-cellulose. *J. Environ. Chem. Eng.* **3**, 2982–2990.

Carey J. C., Tang J., Templer P. H., Kroeger K. D., Crowther T. W., Burton A. J., Dukes J. S., Emmett B., Frey S. D., Heskel M. A., Jiang L., Machmuller M. B., Mohan J., Panetta A. M., Reich P. B., Reinsch S., Wang X., Allison S. D., Bamminger C., Bridgham S., Collins S. L., De Dato G., Eddy W. C., Enquist B. J., Estiarte M., Harte J., Henderson A., Johnson B. R., Larson K. S., Luo Y., Marhan S., Melillo J. M., Peñuelas J., Pfeifer-Meister L., Poll C., Rastetter E., Reinmann A. B., Reynolds L. L., Schmidt I. K., Shaver G. R., Strong A. L., Suseela V. and Tietema A. (2016) Temperature response of soil respiration largely unaltered with experimental warming. *Proc. Natl. Acad. Sci.* **113**, 13797–13802.

Chassé A. W., Ohno T., Higgins S. R., Amirbahman A., Yildirim N. and Parr T. B. (2015) Chemical Force Spectroscopy Evidence Supporting the Layer-by-Layer Model of Organic Matter Binding to Iron (oxy)hydroxide Mineral Surfaces. *Environ. Sci. Technol.* **49**, 9733–9741.

Chorover J. and Amistadi M. K. (2001) Reaction of forest floor organic matter at goethite, birnessite and smectite surfaces. *Geochim. Cosmochim. Acta* **65**, 95–109.

Coward E. K., Ohno T. and Plante A. F. (2018) Adsorption and Molecular Fractionation of Dissolved Organic Matter on Iron-Bearing Mineral Matrices of Varying Crystallinity. *Environ. Sci. Technol.* **52**, 1036–1044.

Craig P. S., Shaw T. J., Miller P. L., Pellechia P. J. and Ferry J. L. (2009) Use of multiparametric techniques to quantify the effects of naturally occurring ligands on the kinetics of Fe(II) oxidation. *Environ. Sci. Technol.* **43**, 337–42.

Daugherty E. E. and Borch T. (2015) Temperature effects on carbon sequestration by iron oxide coated mineral surfaces. In *American Chemical Society Meeting* Spring 2015 Meeting. American Chemical Society, Denver, CO.

Daugherty E. E., Gilbert B., Nico P. and Borch T. (2014) Coordination and redox chemistry of aqueous Fe(II) and dissolved organic matter. In *Goldschmidt Abstracts* Sacramento, CA. p. 501.

Daugherty E. E., Gilbert B., Nico P. S. and Borch T. (2017a) Complexation and Redox Buffering of Iron(II) by Dissolved Organic Matter. *Environ. Sci. Technol.* **51**, 11096–11104.

Daugherty E. E., Lobo G., Pallud C. E. and Borch T. (2017b) Abstract B21J-07 Temperature and chemical composition controls on sorption of DOC to iron hydroxides under dynamic flow conditions. In *Fall Meeting of the American Geophysical Union* 2017 Fall Meeting, AGU. New Orleans, LA.

Emmenegger L., King D. W., Sigg L. and Sulzberger B. (1998) Oxidation Kinetics of Fe(II) in a Eutrophic Swiss Lake. *Environ. Sci. Technol.* **32**, 2990–2996.

Essington M. E. (2004) *Soil and Water Chemistry.*, CRC, New York.

Eusterhues K., Neidhardt J., Hädrich A., Küsel K. and Totsche K. U. (2014) Biodegradation of ferrihydrite-associated organic matter. *Biogeochemistry* **119**, 45–50.

Eusterhues K., Rennert T., Knicker H., Kögel-Knabner I., Totsche K. U. and Schwertmann U. (2011) Fractionation of organic matter due to reaction with ferrihydrite: Coprecipitation versus adsorption. *Environ. Sci. Technol.* **45**, 527–533.

Eusterhues K., Rumpel C., Kleber M. and Kögel-Knabner I. (2003) Stabilisation of soil organic matter by interactions with minerals as revealed by mineral dissolution and oxidative degradation. *Org. Geochem.* **34**, 1591–1600.

Falkowski P. G. (2005) Biogeochemistry of primary production in the sea. In *Biogeochemistry* (ed. W. H. Schlesinger). Elsevier, Boston, MA. p. 206.

Freeman C., Evans C. D., Monteith D. T., Reynolds B. and Fenner N. (2001) Export of organic carbon from peat soils. *Nature* **412**, 785.

Galindo C. and Del Nero M. (2014) Molecular level description of the sorptive fractionation of a fulvic acid on aluminum oxide using electrospray ionization fourier transform mass spectrometry. *Environ. Sci. Technol.* **48**, 7401–8.

Gayer K. H. and Woontner L. (1956) The solubility of ferrous hydroxide and ferric hydroxide in acidic and basic media at 25°. *J. Phys. Chem.* **60**, 1569–1571.

Genest S. C., Simpson M. J., Simpson A. J., Soong R. and McNally D. J. (2014) Analysis of soil organic matter at the solid–water interface by nuclear magnetic resonance spectroscopy. *Environ. Chem.* **11**, 472.

Gledhill M. and Buck K. N. (2012) The organic complexation of iron in the marine environment: A review. *Front. Microbiol.* **3**, 1–17.

Grinhut T., Lansky D., Gaspar A., Hertkorn N., Schmitt-Kopplin P., Hadar Y. and Chen Y. (2010) Novel software for data analysis of Fourier transform ion cyclotron resonance mass spectra applied to natural organic matter. *Rapid Commun. Mass Spectrom.* **24**, 2831–2837.

Gu B., Schmitt J., Chen Z., Liang L. and McCarthy J. F. (1995) Adsorption and desorption of different organic matter fractions on iron oxide. *Geochim. Cosmochim. Acta* **59**, 219–229.

Gu B., Schmitt J., Chen Z., Liang L. and McCarthy J. F. (1994) Adsorption and desorption of natural organic matter on iron oxide: mechanisms and models. *Environ. Sci. Technol.* **28**, 38–46.

Hao J., Liebeke M., Sommer U., Viant M. R., Bundy J. G. and Ebbels T. M. D. (2016) Statistical Correlations between NMR Spectroscopy and Direct Infusion FT-ICR Mass Spectrometry Aid Annotation of Unknowns in Metabolomics. *Anal. Chem.* **88**, 2583–2589.

Hedges J. I. and Keil R. G. (1995) Sedimentary organic matter preservation: an assessment and speculative synthesis. *Mar. Chem.* **49**, 81–115.

Hertkorn N., Frommberger M., Witt M., Koch B. P., Schmitt-Kopplin P. and Perdue E. M. (2008) Natural organic matter and the event horizon of mass spectrometry. *Anal. Chem.* **80**, 8908–19.

von der Heyden B. P., Hauser E. J., Mishra B., Martinez G. A., Bowie A. R., Tyliszczak T., Mtshali T. N., Roychoudhury A. N. and Myneni S. C. B. (2014) Ubiquitous Presence of Fe(II) in Aquatic Colloids and Its Association with Organic Carbon. *Environ. Sci. Technol. Lett.* **1**, 387–392.

von der Heyden B. P., Roychoudhury A. N., Mtshali T. N., Tyliszczak T. and Myneni S. C. B. (2012) Chemically and geographically distinct solid-phase iron pools in the Southern Ocean. *Science* **338**, 1199–201.

Huang W., Peng P., Yu Z. and Fu J. (2003) Effects of organic matter heterogeneity on sorption and desorption of organic contaminants by soils and sediments. *Appl. Geochem.* **18**, 955–972.

Hudson B. D. (1994) Soil organic matter and available water capacity. *J. Soil Water Conserv.* **49**, 189–194.

IPCC (2007) *Climate Change 2007: The Physical Science Basis.*, Cambridge University Press, New York, NY.

Jobbágy E. G. and Jackson R. B. (2000) The vertical distribution of soil organic carbon and its relation to climate and vegetation. *Ecol. Appl.* **10**, 423–436.

Jobin R. and Ghosh M. M. (1972) Effect of buffer intensity and organic matter on the oxygenation of ferrous iron. *J. Am. Water Works Assoc.* **64**, 590–595.

Kaiser K. (2003) Sorption of natural organic matter fractions to goethite (alpha-FeOOH): Effect of chemical composition as revealed by liquid-state 13C NMR and wet-chemical analysis. *Org. Geochem.* **34**, 1569–1579.

Kaiser K. and Guggenberger G. (2000) The role of DOM sorption to mineral surfaces in the preservation of organic matter in soils. *Org. Geochem.* **31**, 711–725.

Kaiser K., Guggenberger G., Haumaier L. and Zech W. (1997) Dissolved organic matter sorption on sub soils and minerals studied by 13C-NMR and DRIFT spectroscopy. *Eur. J. Soil Sci.* **48**, 301–310.

Kallenbach C. M., Grandy A. and Frey S. D. (2016) Direct evidence for microbial-derived soil organic matter formation and its ecophysiological controls. *Nat. Commun.*, 1–10.

Karlsson T. and Persson P. (2012) Complexes with aquatic organic matter suppress hydrolysis and precipitation of Fe(III). *Chem. Geol.* **322–323**, 19–27.

Karlsson T. and Persson P. (2010) Coordination chemistry and hydrolysis of Fe(III) in a peat humic acid studied by X-ray absorption spectroscopy. *Geochim. Cosmochim. Acta* **74**, 30–40.

Karlsson T., Persson P. and Skyllberg U. (2006) Complexation of copper(ll) in organic soils and in dissolved organic matter--EXAFS evidence for chelate ring structures. *Environ. Sci. Technol.* **40**, 2623–8.

Keiluweit M., Bougoure J. J., Nico P. S., Pett-Ridge J., Weber P. K. and Kleber M. (2015) Mineral protection of soil carbon counteracted by root exudates. *Nat. Clim. Change* **5**, 588–595.

Keiluweit M., Nico P. S., Kleber M. and Fendorf S. (2016) Are oxygen limitations under recognized regulators of organic carbon turnover in upland soils? *Biogeochemistry* **127**, 157–171.

Kiem R. and Kögel-Knabner I. (2003) Contribution of lignin and polysaccharides to the refractory carbon pool in C-depleted arable soils. *Soil Biol. Biochem.* **35**, 101–118.

Kleber M., Sollins P. and Sutton R. (2007) A conceptual model of organo-mineral interactions in soils: self-assembly of organic molecular fragments into zonal structures on mineral surfaces. *Biogeochemistry* **85**, 9–24.

Knicker H. (2000) Biogenic nitrogen in soils as revealed by solid-state 13C and 15N nuclear magnetic resonance spectroscopy. *J. Environ. Qual.* **29**, 715–723.

Knorr K. H. (2013) DOC-dynamics in a small headwater catchment as driven by redox fluctuations and hydrological flow paths - Are DOC exports mediated by iron reduction/oxidation cycles? *Biogeosciences* **10**, 891–904.

Koch B. P. and Dittmar T. (2006) From mass to structure: An aromaticity index for high-resolution mass data of natural organic matter. *Rapid Commun. Mass Spectrom.* **20**, 926–932.

Köchy M., Hiederer R. and Freibauer A. (2015) Global distribution of soil organic carbon – Part 1: Masses and frequency distributions of SOC stocks for the tropics, permafrost regions, wetlands, and the world. *SOIL* **1**, 351–365.

Koretsky C. M., Haas J. R., Ndenga N. T. and Miller D. (2006) Seasonal Variations in Vertical Redox Stratification and Potential Influence on Trace Metal Speciation in Minerotrophic Peat Sediments. *Water. Air. Soil Pollut.* **173**, 373–403.

Krachler R., Jirsa F. and Ayromlou S. (2005) Factors influencing the dissolved iron input by river water to the open ocean. , 5.

Kramer R. W., Kujawinski E. B., Zang X., Green-Church K. B., Jones R. B. and Hatcher P. G. (2001) Studies of the structure of humic substances by electrosopray ionization coupled to a

quadrupole-time of flight (QQ-TOF) mass spectrometer. In *Humic Substances: Structures, Models, and Functions* pp. 95–107.

Lal R. (2008) Carbon sequestration. *Philos. Trans. R. Soc. Lond. B Biol. Sci.* **363**, 815–830.

Lalonde K., Mucci A., Ouellet A. and Gelinas Y. (2012) Preservation of organic matter in sediments promoted by iron - SI. *Nature* **483**, 198–200.

Lukas J., Barsugli N., Rangwala I. and Wolter K. (2014) *Climate Change in Colorado, 2nd ed.*, University of Colorado Boulder, Boulder, CO. Available at: http://wwa.colorado.edu/climate/co2014report/index.html.

Lv J., Zhang S., Wang S., Luo L., Cao D. and Christie P. (2016) Molecular-Scale Investigation with ESI-FT-ICR-MS on Fractionation of Dissolved Organic Matter Induced by Adsorption on Iron Oxyhydroxides. *Environ. Sci. Technol.* **50**, 2328–2336.

MacDonald L. H. and Coe D. (2007) Influence of Headwater Streams on Downstream Reaches in Forested Areas. *For. Sci.* **53**, 148–168.

McBride M., Sauve S. and Hendershot W. (2005) Solubility control of Cu, Zn, Cd and Pb in contaminated soils. *Eur. J. Soil Sci.* **48**, 337–346.

McKnight D. M., Bencaia K. E., Zellweger G. W., Aiken G. R., Feder G. L. and Thorn K. A. (1992) Sorption of dissolved organic carbon by hydrous aluminum and iron oxides occurring at the confluence of Deer Creek with the Snake River, Summit County, Colorado. *Environ. Sci. Technol.* **26**, 1388–1396.

Meier M., Namjesnik-Dejanovic K., Maurice P. A., Chin Y. P. and Aiken G. R. (1999) Fractionation of aquatic natural organic matter upon sorption to goethite and kaolinite. *Chem. Geol.* **157**, 275–284.

Mikutta R. and Kaiser K. (2011) Organic matter bound to mineral surfaces: Resistance to chemical and biological oxidation. *Soil Biol. Biochem.* **43**, 1738–1741.

Mikutta R., Kleber M., Torn M. S. and Jahn R. (2006) Stabilization of soil organic matter: Association with minerals or chemical recalcitrance? *Biogeochemistry* **77**, 25–56.

Mitsch W. J. and Gosselink J. G. (2007) *Wetlands*. 4th ed., Wiley, Hoboken, NJ. Available at: https://library.wur.nl/WebQuery/titel/1862523 [Accessed May 21, 2018].

Noël V., Boye K., Kukkadapu R. K., Bone S., Lezama Pacheco J. S., Cardarelli E., Janot N., Fendorf S., Williams K. H. and Bargar J. R. (2017) Understanding controls on redox processes in floodplain sediments of the Upper Colorado River Basin. *Sci. Total Environ.* **603–604**, 663–675.

Prietzel J., Thieme J., Salomé M. and Knicker H. (2007) Sulfur K-edge XANES spectroscopy reveals differences in sulfur speciation of bulk soils, humic acid, fulvic acid, and particle size separates. *Soil Biol. Biochem.* **39**, 877–890.

Pullin M. J. and Cabaniss S. E. (2003) The effects of pH, ionic strength, and iron–fulvic acid interactions on the kinetics of non-photochemical iron transformations. I. Iron(II) oxidation and iron(III) colloid formation. *Geochim. Cosmochim. Acta* **67**, 4067–4077.

Rasmussen C., Heckman K., Wieder W. R., Keiluweit M., Lawrence C. R., Berhe A. A., Blankinship J. C., Crow S. E., Druhan J. L., Hicks Pries C. E., Marin-Spiotta E., Plante A. F., Schädel C., Schimel J. P., Sierra C. A., Thompson A. and Wagai R. (2018) Beyond clay: towards an improved set of variables for predicting soil organic matter content. *Biogeochemistry*. Available at: http://link.springer.com/10.1007/s10533-018-0424-3 [Accessed February 16, 2018].

Reineke W. (2001) Aerobic and anaerobic biodegradation potentials of microorganisms. In *Biodegradation and Persistance* (ed. Bernd Beek). Springer, Berlin. pp. 1–161.

Riedel T., Zak D., Biester H. and Dittmar T. (2013) Iron traps terrestrially derived dissolved organic matter at redox interfaces. *Proc. Natl. Acad. Sci.* **110**, 10101–10105.

Rose A. L. and Waite T. D. (2002) Kinetic model for Fe(II) oxidation in seawater in the absence and presence of natural organic matter. *Environ. Sci. Technol.* **36**, 433–44.

Rose A. L. and Waite T. D. (2003) Kinetics of iron complexation by dissolved natural organic matter in coastal waters. *Mar. Chem.* **84**, 85–103.

Saidy A. R., Smernik R. J., Baldock J. A., Kaiser K. and Sanderman J. (2013) The sorption of organic carbon onto differing clay minerals in the presence and absence of hydrous iron oxide. *Geoderma* **209–210**, 15–21.

Scharlemann J. P., Tanner E. V., Hiederer R. and Kapos V. (2014) Global soil carbon: understanding and managing the largest terrestrial carbon pool. *Carbon Manag.* **5**, 81–91.

Simpson A. J. (2002) Determining the molecular weight, aggregation, structure, and interactions of natural organic matter using diffusion ordered spectroscopy. *Magn. Reson. Chem.* **40**, S72–S82.

Simpson M. J. and Simpson A. J. eds. (2014) *NMR Spectroscopy: A Versatile Tool for Environmental Research.*, John Wiley & Sons, Chichester, UK.

Singer P. C. (1999) Humic substances as precursors for potentially harmful disinfection by-products. *Water Sci. Technol.* **40**, 25–30.

Sleighter R. L. and Hatcher P. G. (2007) The application of electrospray ionization coupled to ultrahigh resolution mass spectrometry for the molecular characterization of natural organic matter. *J. Mass Spectrom.* **42**, 559–574.

Sundman A., Karlsson T., Laudon H. and Persson P. (2014) XAS study of iron speciation in soils and waters from a boreal catchment. *Chem. Geol.* **364**, 93–102.

Tfaily M. M., Chu R. K., Toyoda J., Toli N. and Robinson E. W. (2017) Sequential extraction protocol for organic matter from soils and sediments using high resolution mass spectrometry. *Anal. Chim. Acta* **972**, 54–61.

Tiessen H., Cuevas E. and Chacon P. (1994) The role of soil organic matter in sustaining soil fertility. *Nature* **371**, 783–785.

Tisdall J. M. and Oades J. M. (1982) Organic matter and water-stable aggregates in soils. *J. Soil Sci.* **33**, 141–163.

Toner B. M., Fakra S. C., Manganini S. J., Santelli C. M., Marcus M. A., Moffett J. W., Rouxel O., German C. R. and Edwards K. J. (2009) Preservation of iron(II) by carbon-rich matrices in a hydrothermal plume. *Nat. Geosci.* **2**, 197–201.

Torn M. S., Trumbore S. E., Chadwick O. A., Vitousek P. M. and Hendricks D. M. (1997) Mineral control of soil organic carbon storage and turnover. *Nature* **389**, 170–173.

Van Cappellen P. and Wang Y. (1996) Cycling of iron and manganese in surface sediments: A general theory for the coupled transport and reaction of carbon, oxygen, nitrogen, sulfur, iron, and manganese. *Am. J. Sci.* **296**, 197–243.

Wagai R. and Mayer L. M. (2007) Sorptive stabilization of organic matter in soils by hydrous iron oxides. *Geochim. Cosmochim. Acta* **71**, 25–35.

Wan J., Tyliszczak T. and Tokunaga T. K. (2007) Organic carbon distribution, speciation, and elemental correlations within soil microaggregates: Applications of STXM and NEXAFS spectroscopy. *Geochim. Cosmochim. Acta* **71**, 5439–5449.

Wershaw R. L., Llaguno E. C. and Leenheer J. A. (1996) Mechanism of formation of humus coatings on mineral surfaces 3. Composition of adsorbed organic acids from compost leachate on alumina by solid-state 13C NMR. *Colloids Surf. A* **108**, 213–223.

Williams M. W., Losleben M., Caine N. and Greenland D. (1996) Changes in climate and hydrochemical responses in a high-elevation catchment in the Rocky Mountains, USA. *Limnol. Oceanogr.* **41**, 939–946.

CHAPTER 2: COMPLEXATION AND REDOX BUFFERING OF IRON(II) BY DISSOLVED ORGANIC MATTER[1]

2.1 Introduction

Iron (Fe) is an essential micronutrient for both photosynthesis and respiration, and the two oxidation states of Fe can act as electron donors or acceptors for certain microbial metabolic pathways (Weber et al., 2006; Melton et al., 2014). Iron bioavailability can limit primary production in marine systems (Boyd et al., 2007) and influence the biogeochemical functioning of soils and sediments. The bioavailability of Fe in aquatic environments is strongly affected by redox reactions that cycle Fe between +(II) and +(III) oxidation states and by complexation with organic ligands. Although free Fe(III) has very low solubility at circumneutral pH, organic complexation greatly increases solubility; over 99% of the pool of dissolved oceanic Fe(III) is organically complexed (Rue and Bruland, 1995). Fe(II) is far more soluble than Fe(III), and free Fe(II) can reach high concentrations in reducing environments. However, Fe(II) is also readily complexed by NOM (Yamamoto et al., 2010), a reaction that may influence the redox behavior of Fe(II).

Both pure Fe(II) and mixed Fe(II)/Fe(III) species have been discovered in association with NOM in oxygen-rich aquatic environments. Examples include particles collected from the photic zone in the Southern Ocean (von der Heyden et al., 2012), from hydrothermal plumes at the mid-ocean ridge East Pacific Rise (pH ~9) (Toner et al., 2009), and from freshwater lakes in New Jersey and Puerto Rico, U.S. (von der Heyden et al., 2014). In addition, Sundman *et al.* identified mixed Fe(II)/Fe(III)-NOM complexes in streamwater and soil solutions in a boreal catchment at pH 4.3-5.8

[1] Reproduced with permission from Daugherty, E. E.; Gilbert, B.; Nico, P. S.; Borch, T. Complexation and Redox Buffering of Iron(II) by Dissolved Organic Matter. Environmental Science & Technology 2017, 51 (19), 11096–11104. Copyright 2017, American Chemical Society.

(Sundman et al., 2014). Such observations are contrary to expectations from simple models of Fe(II) oxidation rates and equilibrium calculations that show Fe(III) to be favored under oxic conditions at pH greater than 4. Several mechanisms have been suggested to explain the persistence of reduced Fe, including photochemical reduction (Voelker et al., 1997; Barbeau et al., 2001), microbially mediated reduction (Melton et al., 2014), and enhanced stability as a result of binding with organic ligands (Millero et al., 1987).

Laboratory investigations of Fe–NOM oxidation-reduction chemistry have yielded contradictory results as to whether complexation of Fe by NOM enhances, inhibits, or has no effect upon the rate of Fe(II) oxidation. Such variability likely indicates that the effect of organic association on Fe(II) oxidation is dependent on the molecule and the experimental system. Tannic acid, gallic acid, and pyrogallol have been shown to inhibit Fe(II) oxidation, while salicylate and citrate enhance oxidation (Theis and Singer, 1974; Pham and Waite, 2008), and alanine and glutamic acid have no effect (Santana-Casiano et al., 2000). Studies using environmental samples show that NOM from different sources has variable effects on Fe(II) oxidation kinetics (Jobin and Ghosh, 1972; Davison and Seed, 1983; Emmenegger et al., 1998; Rose and Waite, 2002; Rose and Waite, 2003a; Pullin and Cabaniss, 2003; Rose and Waite, 2003b; Craig et al., 2009; Bligh and Waite, 2010). Most studies lack an explicit consideration of NOM redox activity (Garg et al., 2015; Jiang et al., 2015) and thorough characterization of binding interactions between Fe(II) and the chosen organic molecules. Natural organic matter is capable of acting as both an electron donor and acceptor, and can redox cycle repeatedly (Klüpfel et al., 2014). Aeschbacher *et al.* (2011) have shown that reducible moieties in NOM cover a wide range of standard reduction potentials, many of which can reduce Fe, and some of which may oxidize Fe.

In this study, we used extended X-ray absorption fine structure (EXAFS) spectroscopy to determine the coordination environment of Fe(II) complexed by reduced NOM. Reduced NOM was

used because Fe(II) underwent oxidation in the presence of as-received NOM. Recent EXAFS studies of the structure of Fe(III)-NOM compounds have shown that Fe(III) forms mononuclear complexes with NOM at low pH and Fe concentration and precipitates as Fe(III)-oxyhydroxides at higher pH and Fe content (Karlsson et al., 2008). The mononuclear Fe(III) complexes involve chelate ring structures with carboxyl, hydroxamate, and hydroxyl groups (Mikutta and Kretzschmar, 2011; Karlsson and Persson, 2012). To our knowledge, there are no EXAFS studies of Fe(II) complexation by NOM and few works dedicated to elucidating the binding mechanisms in such complexes (Toner et al., 2009; Catrouillet et al., 2014; von der Heyden et al., 2014). We also studied the consequences of NOM complexation on the rate of Fe(II) oxidation by O_2 for the standard Leonardite humic acid in order to improve our current understanding of mechanisms controlling the fate and stability of Fe(II) in natural oxic waters.

2.2 Materials and Methods

2.2.1 Preparation of samples and standards

Samples for X-ray absorption spectroscopy analysis were prepared using dissolved natural organic matter (NOM) standards from the International Humic Substance Society (IHSS). These were chosen for their range of chemical properties and included Suwannee River fulvic acid (SRFA), humic acid (SRHA), and natural organic matter obtained by reverse osmosis (SRNOM); and Leonardite humic acid (LHA). Solutions were prepared in an anoxic glovebag by adding as-received NOM to O_2-free water and adjusting the pH to between 6.7 and 7.0 using 4 M NaOH (see Table A.2 for exact pH values of NOM solutions).

As-received NOM was capable of oxidizing Fe(II) even under anoxic conditions. To ensure the preservation of ferrous Fe, we used the approach of Ratasuk and Nanny (2007) to reduce some NOM samples by hydrogenation prior to addition of Fe. Reduction of 40-50 mg NOM in 2.75 mL of

Millipore water was performed by gently bubbling H_2 gas through solution in the presence of 100 mg of Pd-Al_2O_3 catalyst for 24 hours. Solutions were then anoxically transferred to centrifuge tubes and centrifuged at 6,000 rpm for 4.0 minutes to pellet out the catalyst. This process did not detectably change the solution pH.

Solutions of Fe(II) in the form of ferrous ammonium sulfate ($(NH_4)_2Fe(SO_4)_2 \bullet 6H_2O$), or Fe(III) in the form of ferric chloride ($FeCl_3$) were added to 1 mL of NOM solution to achieve 1-2 mM concentration and a 10-15 μmol Fe g^{-1} C ratio. The solution was mixed thoroughly, checked again for neutral pH, then lyophilized without exposure to oxygen. Samples were lyophilized in a vacuum flask, which was closed after drying and opened to atmospheric pressure in an anoxic glove bag. [*Reduced samples are indicated with the subscript "red".*] Anoxic preparation and storage effectively prevented the oxidation of Fe(II) by oxygen—a control in which Fe(II) was added to anoxic water in the glove bag showed no evidence of Fe oxidation.

Samples of reference organic molecules were prepared in the same way as the as-received samples, using sodium citrate, pyrocatechol, 2,2'-bipyridine (2,2'-bipy), ethylenediamine (EDA), ethylenediaminetetraacetic acid (EDTA), and mercaptoethanol in place of NOM (Figure A.1). High concentrations were used to minimize the Fe:C ratio and encourage Fe-ligand binding (Table A.1). The lyophilized samples were ground, if necessary, and packed densely into Teflon sample holders inside an anoxic glove bag. They were sealed with Kapton polyimide film and stored under anoxic conditions until transferred to the sample mount at the beam line. Preliminary experiments showed that lyophilized samples were significantly less susceptible than solution samples to X-ray-induced oxidation of Fe(II) (Figure A.2).

2.2.2 Data collection and analysis

2.2.2.1 X-ray absorption spectroscopy

All Fe K-edge X-ray absorption spectroscopic analyses were conducted at Beamline 11-2 at the Stanford Synchrotron Radiation Lightsource (SSRL) in Menlo Park, California, USA. Samples were mounted in an $N_{2\,(l)}$ cryostat to limit beam damage or oxidation. The Si(220) monochromator was detuned 50% to reduce higher order harmonics. Iron X-ray absorption near edge structure (XANES) and EXAFS fluorescence spectra were collected with a 100-element Ge detector simultaneously with the transmission spectrum of Fe foil, which was used for internal energy calibrations. Multiple scans per sample were acquired as necessary to achieve satisfactory data quality. A detector deadtime curve was collected for each beam time using a manganese filter.

Scans were calibrated by setting the first inflection point of the Fe(0) spectrum to 7112 eV, deadtime corrected, and averaged using SixPack software (Webb, 2005). Background removal, normalization, and glitch removal at 7250 and 7600 eV were performed in Athena (Ravel and Newville, 2005). This program was also used to generate and qualitatively compare XANES, EXAFS, and Fourier transform spectra. First-shell fitting of Fourier transforms of the k^3-weighted EXAFS spectra was performed using IFEFFIT code in Artemis, using ferrihydrite as a standard. Fourier transform and k^3-weighted chi spectra were also used to create wavelet transforms using the Igor Pro wavelet transform script developed by Funke *et al.* (2005). Wavelet transforms allow for the qualitative elemental discrimination of signal contributions from backscattering neighboring atoms. Linear combination fitting (LCF) of EXAFS spectra was performed in Artemis. Details of the linear combination fitting procedure can be found in Appendix A (see Figure A.6 and Figure A.7).

2.2.2.2 Fe(II) oxidation experiments[2]

The effect of binding Fe(II) by Leonardite humic acid (LHA) on the rate of Fe(II) oxidation by O_2 was measured in aqueous solution. The initial solutions were prepared under anoxic conditions using O_2-purged Millipore water, reduced LHA, and $FeCl_2$. The Fe(II)-LHA sample was prepared with 2 mg/mL of reduced LHA and 0.79 mM Fe(II). Test samples showed that there was no detectable oxidation of Fe in any sample following the overnight incubation.

To start the experiment, samples were removed from the anoxic glovebag into open air and 1 mL was added into 30-mL glass beakers containing air-equilibrated solutions of 11 mL of 4.2 mM PIPES, a non-complexing buffer (Yu et al., 1997), at pH 7. To test whether PIPES affected the Fe(II) oxidation rate, the kinetics of Fe(II) oxidation were determined at 4.1 mM and 41 μM PIPES concentrations in the absence of LHA (Figure A.8). Pseudo-first-order rate constants of Fe(II) oxidation were consistent with previously published values (Santana-Casiano et al., 2005; Pham and Waite, 2008b). While a difference was observed in the Fe(II) oxidation rates between the two solutions, it was substantially smaller than the effect of adding reduced organic matter, and was likely a result of additions of NaOH required to maintain steady pH. Solutions were kept in the dark and stirred for the length of the oxidation experiments.

Iron(II) concentration as a function of time was determined by extracting 50-μL aliquots and immediately adding them to 150 μL of pH 7 PIPES-buffered, 50-mM solutions of 2,2'-bipyridine (2,2'-bipy) (Moss and Mellon, 1942). After 30-60 seconds of reaction time, these solutions were analyzed by ultraviolet-visible (UV-vis) absorption spectroscopy. At some points, a duplicate 50-μL aliquot was taken, added to the 2,2'-bipy solution, capped, and stored in the dark for >30 minutes.

[2] Work completed by project collaborator Dr. Benjamin Gilbert at Lawrence Berkeley National Laboratory.

The Fe(II) concentration was determined from the average intensity between 568 and 572 nm using a previously measured calibration curve.

Dissolved O_2 was measured simultaneously using the FOXY fiber optic probe (Ocean Optics). There was no detectable difference in the trend in dissolved O_2 between experiments with and without NOM (data not shown). We sought to quantify the generation of hydrogen peroxide (H_2O_2) by the Amplex red assay (A-22188, Molecular Probes, Invitrogen), but found the response to be significantly higher than expected when LHA_{red} was present. Although we were not able to obtain reliable H_2O_2 concentrations in the presence of organic matter, the assay confirmed the generation of this species, and data are shown in Figure A.9.

The oxidizing capacity of as-received LHA was measured by adding Fe(II) to 1 mL of 2 mg/mL LHA to achieve a final Fe concentration of 1 mM. The reducing capacity of reduced LHA was measured by adding Fe(III) to 1 mL of 2 mg/mL LHA to achieve a final Fe concentration of 2 mM (Figure A.10). All reactions were performed in an anoxic chamber. The concentration of Fe(II) was tracked over eight hours using 2,2'-bipy but all redox reactions were completed within the first few minutes.

2.3 Results

2.3.1 XAS data analysis

The position of the absorption threshold of the Fe K-edge XANES spectra approximates the oxidation state of Fe (Figure 2.1). The Fe absorption edge for citrate + Fe(II) appeared at 7124 eV while that of citrate + Fe(III) appeared at a higher energy, 7126 eV. The spectra from all reference compounds with Fe(II) show no signs of oxidation. However, the edges of LHA + Fe(II) and SRFA + Fe(II) are very close to those of LHA + Fe(III) and citrate + Fe(III), clearly indicating that as-received NOM is capable of oxidizing Fe(II). In contrast, the spectra from reduced NOM samples are

aligned with citrate + Fe(II), indicating preeminence of reduced Fe. Electron paramagnetic resonance (EPR) spectroscopy confirmed Fe(II) added to reduced NOM was not oxidized (Figure A.3). The close agreement between the NOM + Fe(III) and the citrate + Fe(III) XANES spectra, as well as the EPR spectroscopy, shows that oxidized Fe remains complexed by NOM and does not form precipitates.

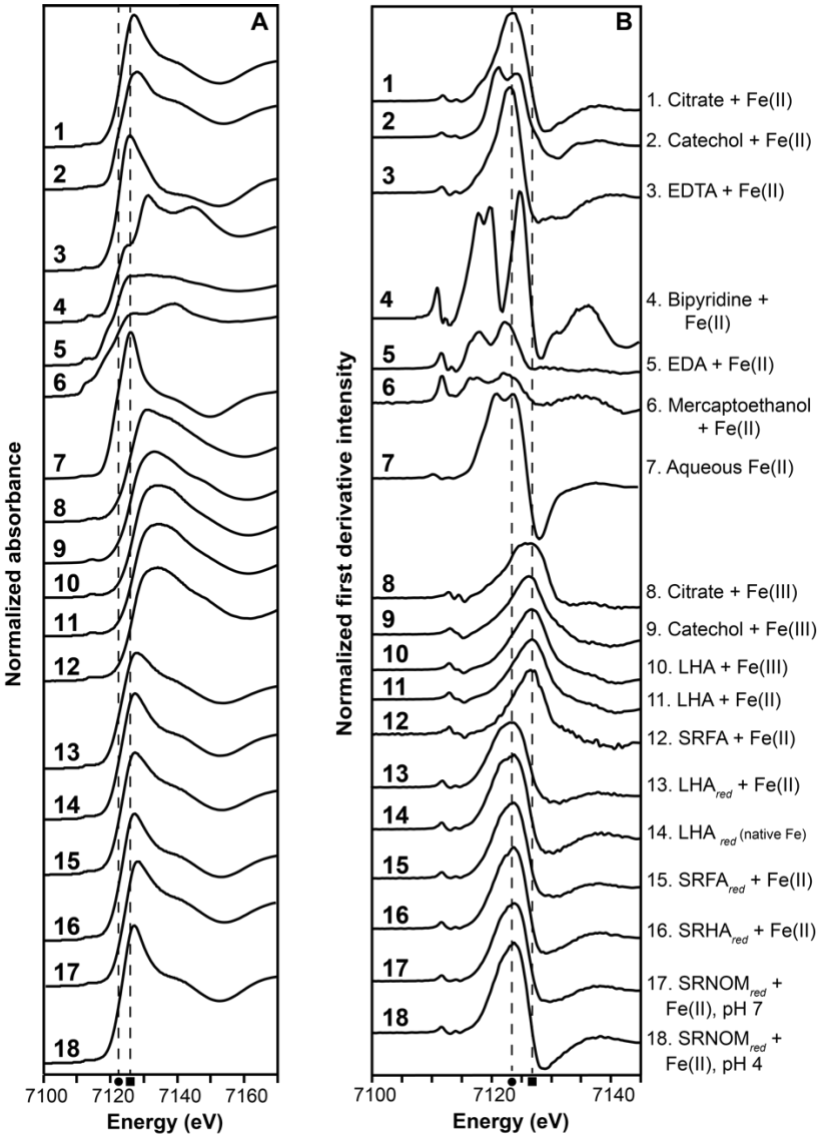

Figure 2.1 (A) Normalized Fe K-edge XANES spectra and (B) first derivatives of Fe-NOM samples and Fe–organic compound references at pH 7 unless indicated otherwise. NOM samples with added Fe have a 10-15 μmol Fe g^{-1} C ratio. Dotted lines show approximate E_0 values for citrate + Fe(II) (● 7124 eV) and citrate + Fe(III) (■ 7126 eV). The E_0 value represents the first well-defined peak in the first derivative.

First-shell fits of the Fe K-edge EXAFS data using a single-scattering oxygen path from ferrihydrite (Figure A.5) provide information about the average coordination number (CN) and bond distances of Fe–O paths (Table 2.1). Complexes containing Fe(III) and Fe(II) added to as-received NOM have high CN values (≥ 6) compared to Fe(II) complexes with reduced NOM or O-containing organic reference ligands (5.0 ≤ CN ≤ 5.7). The bond distances for the Fe(III) complexes analyzed in this study range from 1.99 - 2.02 Å, typical values for Fe(III) octahedral coordination with oxygen in organic ligands (Saines et al., 2011). The bond distances of the Fe(II) complexes range from 2.06 to 2.10 Å. Values above 2.08 Å are consistent with octahedrally coordinated Fe(II) (Strouse et al., 1977; Lundberg et al., 2007; Yang et al., 2007), although path lengths that are shorter could indicate a mixture of Fe(II) and Fe(III) (van Schaik et al., 2008). The longer bond lengths for Fe-O/N complexation in reduced NOM-Fe(II) samples relative to Fe(III)-NOM samples indicate less attraction between Fe(II) and the coordinating ligand and a weaker coordination environment.

Table 2.1 Bond distances (R), coordination numbers (CN), and Debye-Waller factors, (σ^2), derived from Fourier transform fitting of the Fe–O path in NOM samples and Fe citrate complexes.

Sample information				First shell fitting parameters						
		Dominant Fe oxidation state								
OM type	OM redox state[b]	Added	Observed[a]	CN	Error	R (Å)	Error	σ^2 (Å^2)	Error	R-factor
Citrate	as-received	2	2	**5.4**	0.6	**2.10**	0.02	0.0052	0.0016	0.0218
Citrate	as-received	3	3	**6.4**	0.7	**2.02**	0.01	0.0083	0.0018	0.0192
Catechol	as-received	2	2	**5.6**	1.1	**2.08**	0.02	0.0094	0.0030	0.0493
LHA	reduced	--	2	**5.2**	0.6	**2.08**	0.01	0.0073	0.0018	0.0195
LHA	reduced	2	2	**5.0**	0.6	**2.06**	0.01	0.0087	0.0018	0.0175
LHA	as-received	2	3	**6.0**	0.6	**1.990**	0.009	0.0052	0.0012	0.0111
LHA	as-received	3	3	**6.1**	0.5	**1.989**	0.008	0.0052	0.0011	0.0108
SRFA	as-received	2	3	**6.6**	0.8	**2.01**	0.01	0.0042	0.0017	0.0271
SRFA	reduced	2	2	**5.0**	0.5	**2.07**	0.01	0.0073	0.0016	0.0180
SRHA	reduced	2	2	**5.5**	0.6	**2.08**	0.01	0.0076	0.0018	0.0262
SRNOM	reduced	2	2	**5.6**	0.5	**2.07**	0.009	0.0078	0.0013	0.0111
SRNOM	reduced, pH 4	2	2	**5.7**	0.5	**2.09**	0.009	0.0060	0.0012	0.0132

[a]Observed dominant Fe oxidation state is based on E_0 values, visual comparison of XANES spectra, and EPR results.
[b]All samples are at pH 7 unless otherwise indicated.

Wavelet transform (WT) analysis was employed to investigate the nature of the atoms beyond the first coordination shell. WT analysis uses a two-dimensional plot created from the *k*-weighted

EXAFS spectrum and the corresponding Fourier transform to determine the distance and scattering strength of atoms. As can be seen in the WT plot for ferrihydrite in Figure 2.2, second shell Fe contributes a strong feature at about 7 $Å^{-1}$ and 2.75 Å. This feature is absent from WT plots for all complexes of Fe and NOM, demonstrating there is no significant presence of multinuclear Fe clusters or precipitates. Similar observations have been reported for systems containing low concentrations of Fe(III) at low to neutral pH (Karlsson et al., 2008; Karlsson and Persson, 2010; Sjöstedt et al., 2013).

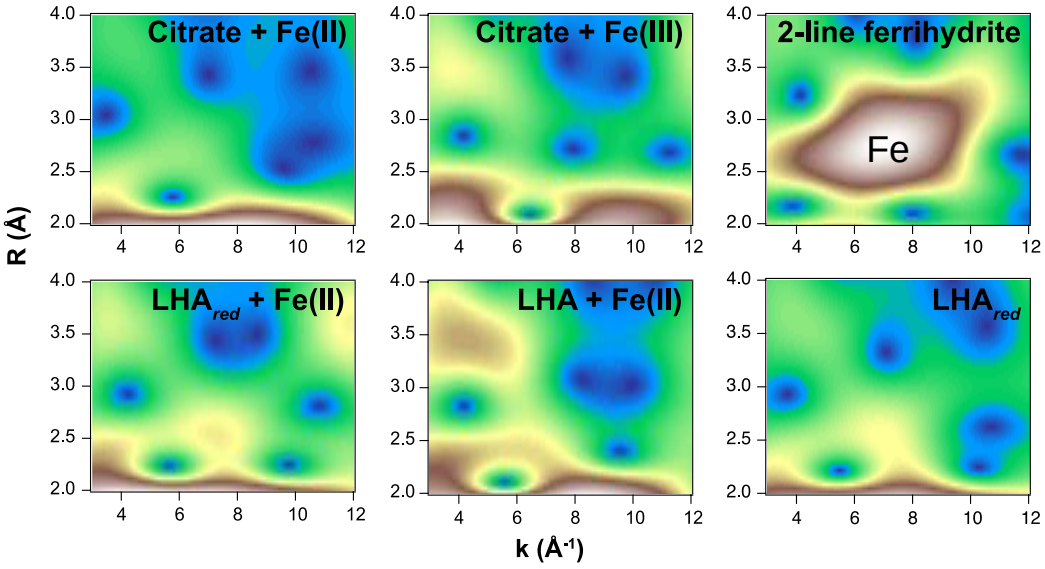

Figure 2.2 Wavelet transform moduli displaying the second and third coordination shells (Morlet wavelet parameters: $\eta = 9$, $\sigma = 1$) of Fe-organic complexes and ferrihydrite. LHA is Leonardite humic acid.

Linear combination fitting (LCF) of Fe EXAFS organic reference spectra to reduced NOM spectra reveals the dominant types of complexes formed (Figure 2.3). The strong contribution from the citrate + Fe(II) reference shows 50 – 75% of Fe was bound by carboxyl and possibly hydroxyl groups (Strouse et al., 1977). Optimal fits to nearly all sample spectra required small contributions from catechol and EDTA. In SRHA$_{red}$ + Fe(II) and SRNOM$_{red}$ + Fe(II) at pH 4, nearly 20% of the Fe exists as hydrated Fe(II), which may represent solvation complexes or outer-sphere complexes, as these are likely indistinguishable. Fe(III)-organic reference complexes (i.e., citrate + Fe(III) or catechol + Fe(III)) were fit, to varying degrees (5-25%), to every sample except SRNOM$_{red}$ + Fe(II) at pH 4.

Though nitrogen- and sulfur-containing organic compounds generally have a higher affinity for Fe(II) than oxygen-containing groups (Harris, 2005), they represent a small proportion of the NOM types studied (0.5 – 2% by weight), and LCF analysis did not reveal any contributions from amine-only or thiol ligands (as determined from ethylenediamine + Fe(II) and mercaptoethanol + Fe(II) references). Bipyridine-like and EDTA-like functional groups, both of which contain nitrogen, were found to complex 5-20% of the Fe (as Fe(II)) in $SRFA_{red}$ + Fe(II), $SRNOM_{red}$ +Fe (II), LHA_{red} + Fe(II), and LHA_{red}. Consistent with the WT analyses, LCF results indicate the absence of significant quantities of polymeric Fe in the reduced NOM samples.

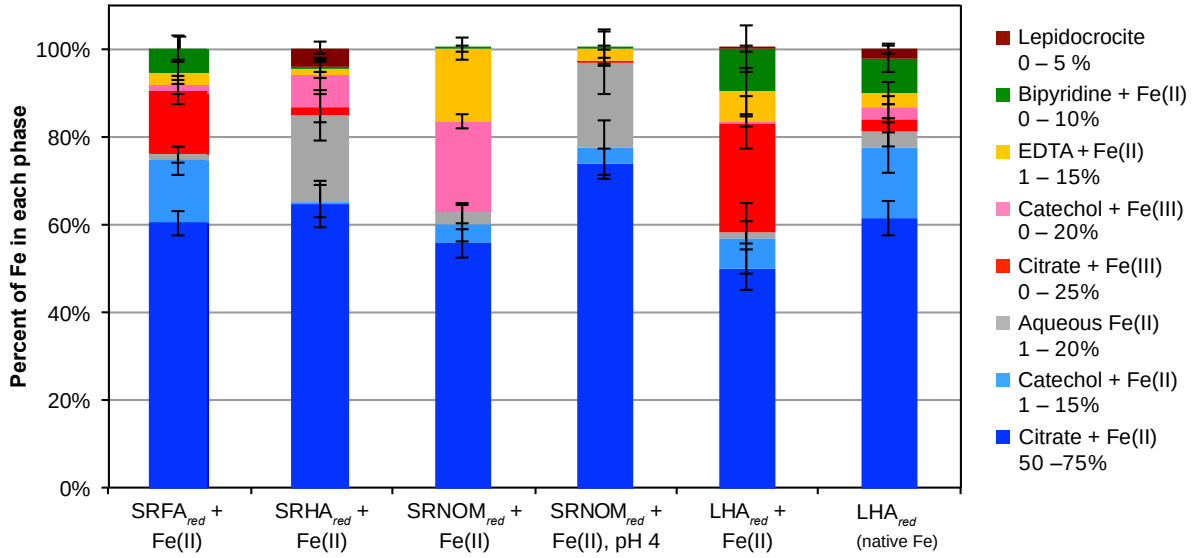

Figure 2.3 Weights of Fe references in linear combination fits of k^3-weighted Fe EXAFS for Fe in reduced NOM complexes (pH 7 unless indicated otherwise). Values shown are the averages of the top 10 combinatorial fits, and error bars represent the standard deviations or the average of the errors given by the fit, whichever is larger. Percentages shown under each legend heading represent the range of that reference present in all the samples.

2.3.2 Fe(II) oxidation experiments

To observe the effect of Fe–NOM complexation on iron redox speciation during oxidation by O_2, we exposed a pH 7 buffered anoxic solution of LHA_{red} + Fe(II) to atmospheric and dissolved O_2 for over three hours. The extent of Fe(II) oxidation decreased substantially in the presence of LHA_{red} compared to a NOM-free control (Figure 2.4). While total oxidation of Fe(II) without LHA_{red}

occurred within about 110 minutes, over 50% of the Fe(II) associated with LHA_{red} remained reduced after four hours of exposure to O_2. Fe(II) assays performed on samples stored in the dark for 30 minutes had approximately a third higher Fe(II) concentrations than those performed immediately following sampling, suggesting that some of the Fe(III) formed through the reaction of Fe(II) and O_2 was re-reduced once open air was excluded via capping. The remaining sample was analyzed for Fe(II) the subsequent day, but no residual Fe(II) was detectable at that point. The exposure of LHA_{red} to O_2 generated hydrogen peroxide (H_2O_2), indicating O_2 directly reacted with redox-active moieties (Figure A.9). In the presence of Fe(II), the measured levels of H_2O_2 were suppressed.

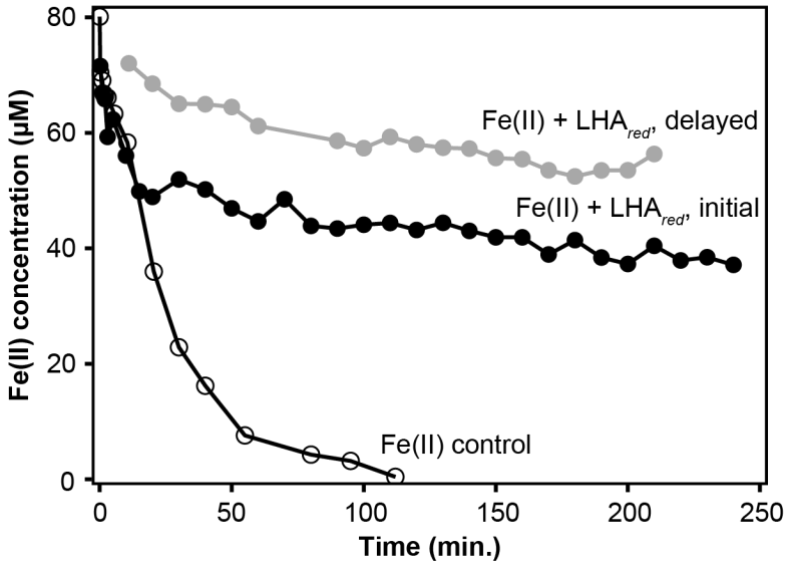

Figure 2.4 Experimental data from Fe(II) oxidation experiments with 67 μM Fe(II), 0.17 mg/mL LHA_{red}, and 4.16 mM PIPES and Fe(II) control data (80 μM Fe(II), 4.16 mM PIPES). The "Fe(II) + LHA_{red}, initial" measurements were made on aliquots immediately after the addition of a dye (2,2'-bipyridine), a colorimetric assay for iron(II), while the "Fe(II) + LHA_{red}, delayed" measurements were made 30 or more minutes after addition of the dye and storage in the dark.

2.4 Discussion

Complexation with organic matter has often been proposed to alter the rate of Fe(II) oxidation—potentially leading to long-term preservation of Fe(II) in oxic circumneutral environments—yet little research has been dedicated to understanding Fe(II)-OM complexation. In this study, we investigated Fe(II) complexation with organic matter using Fe K-edge spectroscopy and determined the impact of reduced organic matter on Fe(II) oxidation.

2.4.1 Oxidation of Fe(II) by as-received LHA

Due to published observations of humic substances reducing Fe(III) (Chen et al., 2003; Bauer and Kappler, 2009) and preserving added Fe(II) (Catrouillet et al., 2014), we expected Fe(II) to remain reduced when added to as-received NOM in anoxic water. Instead, we observed overwhelming oxidation of Fe(II) when added to LHA at pH 7 (Figure A.3). Based on electrochemical studies performed by Aeschbacher *et al.* (2011), a small proportion (~8%) of the reducible moieties in LHA have standard reduction potentials greater than that for the $Fe(OH)_3$/Fe(II) redox couple (0.062 V). At the low Fe:LHA ratio present in the samples, these groups outnumber the amount of added Fe(II) and are likely responsible for oxidation of added Fe(II). Although the identities of these functional groups are unknown, they could include semiquinone radicals, which have been shown to oxidize As(III) under anoxic conditions and were proposed to oxidize Fe(II) following irradiation of SRFA (Jiang et al., 2009; Garg et al., 2015). As a result of Fe(II) oxidation in the presence of as-received NOM, we chose to investigate Fe(II)-NOM complexation using chemically reduced NOM.

2.4.2 Fe(II)-NOM complexation

We expected complexation between Fe(II) and N- and S-containing functional groups to predominate because some of the strongest Fe(II) ligands contain N or S (Harris, 2005), and moles of organic N and S are 1-2 orders of magnitude greater than moles of added Fe(II) in the samples (Chemical Properties of IHSS Samples). However, EXAFS fitting results show that these two elements have low or no representation in the formed Fe(II)-NOM complexes. Instead, approximately 75 – 100% of Fe(II) added to reduced organic matter remained reduced and formed mononuclear oxygen-containing complexes (Figure 2.2 and Figure 2.3). Citrate, which complexes Fe(II) through carboxyl and hydroxyl functional groups (Strouse et al., 1977), better represents the predominant type of complexing ligand than any other reference used, as determined from LCF analysis of the Fe K-edge EXAFS (Figure 2.3). This result generally supports the equilibrium modeling approach used by

Catrouillet *et al.* (2014), which indicated that Fe(II) added to LHA was primarily bound in bidentate complexes with carboxyl groups at acidic to neutral pH. Hence, Fe(II) binding to NOM appears largely analogous to Fe(III)-NOM complexes, but weaker, as indicated by Fe(II) complexation kinetics studies (Rose and Waite, 2003). EXAFS studies of NOM bound to ferric iron indicated mononuclear, bidentate coordination of Fe(III) with oxygen or nitrogen and specific coordination with carboxylate functional groups (Gustafsson et al., 2007; van Schaik et al., 2008; Karlsson et al., 2008; Karlsson and Persson, 2010; Karlsson and Persson, 2012). Since citrate has been shown to accelerate Fe(II) oxidation (Theis and Singer, 1974; Pham and Waite, 2008; Jones et al., 2015), this type of complexation is unlikely to preserve Fe(II) in oxic environments.

While our results support the assertion that the majority of Fe(II) is complexed to carboxyl groups at neutral pH, this type of interaction does not explain the full complexity and extent of Fe(II)-NOM interactions (Figure 2.3). Though contributions from the remaining ligands are less definite than that of citrate; catechol-, EDTA-, and bipyridine-like complexation may account for up to 30% of the Fe in these Fe(II)-NOM mixtures. Catechol and EDTA also form more stable complexes with Fe(III) than Fe(II) (Harris, 2005), so complexation with ligands similar to these may be unlikely to preserve Fe(II). However, phenols like catechol are potentially redox-active moieties in NOM capable of reducing, or preventing the net oxidation of, associated Fe. Phenols and polyphenols may therefore contribute to Fe(II) preservation, as has been shown with tannic acid, a polyphenol, which preserved Fe(II) for over 100 hours in the presence of oxygen (Theis and Singer, 1974). Complexation with pyridinic functional groups as found in 2,2'-bipyridine and 1,10-phenanthroline could potentially prevent oxidation of Fe(II) because tris complexes with these ligands thermodynamically stabilize Fe(II) over Fe(III) (Rizvi et al., 2011; Rizvi, 2015). Pyridinic nitrogen represents a very low proportion of functional groups in NOM—elemental N is only 1% of NOM by weight and only 20-35% of that is pyridinic N (Chemical Properties of IHSS Samples; Vairavamurthy and Wang, 2002). Therefore, the

likelihood of three pyridinic functional groups coming together to bind with Fe(II) and form a tris complex is low.

It remains unclear why Fe(II) is not bound to high-affinity N and S sites at the expected levels. At pH 7, deprotonated carboxyl groups greatly outnumber N, S, and added Fe(II) for the NOM investigated, so their relatively high abundance may account for the prevalence of Fe(II)-carboxyl complexation (Ritchie and Perdue, 2003). Another possible explanation is that complexation with these functional groups occurs at a slower rate, with carboxyl groups complexing Fe(II) more rapidly. Over longer periods, Fe(II) may exchange to lower abundance, higher affinity functional groups, such as N- or S-containing moieties. Such complexation may promote long-term stabilization of Fe(II). Longer-term equilibration studies will be required to determine whether Fe(II) exchanges to lower abundance functional groups and if so, whether these complexes inhibit Fe(II) oxidation.

These results differ from the few published studies that investigated Fe(II)-NOM interactions at the molecular level, none of which targeted Fe(II) complexation using Fe K-edge EXAFS spectroscopy. Toner *et al.* (2009) used scanning transmission X-ray microscopy (STXM) to map the distribution of Fe(II) and different types of carbon in particles collected from a sulfide-rich hydrothermal plume. Based on their results and published stability constant data, the authors suggested organo-sulfur compounds were responsible for preserving Fe(II) after exposure to oxygen. In contrast, the NOM types used in this study do not come from sulfur-rich environments, and therefore have low percentages of sulfur (Chemical Properties of IHSS Samples). Fe(II)-thiol complexation was consistently excluded from the samples by linear combination fits based on the use of a Fe(II)-mercaptoethanol reference. In another recent study, von der Heyden *et al.* (2014) concluded that Fe(II)-containing particles from marine and lacustrine samples were more likely to have alcohol, carboxamide, and/or carbonate C than Fe(III)-containing particles. In contrast to the work presented here, both prior studies show only a correlation between the presence of Fe(II) and certain types of

organic matter—they do not directly probe the coordination environment of Fe(II)-organic complexes.

Differences in NOM source and type were expected to influence Fe(II) complexation, however, the data from this study show that they have small and unpredictable effects. The NOM samples chosen for this study exhibit substantial chemical variation. SRFA has a higher oxygen content, and is more aliphatic and monosaccharide-rich while LHA is highly aromatic and has a lower acidity (Chemical Properties of IHSS Samples; Thorn et al., 1989). Consistent with the higher carboxylic and phenolic acidity of SRFA, added Fe(II) forms complexes with more citrate- and catechol-like groups in $SRFA_{red}$ than LHA_{red} (Figure 2.3). This correlation with chemical characteristics does not appear to hold true for the native Fe(II) in LHA_{red}, which is complexed by citrate- and catechol-like groups in approximately equal proportion to Fe(II) added to $SRFA_{red}$.

Since NOM and Fe can be protonated and hydroxylated, respectively, pH has a substantial impact on Fe–NOM complexation. LCF analysis of Fe(II) + $SRNOM_{red}$ at pH 4 and 7 demonstrates that higher solution acidity promotes the preservation of Fe(II) over Fe(III) but also limits organic complexation (Figure 2.3). At low pH, the oxidation of Fe(II) is slower (Millero et al., 1987) and Fe(II) is thermodynamically favored at a wider range of Eh values (Hem and Cropper, 1962). At pH 4, more carboxyl groups are protonated than at pH 7, so there are fewer available binding sites, leading to a higher proportion of hydrated Fe (fit by "aqueous Fe(II)"). These results are consistent with the findings of Catrouillet *et al.* (2014), which showed a decreasing proportion of LHA-bound Fe(II) with decreasing pH from 8 to 3.

2.4.3 Effect of LHA_{red} on Fe(II) oxidation

During oxidation by O_2, reduced NOM maintained a steady-state concentration of Fe(II) over the course of several hours through what appears to be a redox buffering mechanism (Figure 2.4). During this process, LHA_{red} was oxidized—a reaction likely catalyzed by native Fe or semiquinones

(Roginsky and Barsukova, 2000; Jiang et al., 2015)—resulting in the net production of LHA_{ox} and H_2O_2 (Figure A.9).

$$LHA_{red} + O_2 \rightarrow LHA_{ox} + H_2O_2 \quad (2.1)$$

Along with O_2, H_2O_2 can oxidize Fe(II) in a Fenton-like reaction to form Fe(III)–LHA, OH^- and $OH^\bullet$. The occurrence of this reaction is supported by the suppression of the H_2O_2 concentration in the Fe(II)-LHA_{red} sample (Figure A.9).

$$O_2 + Fe^{(II)}LHA \rightleftharpoons O_2^{\bullet-} + Fe^{(III)}LHA \quad (2.2)$$

$$H_2O_2 + Fe^{(II)}LHA \rightarrow OH^- + OH^\bullet + Fe^{(III)}LHA \quad (2.3)$$

Delayed Fe(II) measurements showed a ~34% increase in Fe(II) concentration when aliquots of the reaction mixture were stored in airtight containers for over 30 minutes prior to Fe(II) measurement (Figure 2.4), suggesting LHA_{red} re-reduced newly-formed Fe(III). This explanation is supported by the results of Bauer and Kappler (2009), who observed humic substances reducing Fe(III), even as they were being oxidized by O_2. Superoxide ($O_2^{\bullet-}$) has been shown to reduce Fe(III)-NOM complexes (Rose and Waite, 2005) and may also contribute to re-reduction of Fe(III).

$$LHA_{red} + Fe^{(III)}LHA \rightarrow LHA_{ox} + Fe^{(II)}LHA \quad (2.4)$$

This redox buffering process may explain the persistence of 50% of the initial Fe(II) after four hours under oxic conditions. Calculations based on measurements of the Fe(III)-reducing capacity of LHA_{red} (Figure A.10) demonstrate that LHA in this system can reduce the total concentration of Fe about 1.6 times. A proposed scheme in Figure 2.5 summarizes the key reactions supported by my findings.

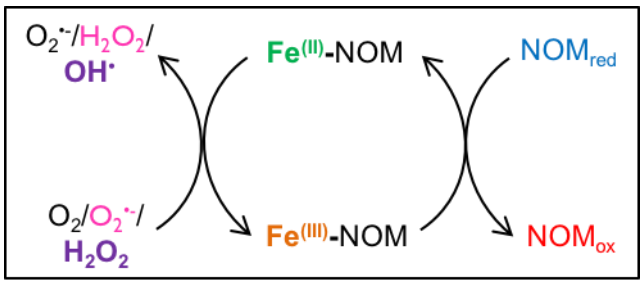

Figure 2.5 Simplified proposed reaction scheme showing Fe redox cycling in the presence of reduced organic matter and oxygen.

Though it is evident that reducing groups in LHA_{red} contribute to the prolonged existence of Fe(II) under oxic conditions, the identities of these groups—in this system—remain unclear. Quinones are responsible for much of the redox behavior of NOM, and our results bear similarities to observations of coupled Fe-quinone cycling. Hydroquinones, which form during reduction via hydrogenation (Ratasuk and Nanny, 2007), can rapidly reduce Fe(III) to Fe(II), outcompeting re-oxidation of Fe(II) to Fe(III) by molecular oxygen or reactive oxygen species (Yuan et al., 2016). Natural organic matter itself appears to be even more adept at cycling Fe than individual quinones. For instance, results published by Jiang *et al.* (2015) show SRFA cycling Fe at rates 10-100 times faster than 1,4-hydroquinone at pH 4. However, our NOM reduction method using H_2-Pd/Al_2O_3 at pH 7 is similar to the one used by Ratasuk and Nanny (2007), which they claimed removed quinone groups via hydrogenolysis. They concluded that the redox active groups responsible for electron transfer under this reduction treatment must be non-quinone moieties, such as thiols and nitrogen functional groups. Therefore, further work is necessary to identify the reducing groups active under the conditions used in this study. In addition, the extent to which Fe(II) complexation affects the Fe(II) oxidation rate and steady-state concentration is not easily discernable and requires further investigation.

2.5 Environmental Implications

The findings from this work clarify important roles of NOM in Fe(II) speciation and Fe redox cycling. Under circumneutral reducing conditions, NOM readily binds low concentrations of Fe(II), primarily forming mononuclear complexes with citrate-like groups. Although additional complexation modes are also identified, for these experiments, the distribution of complexing ligands appears to be determined mostly by abundance rather than expected affinities. The observed Fe(II)-NOM complexes are likely important forms of bioavailable Fe(II) for microorganisms, thereby influencing Fe cycling and primary productivity.

None of the principal ligands observed for Fe(II) are known to thermodynamically stabilize the reduced state. However, the addition of O_2 to Fe(II)–NOM mixtures initiates a dynamic redox cycle that sustains a steady state concentration of Fe(II) for several hours longer than Fe(II) without NOM. Although the redox buffering mechanism does not explain the long-term stabilization of Fe(II), it is likely to occur in the surface waters of streams, lakes, and oceans subjected to diurnal photoredox cycles and in domains of soils and sediments subjected to cycles in microbial metabolisms capable of reducing NOM (Lovley et al., 1996; Voelker et al., 1997; Lovley et al., 1998).

The experimental conditions used in this study were chosen to facilitate the identification of Fe(II)-NOM complexes using XAS spectroscopy and do not represent the full range of possible environmental conditions. Competition from other divalent cations, such as Ca^{2+}, a higher Fe:NOM ratio in some environments, and the presence of unreduced NOM will limit the iron complexation and redox buffering capabilities of NOM. Additional work will be required to confirm that the Fe(II)–NOM interactions observed in these laboratory studies are reproduced in naturally reduced soils and sediments.

REFERENCES

Aeschbacher M., Vergari D., Schwarzenbach R. P. and Sander M. (2011) Electrochemical analysis of proton and electron transfer equilibria of the reducible moieties in humic acids. *Environ. Sci. Technol.* **45**, 8385–8394.

Anon. Chemical Properties of IHSS Samples. *Int. Humic Subst. Soc.*

Barbeau K., Rue E. L., Bruland K. W. and Butler A. (2001) Photochemical cycling of iron in the surface ocean mediated by microbial iron(III)-binding ligands. *Nature* **413**, 409–413.

Bauer I. and Kappler A. (2009) Rates and extent of reduction of Fe(III) compounds and O2 by humic substances. *Environ. Sci. Technol.* **43**, 4902–4908.

Bligh M. W. and Waite T. D. (2010) Role of heterogeneous precipitation in determining the nature of products formed on oxidation of Fe(II) in seawater containing natural organic matter. *Environ. Sci. Technol.* **44**, 6667–6673.

Boyd P. W., Jickells T., Law C. S., Blain S., Boyle E. A., Buesseler K. O., Coale K. H., Cullen J. J., de Baar H. J. W., Follows M., Harvey M., Lancelot C., Levasseur M., Owens N. P. J., Pollard R., Rivkin R. B., Sarmiento J., Schoemann V., Smetacek V., Takeda S., Tsuda A., Turner S. and Watson A. J. (2007) Mesoscale iron enrichment experiments 1993-2005: Synthesis and future directions. *Science (80-.).* **315**, 612–7.

Catrouillet C., Davranche M., Dia A., Bouhnik-Le Coz M., Marsac R., Pourret O. and Gruau G. (2014) Geochemical modeling of Fe(II) binding to humic and fulvic acids. *Chem. Geol.* **372**, 109–118.

Chen J., Gu B., Royer R. A. and Burgos W. D. (2003) The roles of natural organic matter in chemical and microbial reduction of ferric iron. *Sci. Total Environ.* **307**, 167–78.

Craig P. S., Shaw T. J., Miller P. L., Pellechia P. J. and Ferry J. L. (2009) Use of multiparametric

techniques to quantify the effects of naturally occurring ligands on the kinetics of Fe(II) oxidation. *Environ. Sci. Technol.* **43**, 337–42.

Davison W. and Seed G. (1983) The kinetics of the oxidation of ferrous iron in synthetic and natural waters. *Geochim. Cosmochim. Acta* **47**, 67–79.

Emmenegger L., King D. W., Sigg L. and Sulzberger B. (1998) Oxidation Kinetics of Fe(II) in a Eutrophic Swiss Lake. *Environ. Sci. Technol.* **32**, 2990–2996.

Funke H., Scheinost A. and Chukalina M. (2005) Wavelet analysis of extended x-ray absorption fine structure data. *Phys. Rev. B* **71**, 094110.

Garg S., Jiang C. and Waite T. D. (2015) Mechanistic insights into iron redox transformations in the presence of natural organic matter: Impact of pH and light. *Geochim. Cosmochim. Acta* **165**, 14–34.

Gustafsson J. P., Persson I., Kleja D. B. and Van Schaik J. W. J. (2007) Binding of iron(III) to organic soils: EXAFS spectroscopy and chemical equilibrium modeling. *Environ. Sci. Technol.* **41**, 1232–7.

Harris W. R. (2005) Iron Chemistry. In *Molecular and Cellular Iron Transport* (ed. D. M. Templeton). Marcel Dekker, Inc., New York. pp. 1–40.

Hem J. D. and Cropper W. H. (1962) *Survey of ferrous-ferric chemcial equilibria and redox potentials.*, Washington.

von der Heyden B. P., Hauser E. J., Mishra B., Martinez G. A., Bowie A. R., Tyliszczak T., Mtshali T. N., Roychoudhury A. N. and Myneni S. C. B. (2014) Ubiquitous Presence of Fe(II) in Aquatic Colloids and Its Association with Organic Carbon. *Environ. Sci. Technol. Lett.* **1**, 387–392.

von der Heyden B. P., Roychoudhury A. N., Mtshali T. N., Tyliszczak T. and Myneni S. C. B. (2012) Chemically and geographically distinct solid-phase iron pools in the Southern Ocean. *Science*

(80-.). **338**, 1199–201.

Jiang C., Garg S. and Waite T. D. (2015) Hydroquinone-Mediated Redox Cycling of Iron and Concomitant Oxidation of Hydroquinone in Oxic Waters under Acidic Conditions: Comparison with Iron–Natural Organic Matter Interactions. *Environ. Sci. Technol.* **49**, 14076–14084.

Jiang J., Bauer I., Paul A. and Kappler A. (2009) Arsenic redox changes by microbially and chemically formed semiquinone radicals and hydroquinones in a humic substance model quinone. *Environ. Sci. Technol.* **43**, 3639–3645.

Jobin R. and Ghosh M. M. (1972) Effect of buffer intensity and organic matter on the oxygenation of ferrous iron. *J. Am. Water Works Assoc.* **64**, 590–595.

Jones A. M., Griffin P. J. and Waite T. D. (2015) Ferrous iron oxidation by molecular oxygen under acidic conditions: The effect of citrate, EDTA and fulvic acid. *Geochim. Cosmochim. Acta* **160**, 117–131.

Karlsson T. and Persson P. (2012) Complexes with aquatic organic matter suppress hydrolysis and precipitation of Fe(III). *Chem. Geol.* **322–323**, 19–27.

Karlsson T. and Persson P. (2010) Coordination chemistry and hydrolysis of Fe(III) in a peat humic acid studied by X-ray absorption spectroscopy. *Geochim. Cosmochim. Acta* **74**, 30–40.

Karlsson T., Persson P., Skyllberg U., Mörth C.-M. and Giesler R. (2008) Characterization of iron(III) in organic soils using extended X-ray absorption fine structure spectroscopy. *Environ. Sci. Technol.* **42**, 5449–54.

Klüpfel L., Piepenbrock A., Kappler A. and Sander M. (2014) Humic substances as fully regenerable electron acceptors in recurrently anoxic environments. *Nat. Geosci.* **7**, 195–200.

Lovley D. R., Coates J. D., Blunt-Harris E. L., Phillips E. J. P. and Woodward J. C. (1996) Humic substances as electron acceptors for microbial respiration. *Nature* **382**, 445–448.

Lovley D. R., Fraga J. L., Blunt-Harris E. L., Hayes L. A., Phillips E. J. P. and Coates J. D. (1998) Humic Substances as a Mediator for Microbially Catalyzed Metal Reduction. *Acta Hydrochim. Hydrobiol.* **26**, 152–157.

Lundberg D., Ullstrom A.-S., D'Angelo P. and Persson I. (2007) A structural study of the hydrated and the dimethylsulfoxide, N,N'-dimethylpropyleneurea, and N,N -dimethylthioformamide solvated iron(II) and iron(III) ions in solution and solid state. *Inorganica Chim. Acta* **360**, 1809–1818.

Melton E. D., Swanner E. D., Behrens S., Schmidt C. and Kappler A. (2014) The interplay of microbially mediated and abiotic reactions in the biogeochemical Fe cycle. *Nat. Rev. Microbiol.* **12**, 797–809.

Mikutta C. and Kretzschmar R. (2011) Spectroscopic evidence for ternary complex formation between arsenate and ferric iron complexes of humic substances. *Environ. Sci. Technol.* **45**, 9550–9557.

Millero F. J., Sotolongo S. and Izaguirre M. (1987) The oxidation kinetics of Fe(II) in seawater. *Geochim. Cosmochim. Acta* **51**, 793–801.

Moss M. L. and Mellon M. G. (1942) Colorimetric Determination of Iron with 2,2'-Bipyridyl and with 2,2',2'-Terpyridyl. *Ind. Eng. Chem. Anal. Ed.* **14**, 862–865.

Pham A. N. and Waite T. D. (2008a) Modeling the kinetics of Fe(II) oxidation in the presence of citrate and salicylate in aqueous solutions at pH 6.0-8.0 and 25 degrees C. *J. Phys. Chem. A* **112**, 5395–405.

Pham A. N. and Waite T. D. (2008b) Oxygenation of Fe(II) in the Presence of Citrate in Aqueous Solutions at pH 6.0−8.0 and 25 °C: Interpretation from an Fe(II)/Citrate Speciation Perspective. *J. Phys. Chem. A* **112**, 643–651.

Pullin M. J. and Cabaniss S. E. (2003) The effects of pH, ionic strength, and iron–fulvic acid

interactions on the kinetics of non-photochemical iron transformations. I. Iron(II) oxidation and iron(III) colloid formation. *Geochim. Cosmochim. Acta* **67**, 4067–4077.

Ratasuk N. and Nanny M. A. (2007) Characterization and quantification of reversible redox sites in humic substances. *Environ. Sci. Technol.* **41**, 7844–50.

Ravel B. and Newville M. (2005) ATHENA, ARTEMIS, HEPHAESTUS: data analysis for X-ray absorption spectroscopy using IFEFFIT. *J. Synchrotron Radiat.* **12**, 537–41.

Ritchie J. D. and Perdue M. E. (2003) Proton-binding study of standard and reference fulvic acids, humic acids, and natural organic matter. *Geochim. Cosmochim. Acta* **67**, 85–93.

Rizvi M. A. (2015) Complexation modulated redox behavior of transition metal systems (review). *Russ. J. Gen. Chem.* **85**, 959–973.

Rizvi M. A., Syed R. M. and Khan B. (2011) Complexation effect on redox potential of Iron(III) - Iron(II) couple: A simple potentiometric experiment. *J. Chem. Educ.* **88**, 220–222.

Roginsky V. and Barsukova T. (2000) Kinetics of oxidation of hydroquinones by molecular oxygen. Effect of superoxide dismutase. *J. Chem. Soc. Perkin Trans. 2*, 1575–1582.

Rose A. L. and Waite T. D. (2003a) Effect of dissolved natural organic matter on the kinetics of ferrous iron oxygenation in seawater. *Environ. Sci. Technol.* **37**, 4877–4886.

Rose A. L. and Waite T. D. (2002) Kinetic model for Fe(II) oxidation in seawater in the absence and presence of natural organic matter. *Environ. Sci. Technol.* **36**, 433–44.

Rose A. L. and Waite T. D. (2003b) Kinetics of iron complexation by dissolved natural organic matter in coastal waters. *Mar. Chem.* **84**, 85–103.

Rose A. L. and Waite T. D. (2005) Reduction of organically complexed ferric iron by superoxide in a simulated natural water. *Environ. Sci. Technol.* **39**, 2645–2650.

Rue E. L. and Bruland K. W. (1995) Complexation of iron(III) by natural organic ligands in the Central North Pacific as determined by a new competitive ligand equilibration/adsorptive

cathodic stripping voltammetric method. *Mar. Chem.* **50**, 117–138.

Saines P. J., Yeung H. H.-M., Hester J. R., Lennie A. R. and Cheetham A. K. (2011) Detailed investigations of phase transitions and magnetic structure in Fe(III), Mn(II), Co(II) and Ni(II) 3,4,5-trihydroxybenzoate (gallate) dihydrates by neutron and X-ray diffraction. *Dalt. Trans.* **40**, 6401–10.

Santana-Casiano J. M., González-Dávila M. and Millero F. J. (2005) Oxidation of nanomolar levels of Fe(II) with oxygen in natural waters. *Environ. Sci. Technol.* **39**, 2073–9.

Santana-Casiano J. M., González-Dávila M., Rodríguez M. J. and Millero F. J. (2000) The effect of organic compounds in the oxidation kinetics of Fe(II). *Mar. Chem.* **70**, 211–222.

van Schaik J. W. J., Persson I., Kleja D. B. and Gustafsson J. P. (2008) EXAFS study on the reactions between iron and fulvic acid in acid aqueous solutions. *Environ. Sci. Technol.* **42**, 2367–73.

Sjöstedt C., Persson I., Hesterberg D., Kleja D. B., Borg H. and Gustafsson J. P. (2013) Iron speciation in soft-water lakes and soils as determined by EXAFS spectroscopy and geochemical modelling. *Geochim. Cosmochim. Acta* **105**, 172–186.

Strouse J., Layten S. W. and Strouse C. E. (1977) Structural Studies of Transition Metal Complexes of Triionized and Tetraionized Citrate. Models for the Coordination of the Citrate Ion to Transition Metal Ions in Solution and at the Active Site of Aconitase. *J. Am. Chem. Soc.* **99**, 562–72.

Sundman A., Karlsson T., Laudon H. and Persson P. (2014) XAS study of iron speciation in soils and waters from a boreal catchment. *Chem. Geol.* **364**, 93–102.

Theis T. L. and Singer P. C. (1974) Complexation of iron(II) by organic matter and its effect on iron(II) oxidation. *Environ. Sci. Technol.* **8**, 569–573.

Thorn K. A., Folan D. W. and MacCarthy P. (1989) *Characterization of the International Humic Substances*

Society Standard and Reference Fulvic and Humic Acids by Solution State Carbon-13 (13C) and Hydrogen-1 (1H) Nuclear Magnetic Resonance Spectrometry., Denver, CO.

Toner B. M., Fakra S. C., Manganini S. J., Santelli C. M., Marcus M. A., Moffett J. W., Rouxel O., German C. R. and Edwards K. J. (2009) Preservation of iron(II) by carbon-rich matrices in a hydrothermal plume. *Nat. Geosci.* **2**, 197–201.

Vairavamurthy A. and Wang S. (2002) Organic nitrogen in geomacromolecules: Insights on speciation and transformation with K-edge XANES spectroscopy. *Environ. Sci. Technol.* **36**, 3050–3056.

Voelker B. M., Morel F. M. M. and Sulzberger B. (1997) Iron Redox Cycling in Surface Waters: Effects of Humic Substances and Light. *Environ. Sci. Technol.* **31**, 1004–1011.

Webb S. M. (2005) SIXPack: A Graphical User Interface for XAS Analysis Using IFEFFIT. *Phys. Scr.* **T115**, 1011–1014.

Weber K. A., Achenbach L. A. and Coates J. D. (2006) Microorganisms pumping iron: anaerobic microbial iron oxidation and reduction. *Nat. Rev. Microbiol.* **4**, 752–64.

Yamamoto M., Nishida A., Otsuka K., Komai T. and Fukushima M. (2010) Evaluation of the binding of iron(II) to humic substances derived from a compost sample by a colorimetric method using ferrozine. *Bioresour. Technol.* **101**, 4456–4460.

Yang X., Li J., Zhao X.-H., Wang H.-W. and Shan Y.-K. (2007) Hydrogen bonding and π-π stacking in the three-dimensional supramolecular complex bis(4,4'-bipyridinium) diaquadioxalatoferrate(II) bis(hydrogen oxalate). *Acta Crystallogr. C.* **63**, m171-3.

Yu Q., Kandegedara A., Xu Y. and Rorabacher D. B. (1997) Avoiding Interferences from Good's Buffers: A Contiguous Series of Noncomplexing Tertiary Amine Buffers Covering the Entire Range of pH 3–11. *Anal. Biochem.* **253**, 50–56.

Yuan X., Davis J. A. and Nico P. S. (2016) Iron-mediated oxidation of methoxyhydroquinone under dark conditions: kinetic and mechanistic insights. *Environ. Sci. Technol.* **50**, 1731–1740.

CHAPTER 3: TEMPERATURE EFFECTS ON SORPTION OF DISSOLVED ORGANIC MATTER ON FERRIHYDRITE UNDER DYNAMIC FLOW AND BATCH CONDITIONS

3.1 Introduction

The earth's soils store almost 3000 Pg of carbon (C), with most in the form of soil organic carbon (SOC) (Jobbágy and Jackson, 2000; Amundson, 2001; Scharlemann et al., 2014; Köchy et al., 2015). Carbon turnover times, ranging from weeks to millennia, depend in part on SOC biochemical composition, but also on environmental conditions and interactions with mineral phases (Schimel et al., 1994; Torn et al., 1997; Kaiser and Guggenberger, 2000; Mikutta et al., 2006). The complex heterogeneity of soil organic matter (SOM), minerals, vegetation, microbial communities, and soil solution environments hinder our understanding of the interactions governing C stabilization and the impact changing climatic conditions will have on them (Schmidt et al., 2011). A substantial body of literature is devoted to answering the question of how SOC responds to warming, yielding conflicting results, from increased to unaffected to decreased respiration rates (Carey et al., 2016; Pries et al., 2017). The confounding results from macroscale experiments have prompted efforts focusing on the individual constituents of soil systems to discern mechanisms controlling C preservation. While numerous studies have targeted the response of microbial respiration rates to warming (Allison et al., 2010; Carey et al., 2016; Melillo et al., 2017), the temperature effect on mineral-stabilized SOC remains an important outstanding question.

Though the abiotic response may be small in comparison to the biological response (Marschner and Bredow, 2002), respiration rates depend on carbon substrate availability, which in turn is determined by multiple temperature-sensitive factors (Conant et al., 2011). In studies of soil systems, DOM sorption responses to temperature have varied from weakly positive to negative (Jardine et al., 1989; Vance and David, 1992; Kaiser et al., 2001). In such complex and non-sterile

systems, isolation of the mechanisms controlling temperature response is extremely difficult. Baham and Sposito (1994) and Arnarson and Keil (2000) took greater pains to isolate the abiotic temperature response of mineral sorption by filter-sterilizing DOM and using montmorillonite and kaolinite clays. They reported no dependence on temperature from 10 to 35 °C and decreasing sorption with temperature from 3.5 to 21.5 °C, respectively. At low pH, sorption of DOM on the crystalline iron oxide hematite was found to be highly exothermic (Gu et al., 1994), suggesting an increase in temperature would lead to decreased sorption. With high surface area and reactivity, short-range order (SRO) hydrous aluminum and iron oxides contribute substantially—likely more than clays—to SOC stabilization (Kaiser et al., 2007; Wagai and Mayer, 2007; Trumbore, 2009; Mikutta and Kaiser, 2011; Rasmussen et al., 2018). However, to my knowledge, temperature responses of DOM sorption to these important minerals remain uncharacterized.

Hydrous iron oxides such as goethite, lepidocrocite, and ferrihydrite are widely present in soils and reactive towards organic materials (Tipping, 1981; Cornell and Schwertmann, 2003; Kaiser and Guggenberger, 2007). Generally, iron oxides preferentially sorb aromatic, hydrophobic, and carboxylic-rich organic fractions, though some studies also indicate specificity towards aliphatic nitrogen-containing compounds (McKnight et al., 1992; Gu et al., 1994; Gu et al., 1995; Kaiser, 2003; Eusterhues et al., 2011; Chassé et al., 2015; Lv et al., 2016; Coward et al., 2018). Aromatic moieties may associate with the surface via hydrogen bonding of phenolic groups, and with either the surface or previously adsorbed organic material through van der Waals interactions or hydrophobic partitioning (Means et al., 1980; Filius et al., 2000). Carboxylic groups can exchange with hydroxide ligands or associate through cation bridging or electrostatic attraction, depending on solution pH (Gu et al., 1994; Filius et al., 2000; Newcomb et al., 2017). Aliphatic N-containing compounds, such as amino acids, can also form strong associations via ligand exchange (Newcomb et al., 2017).

Each of these interactions is characterized by thermodynamic and kinetic parameters that determine the influence of temperature on sorption. Most are exothermic and spontaneous, such that sorption should decrease with increasing temperatures (ten Hulscher and Cornelissen, 1996; Pignatello, 1999; Moreno-Castilla, 2004; Conant et al., 2011). Ligand exchange interactions are particularly strong, corresponding to high heats of adsorption (Gu et al., 1994). Therefore, they should be especially sensitive to changes in temperature compared to weaker H-bonding, van der Waals, and electrostatic interactions (Conant et al., 2011). Hydrophobic partitioning interactions are likely entropically favored because the process requires the hydrophobic molecule to partially or completely shed the ordered hydration shell and create disorder at the mineral surface or in the organic matrix (ten Hulscher and Cornelissen, 1996; Pignatello, 1999). The greater entropic contribution to these interactions may lead to more variable responses to temperature, including increased sorption with temperature, as suggested by Jardine et al. (1989).

Depending on flow conditions near the mineral surface, temperature may also have a meaningful influence on sorption kinetics, as has been suggested by Thornley and Cannell (2001). The ligand exchange mechanism may include orbital rehybridization and ligand displacement, likely making its activation energy quite large (McBride, 1994; Pignatello, 1999). Weaker H-bonding, polar attraction, and van der Waals interactions have much lower activation energies associated with the reorganization of water molecules around the organic compound and mineral surface (Pignatello, 1999). They may be assumed to reach equilibrium rapidly—in less than an hour. In addition to surface interactions, small molecules can diffuse into mineral pores or "holes" in the organic matrix, a slow process quite sensitive to temperature (Cornelissen et al., 1997). The overall effect of temperature changes on the quantity, quality, and stability of mineral-adsorbed organic matter is likely a combination of these thermodynamic and kinetic factors, as well as solution conditions such as pH and ionic composition and strength.

To determine the effect of temperature on organic matter sorption to a hydrous iron oxide, I implemented temperature-controlled column and batch studies using ferrihydrite-coated sand as sorbent and different types of DOM as sorbates. This study uniquely employed dynamic flow systems, which more accurately represented soil conditions but included a higher degree of complexity than batch studies. Kinetic batch systems were used to aid interpretation of temperature effects. Through these studies, I aimed to gain insight into the mechanisms controlling C stabilization by short-range order hydrous iron oxide and the influence of temperature on the quantity and composition of sorbed C.

3.2 Materials and Methods

3.2.1 Preparation of solutions and columns

A synthetic groundwater medium (SGM) was prepared with the following components: 2.7 mM KCl, 0.3 mM $MgSO_4$, 0.3 mM $CaCl_2$, 1.5 mM NaN_3 as a microbial inhibitor, and 7.9 mM NaCl plus the amount needed to achieve 0.015 M ionic strength, which is within the range for natural groundwater.

To prepare dissolved organic matter solutions, 25 mg of freeze-dried dissolved organic matter (DOM), purchased from the International Humic Substances Society (www.humicsubstances.org), was dissolved in a small volume of 0.5 M NaOH (< 0.5 mL) and SGM (~ 2 mL) prior to addition to a stock bottle. To evaluate the effect of DOM type on sorption to iron oxyhydroxide, several sources and fractions of DOM were used: the acid-soluble ("fulvic acid" - SRFA) and acid-insoluble ("humic acid" - SRHA) fractions and reverse osmosis isolation (SRNOM) of Suwannee River natural organic matter, the acid-insoluble fraction of Elliott prairie soil (ESHA), and the acid-soluble (PPFA) and acid-insoluble (PPHA) fractions of agricultural Pahokee peat soil. After adding 10 mg of KBr as a

conservative tracer and adjusting pH to 7.45 ± 0.1 using 0.5 M NaOH and 0.5 M HCl, solutions were brought to 1 L gravimetrically and filtered through a 5 μm cellulose nitrate filter.

Glass Econo-Columns (1 cm ID x 10 cm length, BioRad) were packed wet with 10 g of 50% (wt/wt) ferrihydrite-coated quartz (FHQ) and uncoated quartz sand between 1 g and 5 g of uncoated quartz sand in SGM. Packed columns had a pore volume of about 3.5 mL and a bulk density of 1.09 g cm^3. Ferrihydrite was synthesized by rapid titration of $FeCl_3$ with 0.4 M NaOH to pH 7.5 and coated on Iota 6 quartz sand as described in Borch et al. (2007) and Hansel et al. (2003). New batches of FHQ were synthesized periodically to avoid aging (Cornell and Schwertmann, 1991; Kaiser et al., 2007), and the presence and purity of 2-line ferrihydrite was verified using X-ray diffraction (XRD). The BET surface area of the FHQ used in all continuous flow experiments at 50 μL min^{-1} was 4.5158 m^2 g^{-1} and Fe concentration was 9.5 mg g^{-1}. FHQ used in kinetics batch studies had a BET surface area of 3.4828 m^2 g^{-1} and Fe concentration of 7.3 mg g^{-1}.

3.2.2 Column studies

Columns and solutions were stored at experimental temperatures either in an incubator (7, 25, and 45 °C) or at room temperature (23 °C) before and during the experiment. A peristaltic pump was used to feed solutions upward through the columns (to prevent preferential flow) at a flow rate of 50 μL min^{-1}. Columns were first equilibrated with at least 12 bed volumes of SGM, then one DOM solution was fed through each column. Fractions of 5-9 mL were collected in glass test tubes using a SpectraChrom CF-2 fraction collector, and effluent volume was determined gravimetrically. To determine the potential kinetic limitations of the continuous flow system, studies were repeated at 10 μL min^{-1} and 250 μL min^{-1} flow rates. Details for these experiments are provided in Appendix B.

3.2.3 Analysis of effluent

DOM concentrations were calculated from UV absorption spectroscopy measurements at 254 nm. To determine breakthrough of the conservative tracer, Br^- concentrations of initial effluent

samples were measured with a Dionex ICS-2100 ion chromatograph and AS-19 anion column. The Br^- tracer reached 100% breakthrough at 6 bed volumes. Total organic carbon (TOC) measurements for SRFA, SRHA, SRNOM, and ESHA experiments at 25 °C were performed using a Shimano TOC-L. Specific ultraviolet absorbance (SUVA) values were calculated by dividing the path length-normalized UV absorbance values (m^{-1}) by TOC values (mg C L^{-1}).

3.2.4 Kinetics batch study

Sorption kinetics of SRNOM and ESHA on FHQ at 7, 23 and 45 °C were evaluated in triplicate batch systems. 50 mL of DOM solution was added to 1 g ferrihydrite-coated sand in 125 mL glass serum bottles. DOM solution consisted of 27 mg/L ESHA or 23 mg/L SRNOM in SGM at pH 6.9 ± 0.1. Prepared bottles were immediately placed in incubator shakers (7 and 45 °C) or on a shaker at room temperature (23 °C) at 80 rpm, and 725 μL aliquots were removed at 5 min, 10 min, 30 min, 1 hr, 2 hr, 4 hr, 24 hr, 32 hr, 48 or 50 hr, 78 hr, 144 hr, and 171 hr. Controls of DOM solutions without FHQ were also prepared and sampled. DOM concentrations of stock solutions and aliquots were calculated from UV absorption spectroscopy measurements at 254 nm. Stock solution and final equilibrium DOC concentrations were also measured by TOC analysis. The amount sorbed was calculated by subtracting solution concentrations of experimental samples from those in the controls.

3.3 Results and Discussion

3.3.1 Temperature effects on adsorption of NOM – continuous flow studies

Breakthrough curves for four types of dissolved organic matter (SRNOM, SRHA, PPHA, and ESHA) changed similarly with temperature (Figure 3.1). Between 7 and 25 °C, there was little change in the retention time or shape of the breakthrough curve, but between 25 and 45 °C, retention time increased for SRNOM, SRHA, and ESHA, and the shape of the curve changed slightly for all DOM types. For the HAs, the top portion of the curve shifted down at higher temperature, while for

SRNOM, the slope of the top portion became steeper. These features suggest slightly more DOM sorbed at 45˚C than at 7 or 25˚C. In addition, sorption of SRNOM appeared to be more sensitive to high temperature than the other types of DOM. These results demonstrate a general trend of increased sorption at high temperature for all DOM types, but some variability in the extent of the response depending on the type.

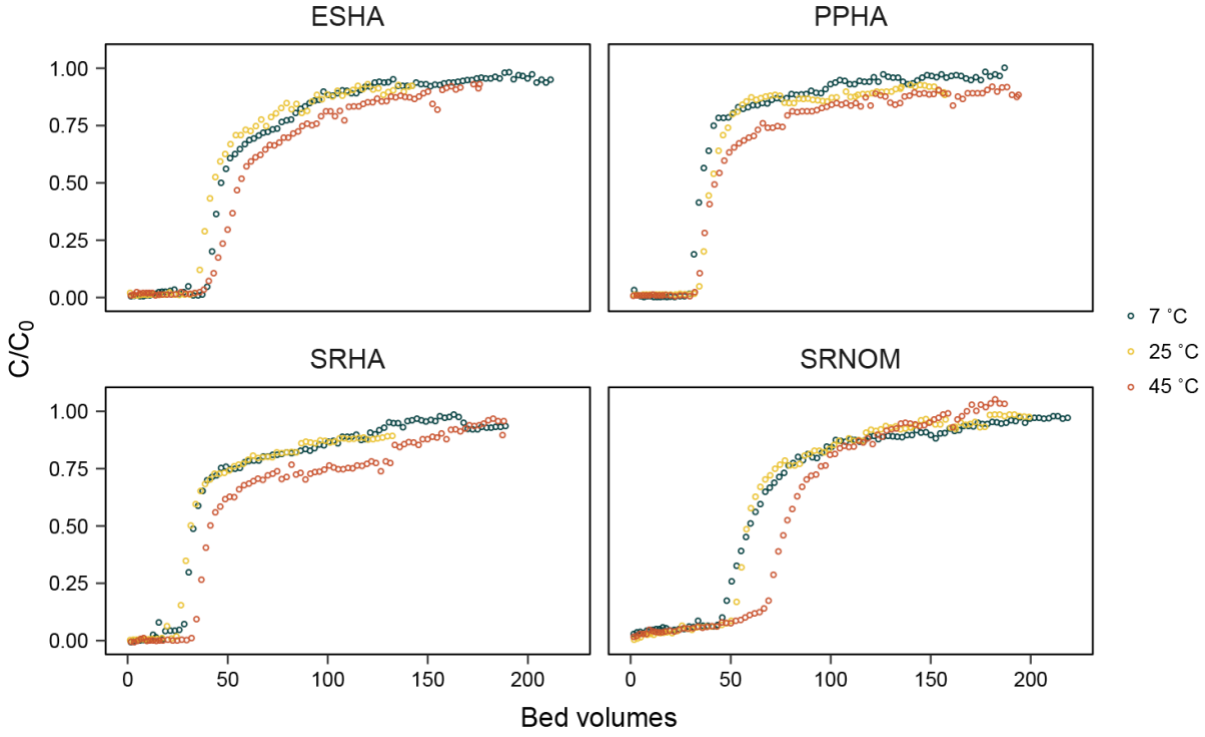

Figure 3.1. Breakthrough curves of four types of DOM at three different temperatures—7 ˚C (blue), 25 ˚C (yellow), and 45 ˚C (red)—in columns containing ferrihydrite-coated sand. Solution conditions: pH 7.4 ± 0.1, and I = 0.015 M, C_0 = 25.3 ± 3.1 mg/L, and flow rate = 50 µL min^{-1}. Complete breakthrough of conservative tracer occurred at 6 pore volumes.

Experimental conditions may also strongly influence the response of sorption to temperature. In experiments conducted with a 10 mg/L ESHA concentration and 100% ferrihydrite-coated quartz (FHQ) sand bedding, temperature impacts on sorption differed substantially from experiments conducted at 25 mg/L ESHA and 1:1 FHQ and uncoated quartz bedding. With twice the amount of FHQ in the column, the number of sorption sites was higher, yielding a greater degree of separation among breakthrough curves as a function of temperature. Under these conditions, ESHA sorption

increased dramatically with temperature, and the shape of the breakthrough curve changed from convex to concave as the steep edge of the curve shifted right (Figure B.1).

The differences in DOM concentration may also have contributed to the sensitivity of sorption to temperature. It is generally accepted that with increasing DOM concentration, hydrophobic groups cluster to reduce free energy, forming macromolecular aggregates. These supramolecular clusters are expected to interact differently with mineral surfaces. One hypothesis is that larger clusters facilitate non-specific sorption to minerals via interactions with surface-bound carboxylic and phenolic compounds, which may bind specifically through ligand exchange or H-bonding. Results from a recent study by Avneri-Katz et al. (2016) support this hypothesis, showing enhanced sorption of oxidized DOM compounds on clay soil at lower DOM concentrations but less fractionation at higher concentrations. Temperature may influence clustering and the specific and non-specific interactions differently, leading to variable effects depending on the DOM type and concentration. For example, solubility generally increases with temperature, so there is likely less clustering at higher temperatures, and therefore a potential for more sorptive fractionation. This may have a greater effect on the higher concentration experiments, in which ESHA would be expected to cluster more than at low concentration (Myneni et al., 1999).

Variations in flow rate altered DOM sorption behavior, revealing the kinetic limitations of the system. I conducted experiments at fast (250 μL min^{-1}) and slow (10 μL min^{-1}) flow rates, monitoring the sorption of ESHA and SRNOM solutions at 23 °C and 45 °C. For both DOM types at both temperatures, there was little difference in breakthrough between flow rates at low DOM loading (Figure B.2). After about 75 – 85% breakthrough, the results for the two flow rates diverged substantially. At low flow, breakthrough rapidly reached 100%, while at high flow, breakthrough gradually approached 100% after an additional 80 – 200 bed volumes. The extra volume necessary to reach steady state at higher flow suggests molecules in solution lacked sufficient time to react with the

stationary phase and reach equilibrium before being pushed through. Interestingly, sorption at low DOM loading responded weakly to the change in flow rate. This unexpected behavior may be attributable to the heterogeneity of DOM and its interactions with hydrous iron oxide. At low DOM loading, specific interactions are more likely (Gu et al., 1994), and these stronger interactions may be less impacted by changing flow rate compared to weaker interactions that likely predominate at high DOM loading.

3.3.2 Desorption of organic matter

Temperature trends for desorption mostly mirrored those for sorption (Figure 3.2). At all temperatures investigated, SRNOM had the highest levels of desorption compared to SRHA, PPHA, and ESHA, suggesting many of its interactions with the solid phase are reversible. SRHA and PPHA desorbed to a similar extent at 7 and 25 °C but desorbed more at 45 °C, with more SRHA desorbing than PPHA at 45 °C. ESHA showed almost no trend in desorption with temperature, while SRNOM desorption increased slightly with each temperature increase. Among all DOM types tested, SRNOM had the greatest amount of both sorption and desorption at all temperatures. This suggests higher levels of sorption do not necessarily indicate that the material interacts strongly with the mineral phase. The apparent reversibility of PPHA, SRHA, and SRNOM sorption at high temperature also implies that at least some of the additional interactions may not be particularly strong.

The high temperature sensitivity of SRNOM and SRHA corresponds with high aliphatic C content (International Humic Substances Society, n.d.). As suggested by Genest et al. (2014) and Coward et al. (2018), aliphatic C may exist in a more water-exchangeable region of coated mineral surfaces and may easily sorb and desorb relative to other types of molecules. Compared to the peat and soil HA fractions, the aquatic DOM types generally comprise smaller molecules more capable of diffusing into the organic matrix or mineral pores (Malcolm, 1990; Wagoner et al., 1997).

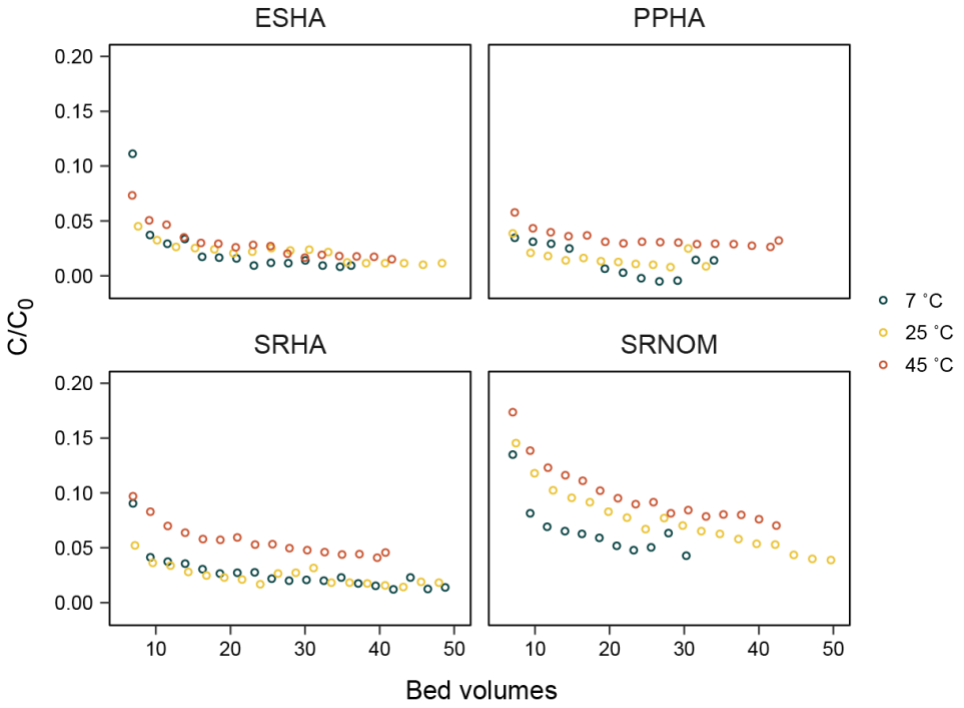

Figure 3.2. Desorption curves of DOM for continuous flow experiments at three temperatures—7 °C (blue), 25 °C (yellow), and 45 °C (red)—in columns containing ferrihydrite-coated sand. Solution conditions: pH 7.4 ± 0.1, and I = 0.015 M, C_0 = 25.3 ± 3.1 mg L^{-1}, and 50 μL min^{-1}. Data from before six bed volumes represents flushing of column pore space and is not included.

The diffusion-controlled "slow sorption" process is highly temperature dependent (ten Hulscher and Cornelissen, 1996; Pignatello, 1999), with both sorption and desorption rates increasing with temperature. This process may account for the temperature sensitivity and high desorption levels of the smaller, aliphatic-rich aquatic DOM.

3.3.3 Kinetic batch experiments

Batch experiments were conducted to determine equilibrium and kinetic parameters for sorption of SRNOM and ESHA on ferrihydrite-coated sand at different temperatures. ESHA sorption reached equilibrium within 78 hours while SRNOM still may not have reached equilibrium by 171 hours, although the sorption rate had slowed substantially by that point (Figure 3.3A). For all conditions, a rapid period of sorption was followed by a much slower approach to equilibrium, features characteristic of diffusion-controlled processes (Wu and Gschwend, 1986). However, no single modeling approach successfully represents the sorption kinetics of both SRNOM and ESHA

at all three temperatures. A possible explanation for the poor fit of models assuming a single sorption mechanism may be that different mechanisms dominate as sorption progresses.

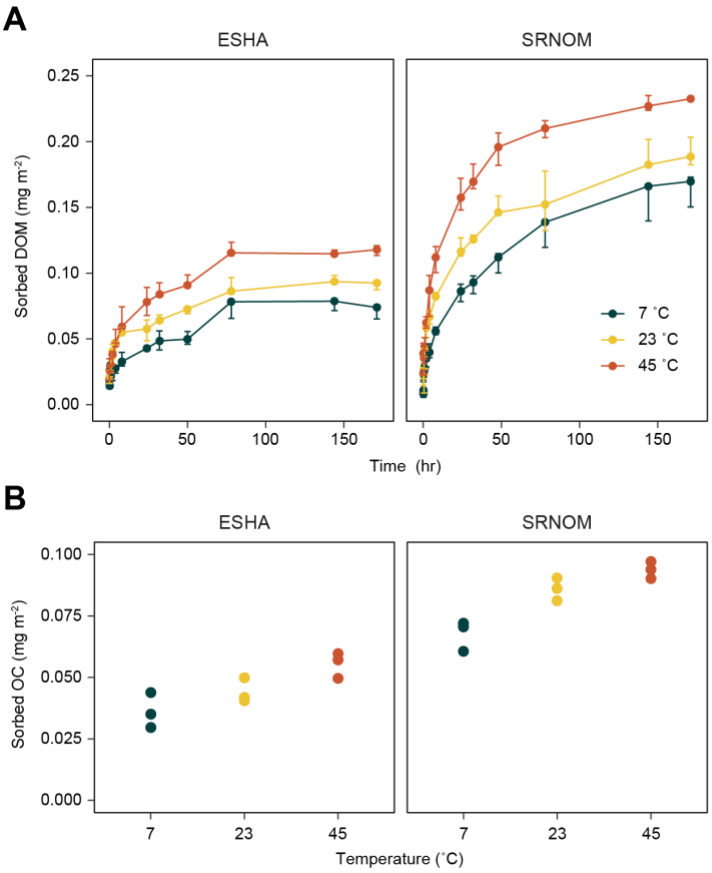

Figure 3.3. Results of batch experiment: (A) Amount of DOM adsorbed to ferrihydrite-coated sand by surface area at each time point (measured by UV absorption spectroscopy at 254 nm) Points represent medians and error bars represent the range of values for triplicates. (B) Final amount of carbon sorbed to ferrihydrite-coated sand normalized by surface area (measured by TOC analysis). 50 mL of 27 mg/L ESHA or 23 mg/L SRNOM in SGM at pH 6.9 ± 0.1 added to 1 g ferrihydrite-coated sand.

Although I was unable to model the entire kinetics curve, I could approximate the initial rate (as determined from UV absorption spectroscopy measurements) from the amount of DOM sorbed in the first 8 hours. This value increased with temperature for both ESHA and SRNOM (Table 3.1), with the rate for SRNOM higher than that for ESHA at each temperature. Since equilibrium sorption values also increased with temperature and were higher for SRNOM than ESHA, the faster rates may not correspond to substantial changes in reaction kinetics, but rather reflect the shift in sorption equilibrium. The batch studies showed increasing sorption from 7 to 23 °C and 23 to 45 °C, while the

column studies performed with 25 mg/L DOM showed an increase in sorption only between 25 and 45 °C. These results demonstrate that differences in reaction conditions, such as the solid to solution ratio, particle mobility, and solution flow, can play crucial roles in the observed temperature responses. However, findings from both experiments are consistent in that they show a trend of increasing sorption with temperature.

Table 3.1. Rate and percent of total DOM sorbed at 8 hours for batch kinetics study at shaker speed of 80 rpm (average and standard deviation of n = 3)

DOM	Temperature (°C)	8-hr rate (μg DOM m^{-2} hr^{-1})	% sorbed in 8 hours	Total DOM sorbed (μg DOM m^{-2})
ESHA	7	4.25 ± 0.66	47.4 ± 7.4	71.7 ± 5.7
	23	6.97 ± 0.33	61.4 ± 2.9	90.9 ± 3.0
	45	8.00 ± 1.14	54.5 ± 7.8	117.4 ± 3.8
SRNOM	7	7.00 ± 0.36	34.1 ± 1.8	164 ± 12
	23	10.36 ± 0.28	43.3 ± 1.2	192 ± 11
	45	13.9 ± 1.3	47.7 ± 4.3	232.6 ± 1.3

A preliminary batch experiment conducted with 0.5 g of ferrihydrite-coated sand and using a much faster shaking speed reached equilibrium in 24-48 hours (Figure B.3), compared to the 78-170+ hours required for the slower shaking batch. At the high shaking speed, ferrihydrite became dislodged from the sand grains during the first few hours, as evidenced by the solution becoming darker and cloudy. This process may have increased the surface area and decreased the size of the ferrihydrite particles. Although the slower shaking speed experiments used nearly twice the amount of coated sand relative to DOM, they took longer to reach equilibrium, suggesting that surface area alone may not account for the change in sorption rate. Instead, increased mixing may account for the more rapid rate.

The very gradual approach of SRNOM to a greater equilibrium sorption maximum than ESHA is consistent with the column studies and may indicate a greater amount of diffusive or partitioning processes involved in its sorption. With a larger proportion of small molecules (or a smaller proportion of supramolecular aggregates), more SRNOM particles may be able to diffuse into

pores in ferrihydrite or "holes" in the accumulating organic coating. The 30-50% decrease in the amount of SRNOM sorbed per unit area in the faster shaker speed experiment (Table B.1) may indicate a substantial amount of weak hydrophobic interactions or partitioning may be taking place at slower shaking speeds. As evidenced by the removal of the ferrihydrite coating, the fast shaking speed increased disturbance among particles relative to the slower shaking speed. This disturbance may have also prevented the formation of weak interactions between DOM molecules and the mineral surface or with an organic matrix beyond the surface.

Despite the overall decrease in the amount of SRNOM sorbed for the higher shaker speed experiment, there was still an evident temperature effect between 25 and 45 °C. (No experiments were conducted at 7 °C for this experiment.) Since the positive effect of temperature on sorption was seen for both the slow and fast shaker speed experiments, temperature may have promoted an increase in relatively strong interactions. From a thermodynamic perspective, this seems counterintuitive—stronger sorption reactions are more exothermic, so they should be less favorable at higher temperatures. Perhaps the impact of temperature on kinetics is responsible—a reaction with high activation energy that occurs very slowly at low temperatures may become fast enough to be noticeable at higher temperatures. Because they involve orbital rehybridization and ligand displacement, ligand exchange mechanisms often have high activation energies (Pignatello, 1999). These may be especially high if the organic ligand must overcome charge repulsion to interact directly with the mineral surface, as is the case with amine groups and ferrihydrite at near-neutral pH. Once bound, these amine groups can be very difficult to remove, due to their strong binding energy (Newcomb et al., 2017). Another possibility is that temperature impacts the "slow sorption" process mentioned above. Higher temperatures may accelerate diffusion into mineral pores and organic "holes", which would be protected from perturbation even at high shaking speeds.

To my knowledge, no published studies have investigated the influence of temperature on sorption of DOM on hydrous iron oxides, but several have evaluated the thermodynamics and effects of temperature on sorption to soils, clays, and hematite. Vance and David (1992), Kaiser et al. (2001), and Jardine et al. (1989) examined the effect of temperature on sorption and desorption of DOM on mineral soils. All three studies conducted experiments at lower pH (3.85 – 5.2) than the range used in this study (~6 – 8). Significantly all studies used soils that already bore organic carbon, so the results do not allow differentiation of the effect of temperature on organic-mineral or organic-organic interactions. Jardine et al. noted a slight increase in sorption from 10 to 23 °C, which they attributed to preferential sorption of hydrophobics, a possibly entropy-driven process. Vance and David observed a weak temperature effect between 3 and 21 °C, similar to my results from 25 mg/L DOM continuous flow experiments. Kaiser et al. reported increasing desorption of DOM with temperature, which is consistent with my results for SRNOM, SRHA, and PPHA. The authors also note that the effect was least pronounced for the soil horizon containing the least amount of Al and Fe minerals.

Arnarson and Keil (2000) studied the temperature response of sorption of marine DOM to montmorillonite clay under saline and slightly alkaline conditions. Their results showed decreasing sorption between 3.5 and 21.5 °C. In a study using DOM from sewage, divalent metal cations, and montmorillonite and kaolinite clays, Baham and Sposito (1994) observed no temperature dependence of DOM sorption between 10, 25, and 35 °C at pH 5.5. Because these clays carry a permanent negative charge, they can interact with DOM molecules differently, including cation exchange with positively charged organic functional groups and cation bridging. Cation bridging is a less significant mechanism of interaction between DOM and hydrous iron oxides, which bear primarily opposite charges from pH 5 - 8.

While no studies report the direct effects of temperature on sorption of DOM to iron oxides, Gu et al. (1994) measured the heat of adsorption of pond DOM associated with industrial hematite at

pH 3.7. The authors observed a high heat of adsorption, suggesting the dominance of strong, exothermic interactions, which would be less thermodynamically favorable at higher temperature (Conant et al., 2011). This information alone could not predict the overall impact of temperature on sorption, since other interactions may be more favored (or less unfavored) at higher temperature, altering the net change in sorption.

The inconsistency in these reported effects of temperature on DOM sorption to soils and minerals is unsurprising given the variety of materials and experimental conditions used. In this study, changes in DOM:mineral ratio, DOM type, and physical reaction conditions all impacted the extent to which temperature influenced sorption. It may therefore be expected that experiments employing a variety of DOC sources, sorbents, and solution conditions would yield highly variable results. The fact that some of these findings contrast with those presented in this work is likely due to very different experimental parameters.

3.3.4 Molecular fractionation of organic matter

Initial breakthrough curve data for continuous flow experiments at 25 °C suggest aromatic moieties may preferentially adsorb to the FHQ column bedding. ESHA, PPHA, PPFA, and SRHA, which contain the highest proportions of aromatic carbon, broke through very little within the first 25 bed volumes (**Error! Reference source not found.**, inset). SRFA and SRNOM, which are chemically quite similar, partially broke through with the conservative tracer. The HAs and PPFA sorb more initially (very little breakthrough in the first few pore volumes), but break through to 50% of the influent concentration before SRFA and SRNOM (Figure 3.4).

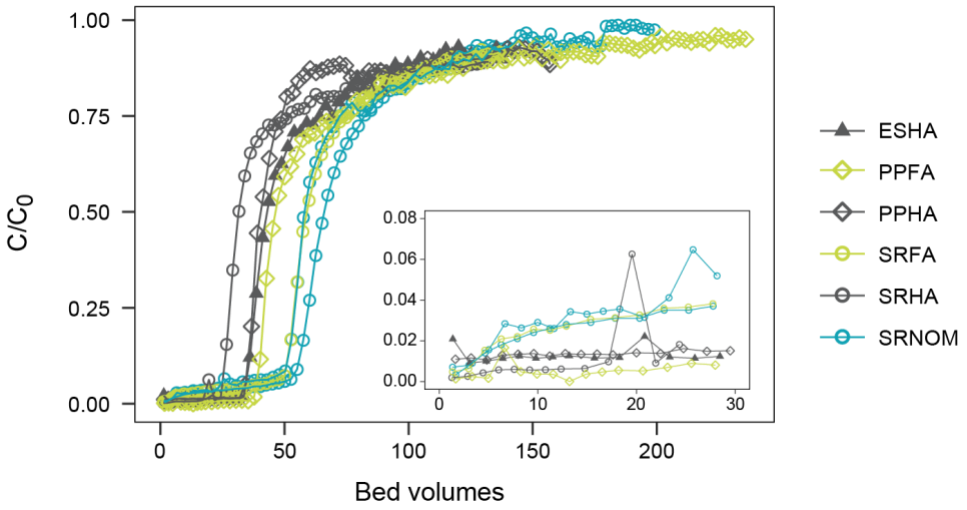

Figure 3.4. Breakthrough curves of six types of DOM at 25 °C, pH 7.4 ± 0.1, and I = 0.015 M, C_0 = 23.8 ± 2.4 mg L^{-1}, and 50 μL min^{-1} flow rate in columns of ferrihydrite-coated sand. Inset shows breakthrough during the first 30 bed volumes. Complete breakthrough of conservative tracer occurred at 6 bed volumes.

In addition, specific ultraviolet absorbance (SUVA) values, which correlate with percent aromatic carbon (Weishaar et al., 2003), are lower for initial effluents than for stock solutions and final effluents (**Error! Reference source not found.**). This suggests aromatic moieties preferentially adsorb initially, but that later stage

sorption is less selective for compounds with high aromaticity. This finding is consistent with a number of studies that have demonstrated preferential sorption of aromatic moieties at mineral surfaces. Using ^{1}H HR-MAS NMR to analyze whole soil, Genest et al. (2014) located aromatic structures buried below the OM-water interface, closer to the mineral surfaces. In an investigation of organic matter associated with different Fe mineral phases, Coward et al. (2018) observed preferential sorption of aromatic and N-aliphatic compounds to short-range order Fe phases, and greater proportions of aliphatic and saturated carbohydrate-like compounds in fractions likely representing colloidal or co-precipitated OM. The fact that DOM types containing higher proportions of aromatic C sorb more completely initially but reach 50% breakthrough at lower bed volumes suggests aromatic components facilitate surface sorption but do not preferentially accumulate beyond the mineral surface.

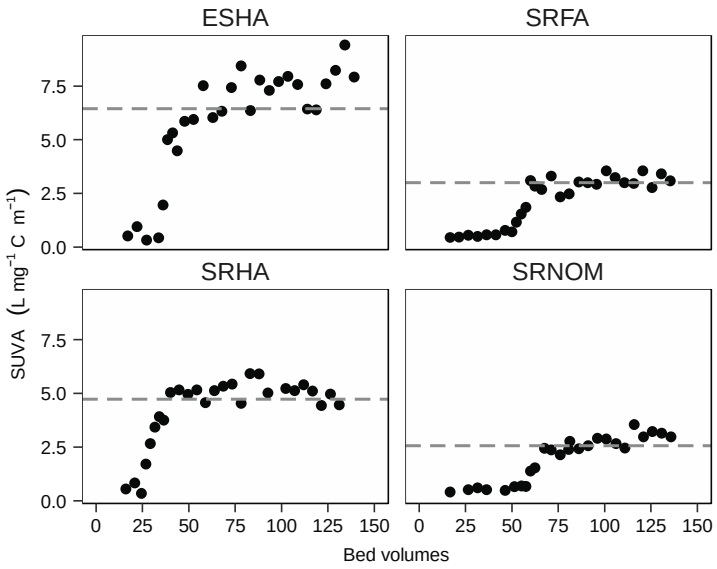

Figure 3.5. $SUVA_{254}$ values for effluent from continuous flow experiments conducted at 25 °C, pH 7.4 ± 0.1, and I = 0.015 M, C_0 = 25.0 ± 2.4 mg L^{-1}, and 50 µL min^{-1} flow rate in columns of ferrihydrite-coated sand. Dashed lines represent the SUVA of stock solutions.

My results share some similarities with a recent study targeting sorption of humic acid on goethite (Qin et al., 2015). In kinetic batch studies and dynamic flow experiments, the authors observed initial (within the first 2 hours for the batch studies and within 13 pore volumes for column studies) sorption of highly aromatic compounds (as determined by low SUVA values of effluent), followed by either the release of these compounds or preferential sorption of non-aromatic compounds (as determined by high SUVA values of effluent). Indeed, the remaining supernatants at the end of my batch experiment had slightly higher or the same or SUVA values as the stocks and controls, suggesting there was no overall preferential sorption of aromatic compounds (Table B.2). It could be possible that aromatic compounds preferentially adsorb only at the mineral surface, forming a layer to which compounds with low aromaticity adsorb, similar to the proposed zonal model (Kleber et al., 2007). Such a process could lead to no net difference in final SUVA values, or even an increase in SUVA, if more non-aromatic moieties sorb than aromatics.

3.4 Summary and Implications/Conclusions

This work presents novel evidence of increasing sorption of DOM to a hydrous iron oxide with increasing temperature. It also shows a trend of increasing desorption with temperature for aquatic and peat DOM types.

In continuous flow experiments, sorption and desorption of SRNOM (aquatic DOM), appeared to be most sensitive to changes in temperature. SRNOM also had the greatest amount of sorption and desorption at all temperatures. In contrast, the soil DOM, ESHA, had lower sorption rates than SRNOM, but experienced far less and less sensitive desorption. Perhaps it is unsurprising that aquatic DOM dissociates more easily from minerals than the soil HA fraction, which was extracted from the solid phase. These findings reinforce the importance of considering both quantity and chemical composition of sorbed DOM—more sorption does not necessarily equate to more protected carbon.

Though these studies were not designed to provide mechanistic insight into sorption processes, there is some indication from SUVA values that aromatic compounds interacted directly with the mineral surface. The mode of interaction is unclear, but solution conditions likely favor interactions such as H-bonding or van der Waals interactions over ligand exchange. Ligand exchange is less favored at more neutral pH (Gu et al., 1995; Persson and Axe, 2005; Norén and Persson, 2007) and probably has higher activation energies than weaker interactions (Pignatello, 1999), making it kinetically unfavorable, and therefore unlikely to dominate initial sorption. The higher SUVA values of later stage effluents and final batch supernatants suggest less-aromatic compounds sorb later on.

An important consideration of these studies is the limitation of the solution environments investigated. DOM solution concentration and Fe:C ratio modulated the influence of temperature on sorption. Other solution conditions such as pH, multi-valent cation concentration, and ionic strength are known to influence DOM aggregation and sorption processes and may also impact the ways in

which sorption changes with temperature. These effects are worth investigating further, since the results from the conditions used in this study may not be scalable to all environments. However, the condition-dependent results highlight the need for studies of temperature effects on specific organo-mineral interactions, since the results from one system may not be applicable to other systems.

Despite broad acceptance of the importance of organo-mineral associations in long-term carbon storage, few studies have investigated the impact of temperature on these interactions. My findings demonstrate there may be some conditions in which increasing temperature contributes to the removal of organic substrates from the accessible carbon pool via sorption to hydrous iron oxides. Although I observed only a slight increase in sorption with temperature, this could have a profound impact on carbon storage when scaled to all applicable systems globally. However, the amount of carbon removed by this mechanism needs to be further quantified, especially in comparison to changes in DOM mineralization rates due to warming, in order to evaluate its relative impact on soil response to climate change.

REFERENCES

Allison S. D., Wallenstein M. D. and Bradford M. A. (2010) Soil-carbon response to warming dependent on microbial physiology. *Nat. Geosci.* **3**, 336–340.

Amundson R. (2001) The carbon budget in soils. *Annu. Rev. Earth Planet. Sci.* **29**, 535–62.

Arnarson T. S. and Keil R. G. (2000) Mechanisms of pore water organic matter adsorption to montmorillonite. *Mar. Chem.* **71**, 309–320.

Avneri-Katz S., Young R. B., McKenna A. M., Chen H., Corilo Y. E., Polubesova T., Borch T. and Chefetz B. (2016) Adsorptive fractionation of dissolved organic matter (DOM) by mineral soil: Macroscale approach and molecular insight. *Org. Geochem.* Available at: http://dx.doi.org/10.1016/j.orggeochem.2016.11.004.

Baham J. and Sposito G. (1994) Adsorption of Dissolved Organic Carbon Extracted from Sewage Sludge on Montmorillonite and Kaolinite in the Presence of Metal Ions. *J. Environ. Qual.* **23**, 147.

Borch T., Masue Y., Kukkadapu R. K. and Fendorf S. (2007) Phosphate imposed limitations on biological reduction and alteration of ferrihydrite. *Environ. Sci. Technol.* **41**, 166–172.

Carey J. C., Tang J., Templer P. H., Kroeger K. D., Crowther T. W., Burton A. J., Dukes J. S., Emmett B., Frey S. D., Heskel M. A., Jiang L., Machmuller M. B., Mohan J., Panetta A. M., Reich P. B., Reinsch S., Wang X., Allison S. D., Bamminger C., Bridgham S., Collins S. L., De Dato G., Eddy W. C., Enquist B. J., Estiarte M., Harte J., Henderson A., Johnson B. R., Larson K. S., Luo Y., Marhan S., Melillo J. M., Peñuelas J., Pfeifer-Meister L., Poll C., Rastetter E., Reinmann A. B., Reynolds L. L., Schmidt I. K., Shaver G. R., Strong A. L., Suseela V. and Tietema A. (2016) Temperature response of soil respiration largely unaltered with experimental warming. *Proc. Natl. Acad. Sci.* **113**, 13797–13802.

Chassé A. W., Ohno T., Higgins S. R., Amirbahman A., Yildirim N. and Parr T. B. (2015) Chemical Force Spectroscopy Evidence Supporting the Layer-by-Layer Model of Organic Matter Binding to Iron (oxy)hydroxide Mineral Surfaces. *Environ. Sci. Technol.* **49**, 9733–9741.

Conant R. T., Ryan M. G., Ågren G. I., Birge H. E., Davidson E. A., Eliasson P. E., Evans S. E., Frey S. D., Giardina C. P., Hopkins F. M., Hyvönen R., Kirschbaum M. U. F., Lavallee J. M., Leifeld J., Parton W. J., Steinweg J. M., Wallenstein M. D., Wetterstedt J. Å. M. and Bradford M. A. (2011) Temperature and soil organic matter decomposition rates - synthesis of current knowledge and a way forward. *Glob. Change Biol.* **17**, 3392–3404.

Cornelissen G., van Noort P. C. M., Parsons J. R. and Govers H. A. J. (1997) Temperature Dependence of Slow Adsorption and Desorption Kinetics of Organic Compounds in Sediments. *Environ. Sci. Technol.* **31**, 454–460.

Cornell R. M. and Schwertmann U. (1991) *Iron Oxides in the Laboratory*., VCH Verlagsgesellschaft, Weinheim, Germany.

Cornell R. M. and Schwertmann U. (2003) *The Iron Oxides: Structure, Properties, Reactions, Occurrences and Uses*., Wiley-VCH, Weinheim, FRG.

Coward E. K., Ohno T. and Plante A. F. (2018) Adsorption and Molecular Fractionation of Dissolved Organic Matter on Iron-Bearing Mineral Matrices of Varying Crystallinity. *Environ. Sci. Technol.* **52**, 1036–1044.

Eusterhues K., Rennert T., Knicker H., Kögel-Knabner I., Totsche K. U. and Schwertmann U. (2011) Fractionation of organic matter due to reaction with ferrihydrite: Coprecipitation versus adsorption. *Environ. Sci. Technol.* **45**, 527–533.

Filius J. D., Lumsdon D. G., Meeussen J. C. L., Hiemstra T. J. and Van Riemsdijk W. H. (2000) Adsorption of fulvic acid on goethite. *Geochim. Cosmochim. Acta* **64**, 51–60.

Genest S. C., Simpson M. J., Simpson A. J., Soong R. and McNally D. J. (2014) Analysis of soil organic matter at the solid–water interface by nuclear magnetic resonance spectroscopy. *Environ. Chem.* **11**, 472.

Gu B., Schmitt J., Chen Z., Liang L. and McCarthy J. F. (1995) Adsorption and desorption of different organic matter fractions on iron oxide. *Geochim. Cosmochim. Acta* **59**, 219–229.

Gu B., Schmitt J., Chen Z., Liang L. and McCarthy J. F. (1994) Adsorption and desorption of natural organic matter on iron oxide: mechanisms and models. *Environ. Sci. Technol.* **28**, 38–46.

Hansel C. M., Benner S. G., Neiss J., Dohnalkova A., Kukkadapu R. K. and Fendorf S. (2003) Secondary mineralization pathways induced by dissimilatory iron reduction of ferrihydrite under advective flow. *Geochim. Cosmochim. Acta* **67**, 2977–2992.

ten Hulscher T. E. M. and Cornelissen G. (1996) Effect of Temperature on Soprtion Equilibrium and Sorption Kinetics of Organic Micropolluants - a Review. *Chemosphere* **32**, 609–626.

International Humic Substances Society Chemical Properties of IHSS Samples. Available at: http://www.humicsubstances.org [Accessed May 11, 2014].

Jardine P. M., Weber N. L. and McCarthy J. F. (1989) Mechanisms of dissolved organic carbon adsorption on soil. *Soil Sci. Soc. Am. J.* **53**, 1378–1385.

Jobbágy E. G. and Jackson R. B. (2000) The vertical distribution of soil organic carbon and its relation to climate and vegetation. *Ecol. Appl.* **10**, 423–436.

Kaiser K. (2003) Sorption of natural organic matter fractions to goethite (alpha-FeOOH): Effect of chemical composition as revealed by liquid-state 13C NMR and wet-chemical analysis. *Org. Geochem.* **34**, 1569–1579.

Kaiser K. and Guggenberger G. (2007) Sorptive stabilization of organic matter by microporous goethite: sorption into small pores vs. surface complexation. *Eur. J. Soil Sci.* **58**, 45–59.

Kaiser K. and Guggenberger G. (2000) The role of DOM sorption to mineral surfaces in the preservation of organic matter in soils. *Org. Geochem.* **31**, 711–725.

Kaiser K., Kaupenjohann M. and Zech W. (2001) Sorption of dissolved organic carbon in soils: effects of soil sample storage, soil-to-solution ratio, and temperature. *Geoderma* **99**, 317–328.

Kaiser K., Mikutta R. and Guggenberger G. (2007) Increased Stability of Organic Matter Sorbed to Ferrihydrite and Goethite on Aging. *Soil Sci. Soc. Am. J.* **71**, 711–711.

Kleber M., Sollins P. and Sutton R. (2007) A conceptual model of organo-mineral interactions in soils: self-assembly of organic molecular fragments into zonal structures on mineral surfaces. *Biogeochemistry* **85**, 9–24.

Köchy M., Hiederer R. and Freibauer A. (2015) Global distribution of soil organic carbon – Part 1: Masses and frequency distributions of SOC stocks for the tropics, permafrost regions, wetlands, and the world. *SOIL* **1**, 351–365.

Lv J., Zhang S., Wang S., Luo L., Cao D. and Christie P. (2016) Molecular-Scale Investigation with ESI-FT-ICR-MS on Fractionation of Dissolved Organic Matter Induced by Adsorption on Iron Oxyhydroxides. *Environ. Sci. Technol.* **50**, 2328–2336.

Malcolm R. L. (1990) The uniqueness of humic substances in each of soil, stream and marine environments. *Anal. Chim. Acta* **232**, 19–30.

Marschner B. and Bredow A. (2002) Temperature effects on release and ecologically relevant properties of dissolved organic carbon in sterilised and biologically active soil samples. *Soil Biol. Biochem.* **34**, 459–466.

McBride M. B. (1994) *Environmental Chemistry of Soils.*, Oxford University Press, New York.

McKnight D. M., Bencaia K. E., Zellweger G. W., Aiken G. R., Feder G. L. and Thorn K. A. (1992) Sorption of dissolved organic carbon by hydrous aluminum and iron oxides occurring at the

confluence of Deer Creek with the Snake River, Summit County, Colorado. *Environ. Sci. Technol.* **26**, 1388–1396.

Means J. C., Wood S. G., Hassett J. J. and Banwart W. L. (1980) Sorption of polynuclear aromatic hydrocarbons by sediments and soils. *Environ. Sci. Technol.* **14**, 1524–1528.

Melillo J. M., Frey S. D., DeAngelis K. M., Werner W. J., Bernard M. J., Bowles F. P., Pold G., Knorr M. A. and Grandy A. S. (2017) Long-term pattern and magnitude of soil carbon feedback to the climate system in a warming world. *Science* **358**, 101–105.

Mikutta R. and Kaiser K. (2011) Organic matter bound to mineral surfaces: Resistance to chemical and biological oxidation. *Soil Biol. Biochem.* **43**, 1738–1741.

Mikutta R., Kleber M., Torn M. S. and Jahn R. (2006) Stabilization of soil organic matter: Association with minerals or chemical recalcitrance? *Biogeochemistry* **77**, 25–56.

Moreno-Castilla C. (2004) Adsorption of organic molecules from aqueous solutions on carbon materials. *Carbon* **42**, 83–94.

Myneni S. C. B., Brown J. T., Martinez G. A. and Meyer-Ilse W. (1999) Imaging of Humic Substance Macromolecular Structures in Water and Soils. *Science* **286**, 1335–1337.

Newcomb C. J., Qafoku N. P., Grate J. W., Bailey V. L. and De Yoreo J. J. (2017) Developing a molecular picture of soil organic matter-mineral interactions by quantifying organo-mineral binding. *Nat. Commun.* **8**. Available at: http://dx.doi.org/10.1038/s41467-017-00407-9.

Norén K. and Persson P. (2007) Adsorption of monocarboxylates at the water/goethite interface: The importance of hydrogen bonding. *Geochim. Cosmochim. Acta* **71**, 5717–5730.

Persson P. and Axe K. (2005) Adsorption of oxalate and malonate at the water-goethite interface: Molecular surface speciation from IR spectroscopy. *Geochim. Cosmochim. Acta* **69**, 541–552.

Pignatello J. J. (1999) The Measurement and Interpretation of Sorption and Desorption Rates for Organic Compounds in Soil Media. *Adv. Agron.* **69**, 1–73.

Pries C. E. H., Castanha C., Porras R. C. and Torn M. S. (2017) The whole-soil carbon flux in response to warming. *Science* **355**, 1420–1423.

Qin X., Liu F., Wang G., Hou H., Li F. and Weng L. (2015) Fractionation of humic acid upon adsorption to goethite: Batch and column studies. *Chem. Eng. J.* **269**, 272–278.

Rasmussen C., Heckman K., Wieder W. R., Keiluweit M., Lawrence C. R., Berhe A. A., Blankinship J. C., Crow S. E., Druhan J. L., Hicks Pries C. E., Marin-Spiotta E., Plante A. F., Schädel C., Schimel J. P., Sierra C. A., Thompson A. and Wagai R. (2018) Beyond clay: towards an improved set of variables for predicting soil organic matter content. *Biogeochemistry*. Available at: http://link.springer.com/10.1007/s10533-018-0424-3 [Accessed February 16, 2018].

Scharlemann J. P., Tanner E. V., Hiederer R. and Kapos V. (2014) Global soil carbon: understanding and managing the largest terrestrial carbon pool. *Carbon Manag.* **5**, 81–91.

Schimel D. S., Braswell B. H., Holland E. A., McKeown R., Ojima D. S., Painter T. H., Parton W. J. and Townsend A. R. (1994) Climatic, edaphic, and biotic controls over storage and turnover of carbon in soils. *Glob. Biogeochem. Cycles* **8**, 279–293.

Schmidt M. W. I., Torn M. S., Abiven S., Dittmar T., Guggenberger G., Janssens I. A., Kleber M., Kögel-Knabner I., Lehmann J., Manning D. A. C., Nannipieri P., Rasse D. P., Weiner S. and Trumbore S. E. (2011) Persistence of soil organic matter as an ecosystem property. *Nature* **478**, 49–56.

Thornley J. H. M. and Cannell M. G. R. (2001) Soil Carbon Storage Response to Temperature: an Hypothesis. *Ann. Bot.* **87**, 591–598.

Tipping E. (1981) The adsorption of aquatic humic substances by iron oxides. *Geochim. Cosmochim. Acta* **45**, 191–199.

Torn M. S., Trumbore S. E., Chadwick O. A., Vitousek P. M. and Hendricks D. M. (1997) Mineral control of soil organic carbon storage and turnover. *Nature* **389**, 170–173.

Trumbore S. (2009) Radiocarbon and Soil Carbon Dynamics. *Annu. Rev. Earth Planet. Sci.* **37**, 47–66.

Vance G. F. and David M. B. (1992) Dissolved Organic Carbon and Sulfate Sorption by Spodosol Mineral Horizons. *Soil Sci.* **154**, 136–144.

Wagai R. and Mayer L. M. (2007) Sorptive stabilization of organic matter in soils by hydrous iron oxides. *Geochim. Cosmochim. Acta* **71**, 25–35.

Wagoner D. B., Christman R. F., Cauchon G. and Paulson R. (1997) Molar Mass and Size of Suwannee River Natural Organic Matter Using Multi-Angle Laser Light Scattering. *Environ. Sci. Technol.* **31**, 937–941.

Weishaar J. L., Aiken G. R., Bergamaschi B. A., Fram M. S., Fujii R. and Mopper K. (2003) Evaluation of specific ultraviolet absorbance as an indicator of the chemical composition and reactivity of dissolved organic carbon. *Environ. Sci. Technol.* **37**, 4702–8.

Wu S.-C. and Gschwend P. M. (1986) Sorption kinetics of hydrophobic organic compounds to natural sediments and soils. *Environ. Sci. Technol.* **20**, 717–25.

CHAPTER 4: HYDROGEOMORPHIC CONTROLS ON SOIL CARBON QUANTITY AND COMPOSITION IN COLORADO SUBALPINE WETLANDS

4.1 Introduction

Wetlands cover only 5 – 8% of the earth's land surface but disproportionately store 20 – 30% of global soil organic carbon (Mitsch and Gosselink, 2007; Lal, 2008). Frequent or permanently saturated conditions create oxygen-depleted soil environments where plant productivity often outpaces decomposition rates, favoring accrual of soil organic carbon (SOC). In addition to sequestering carbon, the unique biogeochemistry and high carbon content of wetlands can have profound influences on water quality. Wetlands can improve or diminish water quality by processing nutrients, retaining sediment, altering the mobility of contaminants, and exporting dissolved organic matter to drinking water sources (Johnston, 1991; Kalbitz and Wennrich, 1998; Freeman et al., 2001). Consequently, understanding C processing in these systems is critical for predicting changes to C storage as a result of environmental disturbances and for effectively managing wetlands.

The flow paths that link wetlands with surrounding landscapes govern seasonal water table fluctuations and redox-related biogeochemical processes. These characteristics vary among wetland classes corresponding to different hydrogeomorphic (HGM) settings and can influence biogeochemical reaction rates and the supply and processing of C (Segnini et al., 2010; Bernal and Mitsch, 2012; Segnini et al., 2013). Furthermore, differences in HGM settings are likely to influence the sensitivity of wetland C stocks to changes in climate.

The effects of water table fluctuations and HGM settings on C processing is not well known (Kayranli et al., 2010). Distinct organic matter supply, reaction and removal rates are likely to generate both quantitative and qualitative differences in soil C among wetland hydrogeomorphic types. In general, wetlands with features promoting anaerobic conditions—a long hydroperiod, minimal flow,

thick organic layers—store more C and have a greater proportion of aliphatic C than wetlands that are drier, minerotrophic, or have shorter hydraulic residence time (Bernal and Mitsch, 2008; Bernal and Mitsch, 2012; Tfaily et al., 2014; Luan et al., 2014; Heller et al., 2015). However, these studies fail to capture the variety of possible conditions among all hydrogeomorphic wetland types, especially with respect to depth, and leave a substantial gap in knowledge regarding C stability in wetlands of the western U.S.

Although wetlands in the western U.S. store less carbon than those in other regions of the country (Nahlik and Fennessy, 2016), many exist in forested headwaters that provide the vast majority of water supplies, including drinking water, for millions of people (USDI, BR, 2012). Because dissolved organic carbon (DOC) affects the efficiency of water treatment operations and can lead to the formation of hazardous disinfection byproducts (Singer, 1999; Lee et al., 2004; Sharp et al., 2004), it is important to understand the processes controlling export of DOC from watersheds. Changes in precipitation patterns due to climate change could have profound impacts on the hydrology regulating wetland C processing, especially in sensitive mountain ecosystems. Therefore, a more detailed understanding of carbon storage and cycling in these wetlands is necessary. In the Rocky Mountains of Colorado, wetlands located in isolated depressions co-occur with slope wetlands in headwater forest watersheds (Carsey et al., 2003) and provide an opportunity to examine how C quantity and composition vary among HGM wetland classes.

Depressional and slope wetlands differ substantially in their dominant hydrodynamics and topographic characteristics. Depressional wetlands occur in topographic depressions and are characterized by primarily seasonally controlled, vertical fluctuations in the water table (NRCS, 2008). Horizontal, downslope flow dominates the hydrodynamics in slope wetlands, which are found on sloping land where groundwater breaches the land surface. In the sites examined in this study, this

feature produces slope wetlands with longer hydroperiods than depressional wetlands (Figure 4.1), which likely influences C storage and decomposition.

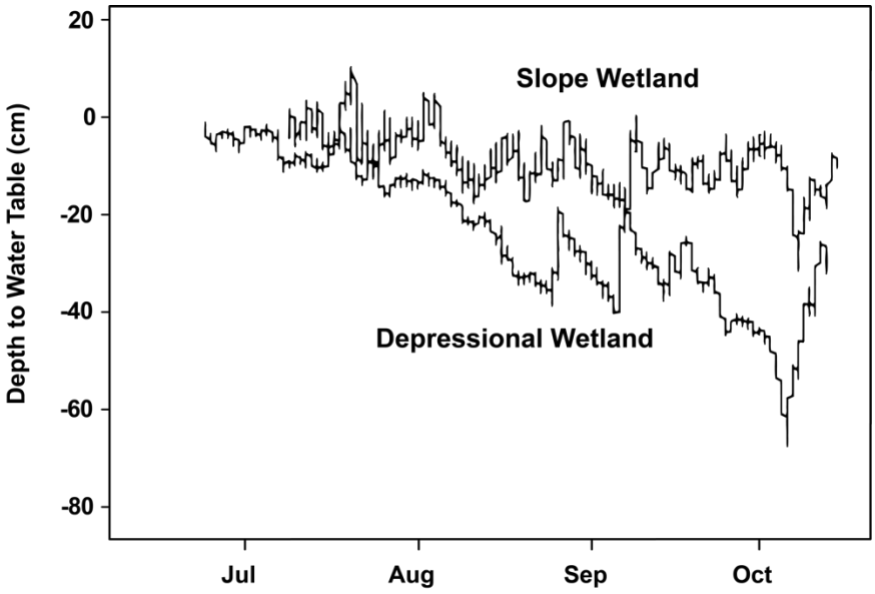

Figure 4.1. Water table height (in cm) of representative depressional (D2) and slope (S2) wetland classes.

To determine the influence of HGM setting on the storage and decomposition of SOC, I examined the chemical composition and quantity of SOC in relation to soil properties and hydrology in six subalpine wetlands in Colorado. I used several techniques to assess C quantity and quality, including total carbon and nitrogen measurements, radiocarbon dating, and solid-state ^{13}C cross-polarization magic angle spinning (CP-MAS) NMR spectroscopy. Solid NMR spectroscopy has been used to provide insight into the chemical composition of soil organic matter and the changes it undergoes during decomposition, providing insights into carbon cycling in different environments (Knicker and Ludemann, 1995; Baldock et al., 1997; Kögel-Knabner, 1997; Rumpel et al., 2002). I hypothesized that longer hydraulic residence times in the depressional wetlands would create anaerobic conditions favoring greater accumulation of carbon and a higher percentage of aliphatic carbon compared to slope wetlands.

4.2 Methods

4.2.1 Site description[3]

I studied six wetlands in the Fraser Experimental Forest (FEF) (39˚ 34' N, 105˚ 30' W), an outdoor research laboratory maintained by the U.S. Department of Agriculture (USDA) Forest Service. The three slope wetlands (S1, S2, S3) resided on hill sides with 15-20% slope gradients where groundwater emerged at the ground surface and passed along near-surface flowpaths in hours to days, resulting in short hydraulic residence times. The three depressional wetlands (D1, D2, D3) formed within topographic depressions and retained water for months, resulting in long hydraulic residence times. In FEF, depressional and slope wetlands occur as 0.1 to 1 ha openings within the subalpine conifer forest at comparable elevation (2700-3300 m) and similar climatic conditions. Detailed descriptions of the wetland sites and soil samples are available in Appendix D. Soils in the wetlands at FEF have developed from Precambrian granite, schist and gneiss bedrock (Retzer, 1962; Kellogg et al., 2008) and are classified as Histic Cryaquolls with 20-100 cm of peat accumulation (Alstatt and Miles, 1983).

Vegetation in the depressional wetlands is dominated by the grass and sedge species *Calamagrostis canadensis*, *Carex aquatilis*, and *Carex utriculata*. Quaking aspen (*Populus tremuloides*) grow immediately adjacent to the wetlands, with Engelmann spruce (*Picea engelmanni*), subalpine fir (*Abies lasiocarpa*), and some lodgepole pine (*Pinus contorta*) located nearby. Slope wetlands are dominated by sedge, but support a greater diversity of species than depressional wetlands, including a variety of forbs

[3] Soil cores were collected by Gina McKee. Soil texture analyses were performed by Robert Bergstrom. Water samples were collected and measurements performed by Kelsey Dean and Gina McKee. Rod Hubbard performed plant biomass and soil respiration measurements. NMR analyses and data analyses were performed by Gina McKee and myself.

and bryophytes (Carsey et al., 2003; LaPerriere Nelson et al., 2011). Two slope wetland sites have scattered Engelmann spruce and subalpine fir, but none have aspen.

4.2.2 Sample collection and analysis

Cores were extracted from two sites in each wetland using a 6-cm diameter steel corer with polyethylene terephthalate liners (Giddings Machine Company, CO). In depressional wetlands, sites were located in the center, lowest part of the wetland (L) and midway (M) between the center and edge. In slope wetlands, site locations were midslope (M) and lower (L). Soil color and evidence of redoximorphic features were recorded and organic and mineral layer depths measured on the intact soil cores. The cores were then divided into 10-cm increments, weighed, air dried, sieved to <2 mm and ground using a ball mill prior to analyses. Soil texture was determined using the hydrometer method (Gavlak et al., 2003). Organic and mineral horizons were defined according to Soil Survey Staff (1999), assuming all soils were saturated for >30 days of the year. Soil Fe, Al, and Ca concentrations were measured using inductively-coupled plasma optical emission spectroscopy (ICP-OES). Samples were prepared as follows: 1 g of dried sample was digested with 5 mL HNO_3 and 5 mL $HClO_4$ at 125 °C until the volume was reduced to 5 mL, then at 200 °C for 2 hrs. Samples were cooled, then diluted to 50 mL. Analysis was performed on a PerkinElmer Optima 7300 DV and data processed in Winlab32 software (PerkinElmer, Inc., Waltham, MA). Total carbon and nitrogen were analyzed by dry combustion on a LECO Tru-Spec CN analyzer (Leco Corp., St. Joseph, MI, USA).

Wetland porewater was sampled from May to September of 2012 from groundwater wells installed at the middle and lower elevation sites in each wetland. Wells were constructed from slotted 2.54-cm diameter polyvinyl chloride (PVC) pipe, sealed at the base and inserted to a depth of 100 cm. Slots extended from about 50-100 cm depth from the ground surface. The wells were capped to limit inputs from surface water and precipitation.

Well water sampling was conducted in a similar method to that described in LaPerriere Nelson (2011). Briefly, wells were purged with a hand pump and allowed to refill with fresh porewater prior to analysis. Dissolved oxygen (DO), reduction oxidation (redox) potential, and temperature measurements were taken using a handheld meter immediately after sampling (results shown in Figure D.1 and Figure D.2). Samples were collected in clean glass bottles for dissolved organic carbon (DOC) analyses and in clean plastic bottles for inorganic ion concentrations and pH. Samples were stored at 4 °C and filtered prior to analysis.

Anion concentrations were determined from ion chromatography using a Dionex AS12A anion-exchange column, an AG12A guard column, and conductivity detection. DOC was determined by high-temperature combustion catalytic oxidation using a Shimadzu TOC-V_{CPN} total organic carbon analyzer (Shimadzu Corporation, Columbia, MD).

Peak herbaceous biomass (annual graminoid and forb growth in August) was clipped from 1 m^2 sample quadrats, dried for 48 hours at 60 °C and weighed. Carbon dioxide flux measurements were collected twice a month from May to September, 2012, by Rob Hubbard.

4.2.3 ^{13}C nuclear magnetic resonance (NMR) spectroscopy

Soil samples of 0-50 cm depth from the middle site at each wetland were analyzed using solid state ^{13}C cross polarization magic angle spinning (CP-MAS) NMR spectroscopy. All samples except for those from the S3-M core were simply dried and ground prior to analysis. The samples from the S3-M core were treated with hydrofluoric acid (HF) prior to analysis to remove paramagnetic material (Schmidt et al., 1997; Smernik and Oades, 2002). These latter samples were prepared and analyzed in a separate batch, and due to unforeseen circumstances, the remaining samples could not be treated prior to analysis. Though several studies have examined whether HF treatment alters the composition of soil organic matter by removal of compound classes that selectively interact with minerals, this issue remains the subject of ongoing scientific debate (Hamdan et al., 2012; Sanderman et al., 2017).

Integration results from the spectra gathered from HF-treated S3 samples followed the same trends as those for the other two slope wetlands, suggesting HF treatment did not cause preferential loss of mineral-bound functional groups.

HF treatment of the S3 samples was conducted as follows: 50 ml of 10% v/v HF was added to 5 g of dry, sieved and ground soil, shaken for 2 hours, and filtered through a 0.2 μm Teflon filter twice. The method was repeated using a 5% v/v HF solution. The soil was rinsed with 18.2 MΩ deionized water (EMD Millipore) three times and then dried in an oven at 40 °C until the mass remained constant. Total mass loss was about 15%.

Vegetation samples from tree litter and grass and sedge leaves were also dried, ground and analyzed using the same instrumental methods as the soil samples. Further details and results are described in Appendix D.

All soils were analyzed at the Environmental Molecular Sciences Laboratory (EMSL) at the Pacific Northwest National Laboratory. 1-D CP-MAS experiments were performed on a 300 MHz Varian instrument operating with a ^{13}C resonance of 400 MHz and a ^{1}H resonance of 100 MHz. Between 30-90 mg of sample was packed in a 4 mm zirconia rotor and spun at 13 kHz at the magic angle (54.78°). The pulse sequence used a ramped pulse applied to the proton for 4 μs before transfer to the ^{13}C nuclei with a contact time of 1 sec. The recycle delay was optimized for each sample between 1-10 sec. Data acquisition used a time domain of 10,000 data points, followed by processing using the Varian vnmrj software, and the application of 1 Hz line broadening of the free induction decay.

Chemical shifts were calibrated using hexamethyl benzene phasing, and the background was subtracted prior to integration. Chemical shift regions were integrated to correspond to broad functional group classifications of 0-45 ppm for alkyl C, 45-110 ppm for O-alkyl C, 110-160 ppm for aromatic C and 160-190 ppm for carbonyl and amide C (Rumpel et al., 2002; Knicker, 2011) (example spectra with integration regions shown in Figure D.3). The ratio of alkyl to O-alkyl C was used to

estimate the extent of decomposition within wetland soil profiles (Baldock et al., 1997), where vegetation is constant.

4.2.4 Carbon dating and $\delta^{13}C$ analysis

Soil samples were selected from surface, intermediate, and basal depths from two sites within a slope wetland (S3-M and S3-L) and one site within a depressional wetland (D2-L) to measure ^{14}C age and $\delta^{13}C$. Radiocarbon dating was completed at Beta Analytic (Miami, FL) using accelerator mass spectrometry (Fifield, 1999). Prior to analysis, samples were air dried and sieved to 2 mm, roots were manually removed, and samples were ground using a ball mill. Samples were then pretreated at Beta Analytic according to standard protocols and resulting spectra were corrected using tree-ring data (Talma and Vogel, 1993). OxCal 4.3 (Bronk Ramsey, C., 2001) was used to calibrate samples with the IntCAL13 (Reimer et al., 2013) calibration curve. I report uncalibrated age, $^{13}C/^{12}C$ ratio, 95.4% probability range, mean and median calibrated age, and 1 sigma error on mean calibrated age in yr BP for each sample.

4.2.5 Calculations and statistical analyses

Bulk density was estimated using the approximate value of 0.224 g cm^{-3} for organic soil horizons and calculated using an estimate for mineral soils according to Rawls (1983) (details in Appendix D). Soil organic carbon stocks (g m^{-2}) were calculated for each soil layer based on data for ~10 cm core samples using the following equation (Gattinger et al., 2012):

$$SOC_{stock} = BD \text{ x } SOC\% \text{ x } D \quad (1)$$

where *BD* is the bulk density in g m^{-3}, SOC% is in g C per 100 g soil, and *D* is the thickness of the soil layer in m.

Statistical comparisons via Wilcoxon rank sum tests were performed using the R statistical package (R Core Team, 2018). Reported p-values less than 0.01 were considered significant.

Table 4.1. Soil texture, soil and water chemistry, and plant biomass values (mean and 1 standard deviation) for sites in three of each wetland class

	Soil texture			Metals in soil			Aqueous		C input
	Sand[a]	Silt[a]	Clay[a]	Fe[b]	Al[b]	Ca[b]	pH[c]	DOC[c]	Plant biomass[d]
Units	%	%	%	g kg^{-1}	g kg^{-1}	g kg^{-1}		mg L^{-1}	g m^{-2}
Depressional	44.3 (10.1)	26.6 (9.5)	29.7 (10.1)	17.5 (3.8)	54.1 (18.6)	6.10 (1.1)	6.04 (0.40)	44.4 (20.9)	514 (165)
Slope	56.7 (6.9)	24.6 (4.4)	18.6 (5.2)	20.6 (5.1)	36.2 (15.4)	11.9 (7.4)	6.71 (0.44)	5.58 (4.48)	167 (83)
p-value	0.0003	>0.05	<0.0001	0.0052	<0.0001	0.0003	<0.0001	<<0.0001	<0.0001

[a] n = 46 and 32 for depressional and slope wetlands, respectively
[b] n = 40 and 39 for depressional and slope wetlands, respectively
[c] n = 34 and 23 for depressional and slope wetlands, respectively
[d] n = 12 and 12 for depressional and slope wetlands, respectively

4.3 Results

4.3.1 Soil, water, and site properties

Soil texture varied between the two wetland classes, with mineral layers in depressional wetlands having significantly more clay (Wilcoxon rank sum test: $p < 0.0001$) and significantly less sand ($p < 0.0005$) than slope wetlands (Table 4.1). Inorganic soil chemistry also differed, with significantly higher Al content in depressional wetlands ($p < 0.0001$) and substantially higher Fe and Ca content in slope wetlands ($p < 0.01$ and $p < 0.0005$, respectively).

The two wetland classes did not differ substantively in mean inorganic aqueous chemistry, and values for anoxic indicators (e.g. dissolved oxygen and redox) did not differ substantially between wetland classes (Figure D.1 and Figure D.2). In both wetland classes, reduction potentials of well-water samples collected from 50 – 100 cm depth varied from about -425 to 350 mV. Throughout the season, 90% of measurements in depressional wetlands and 100% of measurements in slope wetlands were below 300 mV, indicating suboxic and anoxic conditions throughout most of the growing season. Dissolved oxygen (DO) varied between 0.69 and 7.85 mg/L without much trend over the course of the season in slope wetlands. In the depressional wetlands, it generally decreased down to about 0.5-2 mg/L, then increased dramatically shortly before the site desiccated. In all wetlands except for S1, SO_4^{2-} concentrations remained below 5 mg/L for most of the summer. NO_3^- values were very low,

often measuring below detection limits in both wetlands. pH values in depressional wetlands were slightly but consistently lower than in slope wetlands (pH 6.04 vs. 6.71, $p < 0.0001$).

Vegetation cover differed among wetlands. Grass and sedge species covered most of the area in the depressional wetlands, with several aspen growing at the margins (Figure D.4A). Slope wetlands hosted greater plant diversity, with substantial bryophyte coverage and numerous forbs mixed in with grasses and sedges. Spruce and fir comprised the dominant tree species around the perimeter, and a few individuals grew within the wetlands (Figure D.4B) (LaPerriere Nelson et al., 2011). Primary productivity also differed substantially between wetlands. On average, the depressional wetlands produced about three times as much plant biomass per square meter as the slope wetlands during the study period (Table 4.1). In addition to greater aboveground plant productivity and generally higher SOC content, the depressional wetlands had substantially higher mean dissolved organic carbon concentrations (Table 4.1, $p = 3.8 \times 10^{-16}$). Mean soil respiration rates as measured by CO_2 flux were comparable for the two wetland classes (Figure D.5).

4.3.2 Organic carbon quantity

Organic carbon content was higher in the depressional wetlands (164 ± 19 g C kg^{-1}) than in slope wetlands (98 ± 24 g C kg^{-1}). Surface soil layers of both wetland classes had high soil organic carbon (SOC) content, from about 20-40% SOC (Figure 4.2). Generally, carbon content decreased with depth, but declined more rapidly and consistently for slope wetlands. By about 50 cm below the surface, carbon in the slope wetlands dropped to about 0%. In the depressional wetlands, SOC generally remained higher at depth, with as much as 20% SOC at 60-70 cm below the surface. However, the SOC trends with depth were less uniform for depressional wetlands; at some sites, SOC decreased down to 3% by 50-60 cm.

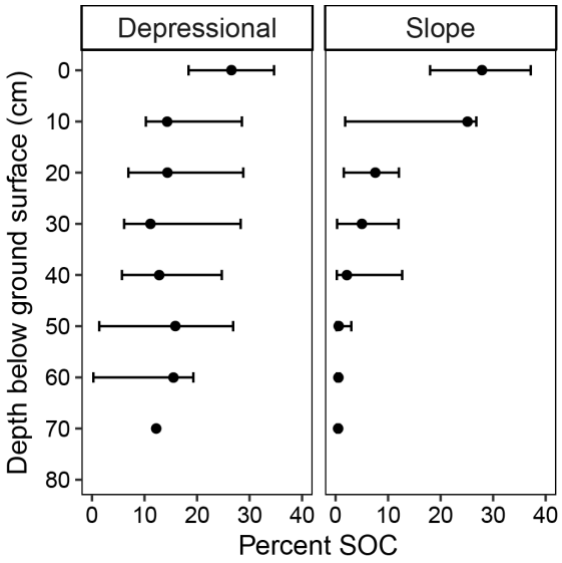

Figure 4.2. Percent soil organic carbon (SOC) means (dots) and ranges (error bars) by depth from both the middle and lower sites in three wetlands of each class.

Estimates of C stocks yielded only slightly larger quantities for depressional wetlands (27.8 ± 5.7 kg m^{-2}) than slope wetlands (21.7 ± 8.0) (Table 4.2). Due to the small sample size (three wetlands of each type), it is difficult to discern the significance of this difference. However, the data clearly show a difference in where the two wetland classes stored carbon. Depressional wetlands stored about four times as much carbon in organic horizons than in mineral horizons. Their organic horizons also contained about twice as much carbon as those in slope wetlands. Slope wetlands stored approximately equal amounts of carbon in mineral and organic horizons, but stored about 70% more carbon in mineral horizons than depressional wetlands. Since soil cores were only taken to about 1-meter depths, there may be some sites, especially in the depressional wetlands, for which the complete mineral layer was not sampled. This may have led to an underestimate of mineral C stocks in depressional wetlands.

Table 4.2. Carbon stock estimates (mean and 1 standard deviation) by wetland class for n = 3 wetlands

	Total	Organic layer	Mineral layer
Units	kg C m^{-2}	kg C m^{-2}	kg C m^{-2}
Depressional	27.8 (5.7)	24.4 (0.6)	6.0 (4.7)
Slope	21.7 (8.0)	11.7 (4.5)	10.0 (3.6)

4.2.3 Organic carbon quality

C:N ratios have been used as a general index of litter quality and degree of decomposition for nearly a century (Waksman, 1924). Overall, C:N ratios ranged from about 8 to 24. They varied little with depth for both wetland classes, and each class had approximately the same C:N ratio in surface and deep soils (Table D.3). Distributions of carbon functional groups (from ^{13}C CP-MAS NMR measurements) showed distinct trends with depth (Figure 4.3). In most profiles studied, a marked change in carbon chemistry occurred around 20 cm below the ground surface, regardless of horizonation. For this reason, results from integration of ^{13}C CP-MAS NMR spectra are displayed as averages of "surface" samples (0-20 cm) and "deep" samples (20-50 cm).

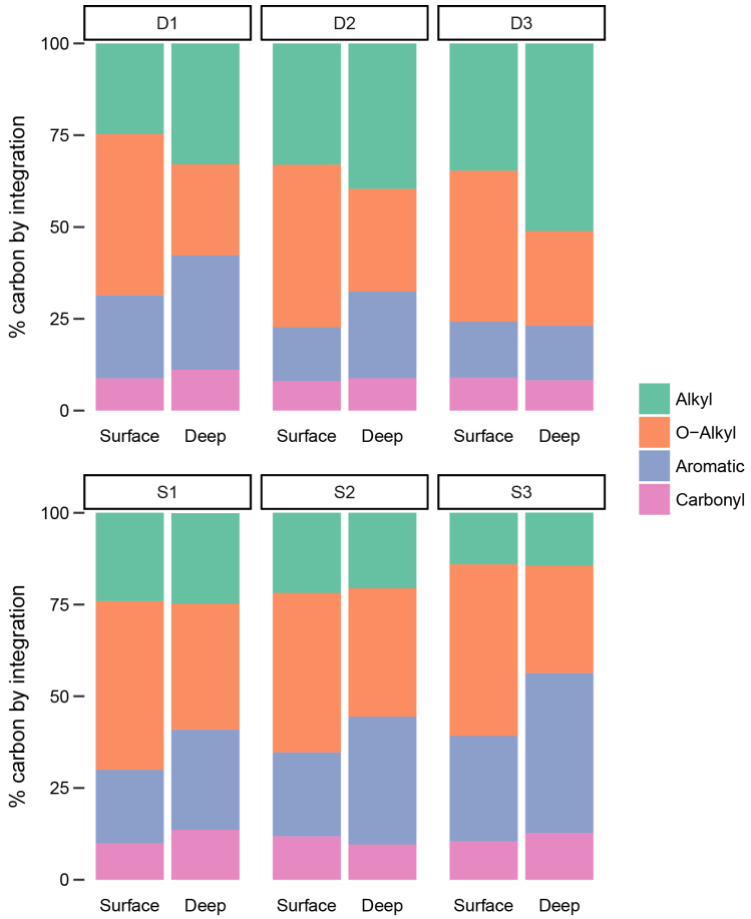

Figure 4.3. Integration results of 13C CP-MAS NMR spectra. Values shown are means from surface (0-20 cm) and deep (20-50 cm) soil samples from the middle sites in three wetlands of each class. Integration regions are alkyl C (0-45 ppm), O-alkyl C (45-110 ppm), aromatic C (110-160), and carbonyl C (160-190).

In surface soils of both slope and depressional wetlands, O-alkyl C, which includes carbohydrate compounds such as cellulose and hemicellulose, dominated (34-39% total C by integration). Deeper in the horizon (20-50 cm), alkyl C content decreased and the relative proportion of aromatic C increased. Aromatic C groups in soils commonly include lignin and tannins. The switch in dominance of O-alkyl C and aromatic C with depth was consistent and obvious for all slope wetlands, but the depressional wetlands demonstrated a different trend. Alkyl C constituted a larger proportion in both surface and deep layers, and it increased with depth. This group represents primarily aliphatic compounds such as cutins and suberins (leaf and root waxes) (Nierop, 1998; Simpson et al., 2008), but can also include microbial membrane lipids (Lorenz et al., 2007). Carbonyl C, which includes amides and carboxylic groups in organic and amino acids, represented much lower proportions (< 15%) of total C and varied little with depth or between wetland classes.

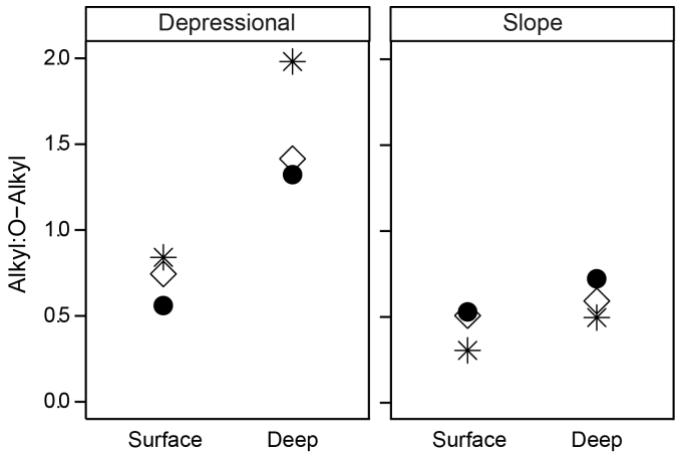

Figure 4.4. Means of alkyl:O-alkyl ratios for surface (0-20 cm) and deep (20-50 cm) soil samples from the middle sites in three wetlands of each class. Circles (●) represent D1 and S1, diamonds (◇) D2 and S2, and stars (✳) D3 and S3.

The ratio of the relative intensities of the alkyl C and O-alkyl C regions of the ^{13}C NMR spectra has been shown to serve as an index of the extent of decomposition of organic matter from soils and litter with a constant vegetational background (Baldock et al., 1997). In both slope and depressional wetlands, the alkyl : O-alkyl (A:O-A) ratio increased with depth (Figure 4.4). Values were slightly higher for surface soil in depressional wetlands, and substantially higher at depth, corresponding with

a much greater increase in the A:O-A ratio from surface to deeper soil horizons compared to the slope wetlands.

4.4 Discussion

4.4.1 Organic carbon storage

Hydrogeomorphic setting likely influenced the higher C content in the depressional wetlands compared to the slope wetlands by regulating C inputs, storage capacity, and processing. Carbon input estimates in the form of plant biomass measurements demonstrated that depressional wetlands supported about three times more plant growth than slope wetlands (Table 4.1). This finding is consistent with the observations of Mitsch et al. (1991), who found higher productivity among wetlands with seasonally pulsing hydroperiods compared to those with slowly flowing water. In another study, Bernal and Mitsch (2012) noted greater C sequestration in isolated depressional wetland communities compared to flow-through riverine wetlands, attributing the difference to primarily differences in vegetation. As topographic low points, depressions may receive groundwater, interflow and surface runoff carrying nutrients, dissolved organic carbon (DOC), and fine sediment from adjacent uplands. Because outflow via groundwater is usually very slow, the deposition of these solutes may increase C and nutrient concentrations as well as soil fertility in depressional wetlands. Slope wetlands, in contrast, are characterized by primarily downslope water flow, which originates dominantly from groundwater and passes across the surface or just below the surface. Flowing water can transport DOC downslope, preventing considerable accumulation of DOC (Rosenbloom et al., 2001). Nutrients may be retained or exported from slope wetlands, depending on soil composition, flow, and vegetation (Harms and Ludwig, 2016). Concentrations of the macronutrients N, P, and K differed irrespective of wetland type (data not shown), so higher plant productivity in depressional wetlands is likely due to factors other than nutrient enrichment, such as hydroperiod. Though import

and export of DOC were not measured, average DOC concentrations within depressional wetlands were about eight times higher than in slope wetlands, confirming depressional wetlands retain higher amounts of dissolved carbon (Table 4.1). In total, these results indicate depressional wetlands receive higher C inputs than slope wetlands, which may contribute to their higher C content.

Once organic carbon enters a wetland, it can be exported, stored, or processed. Based on the hydrogeomorphic characteristics of these wetlands, it can reasonably be assumed that export occurs to a greater extent from slope wetlands than from depressional wetlands. Storage is a function of physical and chemical stabilization as well as decomposition rates. Clays and Al and Fe oxides have high surface areas that can adsorb and occlude organic carbon, protecting it from decomposition (Oades, 1988; Schimel et al., 1994; Sposito et al., 1999). The hydrogeomorphic setting of depressional wetlands promotes deposition and retention of fine sediments (e.g. clays) transported from upland soils (Rosenbloom et al., 2001). Indeed, the soils in depressional wetlands had significantly more clay than those in slope wetlands (29.7% vs. 18.6 %, $p < 0.0001$). This higher clay content could be partially responsible for the greater carbon storage observed in depressional wetlands, although it likely does not play a substantial role, since much more C was stored in organic layers than mineral layers in these wetlands. Erosion of hillslope soils preferentially removes fine particles, which can diminish the proportion of adsorptive clay minerals (Rosenbloom et al., 2001). The slope wetlands in this study had coarser soil textures compared to the depressional wetlands (56.7% vs. 44.3% sand, $p = 0.0003$), but slightly higher Fe content (20.6 vs. 17.5 g kg^{-1}, $p = 0.0052$). Iron oxides can contribute to OC stabilization, as evidenced by positive correlations between Fe oxide and OC concentrations in soils and sediments (Kaiser and Guggenberger, 2000; Lalonde et al., 2012) and negative correlations with OC age (Torn et al., 1997; Eusterhues et al., 2003). Although the data do not distinguish among Fe oxidation states, mottling in soil cores from slope wetlands was visually observable, indicating the presence of Fe oxides. Sorption of OC on these minerals may contribute to the relatively high OC

content of some mineral layers in the slope wetlands—up to 11% OC in samples from 10-50 cm deep (Figure 4.2).

Sorption is likely a more important process in slope wetlands, where DOC that is not stabilized by minerals can be both decomposed by microbes and removed by downslope water flows. In depressional wetlands, outflow is much slower, and DOC has much longer residence time. The dominant vertical fluctuations in the water tables of depressional wetlands may also facilitate translocation of DOC deeper into the soil column, where it may associate with the mineral layer (Kögel-Knabner et al., 2010).

Table 4.3. $^{13}C/^{12}C$ ratio, uncalibrated ^{14}C age, 95.4% probability range, mean and median calibrated age, and corresponding horizons of soil samples from D2 (central/lower site (L)) and S3 (middle (M) and lower (L) sites)

Site	Depth	Soil Horizon	$^{13}C/^{12}C$	Uncalibrated ^{14}C age	95.4% range	Mean calibrated age (error)[b]	Median calibrated age
	(cm)		(‰)	(yr BP)	(yr BP)	(yr BP)	(yr BP)
D2-L	0-10	Organic	-27.4	101.8 ± 0.4 pMC[a]	modern	modern	modern
	40-50	Organic	-26.9	1163 ± 30	1178-983	1087 (56)	1087
	90-100	Mineral	-26.3	2945 ± 30	3207-2998	3100 (51)	3104
S3-M	10-20	Organic	-25.4	105 ± 30	269-13	132 (78)	113
	40-50	Mineral	-24.8	3006 ± 30	3331-3076	3196 (59)	3194
	110-120	Mineral	-24.9	3984 ± 30	4525-4410	4465 (39)	4473
S3-L	10-20	Organic	-26.4	175 ± 30	294-modern	160 (88)	179
	20-30	Mineral	-25.0	1471 ± 30	1406-1306	1357 (30)	1356
	70-80	Mineral	-24.7	3882 ± 30	4417-4193	4322 (58)	4326

[a] pMC = percent modern carbon
[b] 1 sigma error on mean calibrated age

In many soils, long-term carbon storage occurs in mineral layers, where sorption, co-precipitation and physical occlusion of organic matter deter microbial decomposition. Radiocarbon dates of samples selected from one depressional (D2) and one slope (S3) wetland generally showed this to be the case. Calibrated median ^{14}C ages in surface organic layers of 0-10 or 10-20 cm depth ranged from modern to 180 years before present (yr BP, Table 4.3), suggesting fresh inputs and rapid cycling regulated C located in these layers. Radiocarbon age increased with depth in all profiles tested. Samples from mineral layers at intermediate depths (20-30 and 40-50 cm) from two cores in the slope wetland were substantially older than in the surface layer, 1356 and 3194 yr BP respectively. In the

depressional wetland, the intermediate depth sample was taken from an organic layer, which despite its low mineral content, contained quite old carbon (1087 yr BP). This old age is consistent with other peat soils, in which saturated and anoxic conditions hinder decomposition and preserve carbon, even in organic layers, for hundreds of years (Tfaily et al., 2014). Deep samples from the slope wetland had median ^{14}C carbon ages of around 4400 yr BP, while the one taken from the depressional wetland was about 1000 years younger.

A number of factors could contribute to the faster turnover of deep carbon in the depressional wetland. One possibility is that the dropping water table over the course of the season allows young DOC from upper layers to translocate deeper into the soil column, reducing the median age of the deep carbon. In slope wetlands, downhill flow dominates hydrodynamics, potentially limiting vertical translocation of DOC and removing any organic carbon that is not protected by minerals. Once the organic carbon interacts with minerals, it likely remains protected for long periods of time. This latter explanation is consistent with the very small but stable C fraction found at the lower depths of the slope wetland (Figure 4.2, Table 4.3).

Decomposition rates in wetlands are highly dependent on hydrology, which exerts control on oxygen levels. Despite higher plant inputs in depressional wetlands, they maintained approximately the same soil respiration rates (Figure D.5), providing further indication that depressional wetlands retained more carbon than slope wetlands. In depressional wetlands, the higher clay content likely limits oxygen infiltration and promotes water retention, and along with the long hydraulic residence time and high organic matter content, should create anaerobic conditions. Bulk redox potential and dissolved oxygen (DO) measurements of porewater indicated reducing conditions existed while the wetland was saturated (Figure D.1 and Figure D.2). As the water table declined below the sampling well, oxygen levels increased, but redox potentials remained low. The lack of correlation between redox potential and DO levels under drier conditions may be explained by the presence of anoxic

microsites. Bulk DO measurements have been shown to poorly characterize the extent of oxidation in upland soils (Keiluweit et al., 2018), demonstrating that high values do not preclude the existence of anaerobic activity. Moreover, fine texture and high carbon content, both characteristic of the depressional wetland soils, correlate with anoxic volume, reducing conditions, and decreased mineralization rates (Keiluweit et al., 2017; Noël et al., 2017; Keiluweit et al., 2018). Plant roots may also contribute to anaerobic microsite formation through root respiration (Bidel et al., 2000), stimulation of microbial respiration (Keiluweit et al., 2015a), or the release of organic reductants (Fimmen et al., 2008). The likely persistence of anoxic microsites under dry conditions may keep decomposition rates low, facilitating accumulation of organic carbon in depressional wetlands.

4.4.2 Processing of organic carbon

Carbon composition data from ^{13}C NMR further demonstrates the influence of hydrogeomorphic setting on carbon decomposition processes. In both wetland classes, the surface layers contained high proportions of O-alkyl C, such as that in the cellulose and hemicellulose present in fresh plant litter, and is consistent with previous reports for both wetland and upland soils (Rumpel et al., 2002; Jokic et al., 2003; Grover and Baldock, 2010; Grover and Baldock, 2013; Luan et al., 2014). These compounds typically decompose relatively quickly (Berg and McClaugherty, 2014; McKee et al., 2016), even in anaerobic environments under thermodynamic limitations (Keiluweit et al., 2016). Their abundance in the upper soil layers likely indicates frequent input of new plant material relative to decomposition rates. The relative contribution of the O-alkyl fraction to the total organic carbon pool decreased with depth, suggesting it entered the soil through the upper layers of the profile and that most of it decomposed before it had the opportunity to translocate deeper (Kaiser and Kalbitz, 2012; Cotrufo et al., 2015; Leinemann et al., 2018).

In two of the three depressional wetlands, the surface layers also contained large quantities of C in the alkyl region, likely representing substantial input from leaf cutins or root suberins (Nierop,

1998; Simpson et al., 2008). Greater representation of this fraction in the surface soils of depressional wetlands suggests differences in litter chemistry may exist between the two wetland classes. Plant cover and diversity at the sites differed noticeably—depressional wetlands hosted almost exclusively grasses and sedges, with aspen dominating the tree species at the perimeter, while slope wetlands supported a more diverse set of plant species and lacked aspen at their edges. Leaf litter from these deciduous trees contains high proportions of alkyl C relative to coniferous fir and spruce litter and leaves from grasses and sedges (Figure D.6). Consequently, the presence of aspen around depressional wetlands may lead to aliphatic-rich litter compared to the slope wetlands, which are surrounded by primarily spruce and fir trees. Vegetation type has been shown to influence soil organic matter chemistry (Quideau et al., 2000; Quideau et al., 2001; Ussiri and Johnson, 2003) and decomposition rates (Keiluweit et al., 2015b), and this explanation may plausibly account for the differences observed in the carbon chemistry of the surface soils. Alternatively, the submersion of surface soils in depressional wetlands for substantial portions of the growing season could lead to longer periods of anaerobic conditions compared to the surface layers in the slope wetlands, promoting preferential decomposition of more oxidized compounds.

For all of the depressional wetlands, alkyl C made up an increasing proportion of total carbon with depth. This trend is consistent with numerous studies showing persistence of aliphatic compounds in saturated subsoils (Tfaily et al., 2014; Heller et al., 2015; Noël et al., 2017). The long hydraulic residence time, high SOC content, and high clay content of the subsoils in the depressional wetlands likely lead to more reducing conditions than in the slope wetlands (Boye et al., 2017; Keiluweit et al., 2018). Under anaerobic conditions, the use of highly reduced aliphatic compounds as electron donors in microbial respiration becomes thermodynamically unfavorable (Keiluweit et al., 2016; Boye et al., 2017; Keiluweit et al., 2017). Microbes utilizing Fe(III) or SO_4^{2-} as terminal electron acceptors may be unable to couple their reduction with the oxidation of reduced aliphatic substrates,

leading to preferential preservation of these compounds. Even as the water table dropped over the course of the season, the high organic carbon and clay content of the depressional wetland soils may have preserved anaerobic microsites where decomposition of aliphatic compounds remained unfavorable. Indeed, one study found that in moist upland soils with even lower clay content than the wetland soils examined here, anaerobic microsites composed approximately 14-85% of the total pore volume (Keiluweit et al., 2018). Thus, anaerobic decomposition and preferential preservation of aliphatic carbon could continue all season in the depressional wetlands.

In contrast, alkyl C represented a smaller proportion of total carbon in the surface soils of slope wetlands and remained fairly constant with increasing depth (Figure 4.3). This trend has been observed in soil samples from a drained peat, where oxygen permeated deeper into the profile (Heller et al., 2015). The slope wetlands remained saturated for most of the growing season, but experienced frequent oscillations in DO concentrations, which have been shown to accelerate the decomposition of refractory compounds relative to prolonged anaerobic or aerobic conditions (Reddy and Patrick, 1975; Hulthe et al., 1998). These fluctuating DO levels may have enhanced decomposition of aliphatic compounds in the slope wetlands compared to the depressional wetlands.

The relative proportion of the aryl C region, which includes aromatic compounds such as lignins, tannins, and pyrolyzed organic matter, increased with depth in all wetlands but D3 (Figure 4.3). In general, aromatic compounds take longer to decompose, and their accumulation in deeper soils is well documented (Leifeld et al., 2012; Grover and Baldock, 2013; Berg and McClaugherty, 2014; Tfaily et al., 2014). A possible explanation for their persistence in deeper layers, especially in slope wetlands, could be the preferential sorption of aromatics to minerals, which has been broadly reported (Kaiser and Guggenberger, 2000; Kramer et al., 2012; Hernes et al., 2013; Galindo and Del Nero, 2014; Avneri-Katz et al., 2016; Young et al., 2018). The preferential sorption of carboxylic

groups (Gu et al., 1994; Kaiser and Guggenberger, 2000; Kramer et al., 2012) may also explain their persistence in the more mineral-rich slope wetlands.

The quantitative indexes of decomposition—alkyl C: O-alkyl C (A:O-A) and C:N ratios—provide divergent results as to the extent of decomposition with depth in the two wetland classes. The A:O-A ratio is a well-established method for estimating the extent of decomposition when vegetation is constant (Baldock et al., 1997; Leifeld et al., 2012; Incerti et al., 2017). Because vegetation differs among wetlands, only values within sites can be compared. In depressional wetlands, the A:O-A ratio increased substantially (90-136%) between the surface and deeper layers (Figure 4.4), reflective of both the decrease in O-alkyl C and increase in alkyl C with depth (Figure 4.3). Slope wetlands had a much smaller increase in this metric, since O-alkyl C decreased but alkyl C remained fairly constant between layers. The difference in the magnitude of the increase may indicate less decomposition occurred in the slope wetlands, or that its hydrogeomorphic conditions promoted decomposition of different compound classes. Carbon isotope measurements generally support the overall trend of increasingly decomposed organic material with depth for both wetlands. For the three profiles measured, $\delta^{13}C$ values increased by 0.5–1.7‰ (Table 4.3), suggesting an increase in microbial biomass relative to plant biomass between surface and deep soil layers (Taylor et al., 2003; Tfaily et al., 2014).

C:N ratios displayed no consistent trend with depth and varied little among wetlands (Table D.3). This lack of change contrasts results from some studies of wetlands showing decreasing C:N ratio with depth (Vardy et al., 2000; Tfaily et al., 2014). However, others have observed little difference in C:N values between surface and basal samples from wetlands (Grover and Baldock, 2010). Indeed, the reliability of this metric has been contested, and several studies have found ratios of certain C functional groups in litter and decaying OM, such as the A:O-A ratio, to be better indicators of carbon quality and decomposition rates (Leifeld et al., 2012; Bonanomi et al., 2013; Incerti et al., 2017).

Evidently, the bulk index of C:N poorly conveys trends in decomposition in comparison to the compositional measure of A:O-A.

4.5 Conclusions and Implications

The findings presented in this work demonstrate subtle yet distinct differences in carbon storage and processing in subalpine wetlands from two hydrogeomorphic classes: depressional and slope. Though the estimated amount of carbon stored in depressional wetlands was only slightly greater than that estimated for slope wetlands, the locations of SOC stocks were quite different. Approximately 88% of C stocks in measured soils from depressional wetlands resided in potentially younger organic layers, while almost 50% of C stocks in slope wetlands were located in mineral layers. This implies that though somewhat larger, C stocks in depressional wetlands likely turn over faster than those in slope wetlands and represent a less stable SOC pool. However, a more accurate understanding of C stocks and turnover in these wetlands would require a larger set of study sites, radiocarbon data, and a better understanding of C protection within microsites. In addition, these estimates are limited by the depths to which samples could be taken. Depressional wetland soils in particular were very deep and these estimates may not include the full extent of SOC-bearing layers.

According to compositional data from ^{13}C NMR analyses, the two wetland classes also process carbon differently. The surface layers of slope wetlands were dominated by labile carboxylic compounds while those of depressional wetlands also contained large proportions of aliphatic carbon, likely due to the differences in vegetation composition between wetlands. In deeper soils, aromatic C dominated total C in slope wetlands while aliphatic C increased in proportion in depressional wetlands. It seems likely that more extensive anaerobic conditions existed in the depressional wetlands and led to the accumulation of aliphatic C, but from my data, it is not possible to discriminate the exact mechanisms contributing to these differences. Further investigation of chemical composition of plant

inputs, microbial community structure and activity, redox gradients, concentrations of electron acceptors, and extent of mineral sorption and physical protection could elucidate the biochemical and physical pathways responsible for the differences in SOC chemistry between these wetlands.

Methods of carbon accounting rarely consider differences in hydrogeomorphic wetland classes, assuming substantial similarity in C stocks of wetlands in broad categories (Nahlik and Fennessy, 2016). The results presented here suggest it may be necessary to differentiate among hydrogeomorphic classes of wetlands, especially when considering C processing and turnover times.

REFERENCES

Alstatt D. and Miles R. L. (1983) *Soil survey of Grand County area, Colorado*., USDA Soil Conservation Service and Forest Service and Colorado Agriculture Experiment Station, U.S. Government Printing Office.

Avneri-Katz S., Young R. B., McKenna A. M., Chen H., Corilo Y. E., Polubesova T., Borch T. and Chefetz B. (2016) Adsorptive fractionation of dissolved organic matter (DOM) by mineral soil: Macroscale approach and molecular insight. *Org. Geochem.* Available at: http://dx.doi.org/10.1016/j.orggeochem.2016.11.004.

Baldock J. A., Oades J. M., Nelson P. N., Skene T. M., Golchin A. and Clarke P. (1997) Assessing the extent of decomposition of natural organic materials using solid-state 13C NMR spectroscopy. *Soil Res.* **35**, 1061–1084.

Berg B. and McClaugherty C. (2014) *Plant Litter: Decomposition, Humus Formation, Carbon Sequestration*. 3rd ed., Springer Berlin Heidelberg, Berlin, Heidelberg.

Bernal B. and Mitsch W. J. (2008) A comparison of soil carbon pools and profiles in wetlands in Costa Rica and Ohio. *Ecol. Eng.* **34**, 311–323.

Bernal B. and Mitsch W. J. (2012) Comparing carbon sequestration in temperate freshwater wetland communities. *Glob. Change Biol.* **18**, 1636–1647.

Bidel L. P. R., Renault P., Pagès L. and Rivière L. M. (2000) Mapping meristem respiration of Prunus persica (L.) Batsch seedlings: potential respiration of the meristems, O2 diffusional constraints and combined effects on root growth. *J. Exp. Bot.* **51**, 755–768.

Bonanomi G., Incerti G., Giannino F., Mingo A., Lanzotti V. and Mazzoleni S. (2013) Litter quality assessed by solid state 13C NMR spectroscopy predicts decay rate better than C/N and Lignin/N ratios. *Soil Biol. Biochem.* **56**, 40–48.

Boye K., Noël V., Tfaily M. M., Bone S. E., Williams K. H., Bargar J. R. and Fendorf S. (2017) Thermodynamically controlled preservation of organic carbon in floodplains. *Nat. Geosci.* **10**, 415–419.

Bronk Ramsey, C. (2001) Development of the radiocarbon calibration program. *Radiocarbon* **43**, 355–363.

Carsey K., Kittel G., Decker K., Cooper D. J. and Culver D. R. (2003) *Field guide to the wetland and riparian plant associations of Colorado.*, Colorado National Heritage Program, Colorado State University, Fort Collins, CO.

Cotrufo M. F., Soong J. L., Horton A. J., Campbell E. E., Haddix M. L., Wall D. H. and Parton W. J. (2015) Formation of soil organic matter via biochemical and physical pathways of litter mass loss. *Nat. Geosci.* **8**, 776–779.

Eusterhues K., Rumpel C., Kleber M. and Kögel-Knabner I. (2003) Stabilisation of soil organic matter by interactions with minerals as revealed by mineral dissolution and oxidative degradation. *Org. Geochem.* **34**, 1591–1600.

Fifield L. K. (1999) Accelerator mass spectrometry and its applications. *Rep. Prog. Phys.* **62**, 1223–1274.

Fimmen R. L., Richter D. deB, Vasudevan D., Williams M. A. and West L. T. (2008) Rhizogenic Fe–C redox cycling: a hypothetical biogeochemical mechanism that drives crustal weathering in upland soils. *Biogeochemistry* **87**, 127–141.

Freeman C., Evans C. D., Monteith D. T., Reynolds B. and Fenner N. (2001) Export of organic carbon from peat soils. *Nature* **412**, 785.

Galindo C. and Del Nero M. (2014) Molecular level description of the sorptive fractionation of a fulvic acid on aluminum oxide using electrospray ionization fourier transform mass spectrometry. *Environ. Sci. Technol.* **48**, 7401–8.

Gattinger A., Muller A., Haeni M., Skinner C., Fliessbach A., Buchmann N., Mäder P., Stolze M., Smith P., Scialabba N. E.-H. and Niggli U. (2012) Enhanced top soil carbon stocks under organic farming. *Proc. Natl. Acad. Sci.* **109**, 18226–31.

Gavlak R., Hornek R., Miller R. O. and Kotuby-Amacher J. (2003) *Soil, Plant and Water Reference Methods for the Western Region*., WREP-125.

Grover S. P. P. and Baldock J. A. (2010) Carbon decomposition processes in a peat from the Australian Alps. *Eur. J. Soil Sci.* **61**, 217–230.

Grover S. P. P. and Baldock J. A. (2013) The link between peat hydrology and decomposition: Beyond von Post. *J. Hydrol.* **479**, 130–138.

Gu B., Schmitt J., Chen Z., Liang L. and McCarthy J. F. (1994) Adsorption and desorption of natural organic matter on iron oxide: mechanisms and models. *Environ. Sci. Technol.* **28**, 38–46.

Hamdan R., El-Rifai H. M., Cheesman A. W., Turner B. L., Reddy K. R. and Cooper W. T. (2012) Linking Phosphorus Sequestration to Carbon Humification in Wetland Soils by ^{31}P and ^{13}C NMR Spectroscopy. *Environ. Sci. Technol.* **46**, 4775–4782.

Harms T. K. and Ludwig S. M. (2016) Retention and removal of nitrogen and phosphorus in saturated soils of arctic hillslopes. *Biogeochemistry* **127**, 291–304.

Heller C., Ellerbrock R. H., Roßkopf N., Klingenfuß C. and Zeitz J. (2015) Soil organic matter characterization of temperate peatland soil with FTIR-spectroscopy: effects of mire type and drainage intensity. *Eur. J. Soil Sci.* **66**, 847–858.

Hernes P. J., Kaiser K., Dyda R. Y. and Cerli C. (2013) Molecular trickery in soil organic matter: hidden lignin. *Environ. Sci. Technol.* **47**, 9077–85.

Hulthe G., Hulth S. and Hall P. O. J. (1998) Effect of oxygen on degradation rate of refractory and labile organic matter in continental margin sediments. *Geochim. Cosmochim. Acta* **62**, 1319–1328.

Incerti G., Bonanomi G., Giannino F., Cartenì F., Spaccini R., Mazzei P., Piccolo A. and Mazzoleni S. (2017) OMDY: a new model of organic matter decomposition based on biomolecular content as assessed by 13C-CPMAS-NMR. *Plant Soil* **411**, 377–394.

Johnston C. A. (1991) Sediment and nutrient retention by freshwater wetlands: Effects on surface water quality. *Crit. Rev. Environ. Control* **21**, 491–565.

Jokic A., Cutler J. N., Ponomarenko E., van der Kamp G. and Anderson D. W. (2003) Organic carbon and sulphur compounds in wetland soils: insights on structure and transformation processes using K-edge XANES and NMR spectroscopy. *Geochim. Cosmochim. Acta* **67**, 2585–2597.

Kaiser K. and Guggenberger G. (2000) The role of DOM sorption to mineral surfaces in the preservation of organic matter in soils. *Org. Geochem.* **31**, 711–725.

Kaiser K. and Kalbitz K. (2012) Cycling downwards - dissolved organic matter in soils. *Soil Biol. Biochem.* **52**, 29–32.

Kalbitz K. and Wennrich R. (1998) Mobilization of heavy metals and arsenic in polluted wetland soils and its dependence on dissolved organic matter. *Sci. Total Environ.* **209**, 27–39.

Kayranli B., Scholz M., Mustafa A. and Hedmark Å. (2010) Carbon Storage and Fluxes within Freshwater Wetlands: a Critical Review. *Wetlands* **30**, 111–124.

Keiluweit M., Bougoure J. J., Nico P. S., Pett-Ridge J., Weber P. K. and Kleber M. (2015a) Mineral protection of soil carbon counteracted by root exudates. *Nat. Clim. Change* **5**, 588–595.

Keiluweit M., Gee K., Denney A. and Fendorf S. (2018) Anoxic microsites in upland soils dominantly controlled by clay content. *Soil Biol. Biochem.* **118**, 42–50.

Keiluweit M., Nico P., Harmon M. E., Mao J., Pett-Ridge J. and Kleber M. (2015b) Long-term litter decomposition controlled by manganese redox cycling. *Proc. Natl. Acad. Sci.* **112**, E5253–E5260.

Keiluweit M., Nico P. S., Kleber M. and Fendorf S. (2016) Are oxygen limitations under recognized regulators of organic carbon turnover in upland soils? *Biogeochemistry* **127**, 157–171.

Keiluweit M., Wanzek T., Kleber M., Nico P. and Fendorf S. (2017) Anaerobic microsites have an unaccounted role in soil carbon stabilization. *Nat. Commun.* **8**, 1771.

Kellogg K. S., Shroba R. R., Bryant B. and Premo W. R. (2008) Geologic Map of the Denver West 30' x 60' Quadrangle, North-Central Colorado. Available at: https://pubs.usgs.gov/sim/3000/.

Knicker H. (2011) Solid state CPMAS 13C and 15N NMR spectroscopy in organic geochemistry and how spin dynamics can either aggravate or improve spectra interpretation. *Org. Geochem.* **42**, 867–890.

Knicker H. and Ludemann H. D. (1995) 15 N and 13 C CP-MAS and solution NMR-studies of 15 N enriched plant material during 600 days of microbial degradation. *Org. Geochem.* **23**, 329–341.

Kögel-Knabner I. (1997) 13C and 15N NMR spectroscopy as a tool in soil organic matter studies. *Geoderma* **80**, 243–270.

Kögel-Knabner I., Amelung W., Cao Z., Fiedler S., Frenzel P., Jahn R., Kalbitz K., Kölbl A. and Schloter M. (2010) Biogeochemistry of paddy soils. *Geoderma* **157**, 1–14.

Kramer M. G., Sanderman J., Chadwick O. A., Chorover J. and Vitousek P. M. (2012) Long-term carbon storage through retention of dissolved aromatic acids by reactive particles in soil. *Glob. Change Biol.* **18**, 2594–2605.

Lal R. (2008) Carbon sequestration. *Philos. Trans. R. Soc. Lond. B Biol. Sci.* **363**, 815–830.

Lalonde K., Mucci A., Ouellet A. and Gelinas Y. (2012) Preservation of organic matter in sediments promoted by iron - SI. *Nature* **483**, 198–200.

LaPerriere Nelson M., Rhoades C. C. and Dwire K. A. (2011) Influence of Bedrock Geology on Water Chemistry of Slope Wetlands and Headwater Streams in the Southern Rocky Mountains. *Wetlands* **31**, 251–261.

Lee N., Amy G., Croué J.-P. and Buisson H. (2004) Identification and understanding of fouling in low-pressure membrane (MF/UF) filtration by natural organic matter (NOM). *Water Res.* **38**, 4511–4523.

Leifeld J., Steffens M. and Galego-Sala A. (2012) Sensitivity of peatland carbon loss to organic matter quality. *Geophys. Res. Lett.* **39**. Available at: https://agupubs.onlinelibrary.wiley.com/doi/epdf/10.1029/2012GL051856 [Accessed May 19, 2018].

Leinemann T., Preusser S., Mikutta R., Kalbitz K., Cerli C., Höschen C., Mueller C. W., Kandeler E. and Guggenberger G. (2018) Multiple exchange processes on mineral surfaces control the transport of dissolved organic matter through soil profiles. *Soil Biol. Biochem.* **118**, 79–90.

Lorenz K., Lal R., Preston C. M. and Nierop K. G. J. (2007) Strengthening the soil organic carbon pool by increasing contributions from recalcitrant aliphatic bio(macro)molecules. *Geoderma* **142**, 1–10.

Luan J., Cui L., Xiang C., Wu J., Song H. and Ma Q. (2014) Soil carbon stocks and quality across intact and degraded alpine wetlands in Zoige, east Qinghai-Tibet Plateau. *Wetl. Ecol. Manag.* **22**, 427–438.

McKee G. A., Soong J. L., Caldéron F., Borch T. and Cotrufo M. F. (2016) An integrated spectroscopic and wet chemical approach to investigate grass litter decomposition chemistry. *Biogeochemistry* **128**, 107–123.

Mitsch W. J. and Gosselink J. G. (2007) *Wetlands*. 4th ed., Wiley, Hoboken, NJ. Available at: https://library.wur.nl/WebQuery/titel/1862523 [Accessed May 21, 2018].

Mitsch W. J., Taylor J. R. and Benson K. B. (1991) Estimating primary productivity of forested wetland communities in different hydrologic landscapes. *Landsc. Ecol.* **5**, 75–92.

Nahlik A. M. and Fennessy M. S. (2016) Carbon storage in US wetlands. *Nat. Commun.* **7**, 13835.

Nierop K. G. J. (1998) Origin of aliphatic compounds in a forest soil. *Org. Geochem.* **29**, 1009–1016.

Noël V., Boye K., Kukkadapu R. K., Bone S., Lezama Pacheco J. S., Cardarelli E., Janot N., Fendorf S., Williams K. H. and Bargar J. R. (2017) Understanding controls on redox processes in floodplain sediments of the Upper Colorado River Basin. *Sci. Total Environ.* **603–604**, 663–675.

NRCS (2008) Hydrogeomorphic Wetland Classification System: An Overview and Modification to Better Meet the Needs of the Natural REsources Conservation Service. Technical Note No. 190-8-76. Available at: https://www.nrcs.usda.gov/Internet/FSE_DOCUMENTS/nrcs143_010784.pdf [Accessed May 20, 2018].

Oades J. M. (1988) The retention of organic matter in soils. *Biogeochemistry* **5**, 35–70.

Quideau S. A., Anderson M. A., Graham R. C., Chadwick O. A. and Trumbore S. E. (2000) Soil organic matter processes: characterization by 13C NMR and 14C measurements. *For. Ecol. Manag.* **138**, 19–27.

Quideau S. A., Chadwick O. A., Benesi A., Graham R. C. and Anderson M. A. (2001) A direct link between forest vegetation type and soil organic matter composition. *Geoderma* **104**, 41–60.

R Core Team (2018) *R: A language and environment for statistical computing*., R Foundation for statistical computing, Vienna, Austria. Available at: https://www.R-project.org/.

Ramsey C. B. (2001) Development of the radiocarbon calibration program. *Radiocarbon* **43**, 355–363.

Rawls W. J. (1983) Estimating soil bulk density from particle size analysis and organic matter content. *Soil Sci.* **135**, 123–125.

Reddy K. R. and Patrick W. H. (1975) Effect of alternate aerobic and anaerobic conditions on redox potential, organic matter decomposition and nitrogen loss in a flooded soil. *Soil Biol. Biochem.* **7**, 87–94.

Reimer P. J., Bard E., Bayliss A., Beck J. W., Blackwell P. G., Ramsey C. B., Buck C. E., Cheng H., Edwards R. L., Friedrich M., Grootes P. M., Guilderson T. P., Haflidason H., Hajdas I., Hatté C., Heaton T. J., Hoffmann D. L., Hogg A. G., Hughen K. A., Kaiser K. F., Kromer B., Manning S. W., Niu M., Reimer R. W., Richards D. A., Scott E. M., Southon J. R., Staff R. A., Turney C. S. M. and van der Plicht J. (2013) IntCal13 and Marine13 Radiocarbon Age Calibration Curves 0–50,000 Years cal BP. *Radiocarbon* **55**, 1869–1887.

Retzer J. L. (1962) *Soil Survey of Fraser Alpine Area, Colorado.*, U.S. Department of Agriculture, Washington, D.C. Available at: https://www.fs.fed.us/rm/pubs_journals/1962/rmrs_1962_retzer_j001.pdf.

Rosenbloom N. A., Doney S. C. and Schimel D. S. (2001) Geomorphic evolution of soil texture and organic matter in eroding landscapes. *Glob. Biogeochem. Cycles* **15**, 365–381.

Rumpel C., Kögel-Knabner I. and Bruhn F. (2002) Vertical distribution, age, and chemical composition of organic carbon in two forest soils of different pedogenesis. *Org. Geochem.* **33**, 1131–1142.

Sanderman J., Farrell M., Macreadie P. I., Hayes M., McGowan J. and Baldock J. (2017) Is demineralization with dilute hydrofluoric acid a viable method for isolating mineral stabilized soil organic matter? *Geoderma* **304**, 4–11.

Schimel D. S., Braswell B. H., Holland E. A., McKeown R., Ojima D. S., Painter T. H., Parton W. J. and Townsend A. R. (1994) Climatic, edaphic, and biotic controls over storage and turnover of carbon in soils. *Glob. Biogeochem. Cycles* **8**, 279–293.

Schmidt M. W. I., Knicker H., Hatcher P. G. and Kogel-Knabner I. (1997) Improvement of 13-C and 15-N CPMAS NMR spectra of bulk soils, particle size fractions and organic material by treatment with 10% hydrofluoric acid. *Eur. J. Soil Sci.* **48**, 319–328.

Segnini A., Posadas A., Quiroz R., Milori D. M. B. P., Saab S. C., Neto L. M. and Vaz C. M. P. (2010) Spectroscopic Assessment of Soil Organic Matter in Wetlands from the High Andes. *Soil Sci. Soc. Am. J.* **74**, 2246–2253.

Segnini A., Souza D., Alves A., Novotny E. H., Milori D. M. B. P., Silva D., Lopes W. T., Bonagamba T. J., Posadas A. and Quiroz R. (2013) Characterization of Peatland Soils from the High Andes through 13 C Nuclear Magnetic Resonance Spectroscopy. *Soil Sci. Soc. Am. J.* **77**, 673–679.

Sharp E. L., Parsons S. A. and Jefferson B. (2004) The effects of changing NOM composition and characteristics on coagulation performance, optimisation and control. *Water Sci. Technol. Water Supply* **4**, 95–102.

Simpson M. J., Otto A. and Feng X. (2008) Comparison of Solid-State Carbon-13 Nuclear Magnetic Resonance and Organic Matter Biomarkers for Assessing Soil Organic Matter Degradation. *Soil Sci. Soc. Am. J.* **72**, 268–276.

Singer P. C. (1999) Humic substances as precursors for potentially harmful disinfection by-products. *Water Sci. Technol.* **40**, 25–30.

Smernik R. J. and Oades J. M. (2002) Paramagnetic effects on solid state carbon-13 nuclear magnetic resonance spectra of soil organic matter. *J. Environ. Qual.* **31**, 414–20.

Soil Survey Staff (1999) Differentiae for Mineral and Organic Soils. In *Soil taxonomy: A basic system of soil classification for making and interpreting soil surveys* U.S. Department of Agriculture Natural Resources Conservation Service. pp. 19–20. Available at: https://www.nrcs.usda.gov/Internet/FSE_DOCUMENTS/nrcs142p2_051232.pdf [Accessed May 4, 2018].

Sposito G., Skipper N. T., Sutton R., Park S., Soper A. K. and Greathouse J. A. (1999) Surface geochemistry of the clay minerals. *Proc. Natl. Acad. Sci.* **96**, 3358–3364.

Talma A. S. and Vogel J. C. (1993) A simplified approach to calibrating 14C dates. *Radiocarbon* **35**, 317–322.

Taylor A. F. S., Fransson P. M., Högberg P., Högberg M. N. and Plamboeck A. H. (2003) Species level patterns in 13C and 15N abundance of ectomycorrhizal and saprotrophic fungal sporocarps. *New Phytol.* **159**, 757–774.

Tfaily M. M., Cooper W. T., Kostka J. E., Chanton P. R., Schadt, Hanson P. J., Iversen C. M. and Chanton J. P. (2014) Organic matter transformation in the peat column at Marcell Experimental Forest: Humification and vertical stratification. *J. Geophys. Res. Biogeosciences* **119**, 661–675.

Torn M. S., Trumbore S. E., Chadwick O. A., Vitousek P. M. and Hendricks D. M. (1997) Mineral control of soil organic carbon storage and turnover. *Nature* **389**, 170–173.

USDI, BR (2012) *Colorado River Basin Water Supply and Demand Study: Executive Summary*., U.S. Department of the Interior, Bureau of Reclamation.

Ussiri D. A. N. and Johnson C. E. (2003) Characterization of organic matter in a northern hardwood forest soil by 13C NMR spectroscopy and chemical methods. *Geoderma* **111**, 123–149.

Vardy S. R., Warner B. G., Turunen J. and Aravena R. (2000) Carbon accumulation in permafrost peatlands in the Northwest Territories and Nunavut, Canada. *The Holocene* **10**, 273–280.

Waksman S. A. (1924) Influence of microorganisms upon the carbon-nitrogen ratio in the soil. *J. Agric. Sci.* **14**, 555–562.

Young R., Avneri-Katz S., McKenna A., Chen H., Bahureksa W., Polubesova T., Chefetz B. and Borch T. (2018) Composition-Dependent Sorptive Fractionation of Anthropogenic Dissolved Organic Matter by Fe(III)-Montmorillonite. *Soil Syst.* **2**, 14.

CHAPTER 5: SUMMARY

The purpose of the work presented in this dissertation is to elucidate the impacts of complexation, temperature, and hydrology on the mobility and stability of Fe and natural organic matter. The research detailed here examines the key role of organic carbon chemistry in carbon and iron cycling by (I) determining the dominant modes of complexation of Fe(II) and dissolved organic matter (DOM) and the resulting impacts on Fe(II) redox chemistry (Chapter 2); (II) investigating the impact of temperature and DOM type on the sorption of DOM to a hydrous Fe oxide (Chapter 3); and (III) examining differences in organic carbon storage and biogeochemical processing in subalpine wetlands from two hydrogeomorphic classes (Chapter 4). This chapter summarizes key findings and describes implications of the work reported in the preceding three chapters and provides recommendations for future research.

Iron bioavailability depends upon its solubility and oxidation state, which are strongly influenced by complexation with natural organic matter (NOM). Despite observations of Fe(II)–NOM associations under conditions favorable for Fe oxidation, the molecular mechanisms by which NOM influences Fe(II) oxidation remain poorly understood. I characterized the coordination environment of Fe(II) associated with DOM using Fe K-edge X-ray absorption spectroscopy and evaluated the effect of complexation on Fe redox stability in oxidation experiments. Linear combination fitting of extended X-ray absorption fine structure (EXAFS) data using reference organic ligands demonstrated that Fe(II) was complexed primarily by carboxyl functional groups in reduced NOM. Functional groups more likely to preserve Fe(II), such as bipyridine, represented much smaller fractions of NOM-bound Fe(II), and there was no evidence of complexation with sulfur groups. Iron(II) added to anoxic solutions of as-received NOM oxidized to Fe(III) and remained organically complexed. Iron oxidation experiments revealed that the presence of reduced NOM limited Fe(II)

oxidation, with over 50% of initial Fe(II) remaining after four hours. The findings from this work provide crucial insight into Fe cycling in oceans, lakes, streams, and porewaters of soils and sediments. In oceans, where low concentrations of bioavailable Fe can limit primary productivity, understanding Fe speciation is essential to accurately modeling carbon cycling. This work contributes to the improvement of carbon models by providing a refined understanding of Fe(II) complexation and redox transformations in the presence of DOM. Because both organic contaminants and toxic metal(loid)s commonly react with Fe and DOM, the findings presented here also enhance our understanding of redox processes affecting the fate and transport of environmental contaminants. Future research should consider using the Fe K-edge X-ray absorption spectroscopy technique to identify Fe(II)–DOM complexes from natural systems and to further investigate the effects of pyridine or pyridine-like ligands on Fe redox transformations. Because the model DOM types used in this study contained low sulfur fractions compared to some other DOM types (e.g. near deep ocean vents), the lack of sulfur binding may not necessarily indicate that Fe(II)–organosulfur complexes are not possible. Since such complexes could contribute to Fe(II) stabilization, future work should characterize coordination of Fe(II) with sulfur-rich DOM to determine if Fe(II)-organosulfur complexes may be more prevalent in different systems.

The response of global carbon stocks to warming remains a key uncertainty in climate models. While numerous studies have investigated the temperature sensitivity of decomposition and microbial carbon use efficiency, the effects of temperature on sorption interactions between organic matter and minerals are inadequately characterized. I examined the impacts of temperature (7, 25 and 45 °C) and DOM type on sorption of DOM to ferrihydrite-coated sand in continuous flow and batch systems at circumneutral pH. Findings demonstrated a positive relationship between temperature and sorption, especially between 25 and 45 °C. Desorption of aquatic DOM increased appreciably with temperature, while desorption of peat and soil DOM was less sensitive. The amount of material that sorbed also

depended on DOM type: more aquatic natural OM adsorbed than soil DOM at all temperatures. Specific ultraviolet absorbance values (SUVA) of initial column effluents were low, suggesting aromatic-rich compounds preferentially adsorbed to the mineral surface. These results indicate that some circumstances may favor the accumulation of DOM on iron mineral surfaces as temperature increases, potentially removing organic substrates from the accessible dissolved carbon pool. However, they also imply that the stability of newly associated material likely depends on its chemical characteristics and the conditions under which it sorbed. In total, the results from this novel investigation of temperature effects on DOM sorption to an iron oxide indicate that some abiotic mechanisms of carbon storage may provide negative feedbacks to climate change. However, given the variability among published results as well as those presented in this study, it is clear that the effect of temperature on sorption in one system is not scalable to all environments. Mineral type as well as solution conditions such as pH, ionic strength, and multivalent cation and DOM concentrations can impact dominant sorption mechanisms and therefore temperature sensitivity of organo-mineral associations. Further studies identifying sorption temperature sensitivity under varying conditions are necessary for broad-scale understanding of abiotic feedback mechanisms in warming soils.

Despite the importance of wetlands for water quality and carbon storage, our understanding of biogeochemical processes in these systems remains inadequate for effective management of these biogeochemical "hotspots". In particular, the variability in carbon storage and processing among different wetland types within the same ecoregion is insufficiently characterized. To determine how differences in hydrology and topographic setting (also known as the hydrogeomorphic setting) influence organic carbon storage and decomposition processes, I compared carbon content and composition between depressional and slope wetlands in the Rocky Mountains. Results of soil organic carbon measurements showed that depressional wetlands had slightly larger carbon stocks than slope wetlands, and they stored substantially more carbon in organic layers compared to mineral layers. By

contrast, slope wetlands stored approximately equal amounts of C in mineral and organic layers. Carbon dating suggests that though carbon in deep organic layers was quite old, the carbon stored in mineral layers was older than that in organic layers. Analysis of soil organic carbon composition by solid-state ^{13}C nuclear magnetic resonance (NMR) demonstrated a higher prevalence of aliphatic compounds in depressional wetlands, especially at depth, while carbon content in the subsoils of slope wetlands was dominated by aromatic compounds. It is likely that these differences in carbon chemistry arise from different decomposition pathways and stabilization mechanisms imposed by different hydrologically controlled redox conditions. As a whole, the results from this study illustrate that differences in hydrogeomorphic setting can lead to divergent decomposition processes and carbon storage mechanisms. Because depressional wetlands disproportionately store carbon in less stable organic layers, their carbon stocks may be more sensitive to disturbance than those in slope wetlands. The variability in carbon processing and storage between these wetland types also indicates that different hydrogeomorphic classes of wetlands should be considered independently when evaluating wetland carbon cycling and sequestration on broad scales. Further research to refine our understanding of the decomposition and stabilization mechanisms in these wetlands should include the examination of the chemical composition of plant inputs and oxidation state of organic matter, microbial community structure and activity, redox gradients, diffusion limitations, concentrations of electron acceptors, and extent of mineral sorption and physical protection. General carbon accounting and compositional analysis of wetland soils for other hydrogeomorphic classes of wetlands could extend this comparison beyond the two wetland types evaluated here.

APPENDIX A: SUPPORTING INFORMATION FOR CHAPTER 2 - COMPLEXATION AND REDOX BUFFERING OF IRON(II) BY DISSOLVED ORGANIC MATTER

A.1 Selection of organic references

Organic ligands were chosen to emulate functional groups found in organic matter. The chosen references contained the following functional groups: carboxylic acid, alcohol, phenol, amine, thiol, and aromatic heterocyclic amine. While multiple compounds could have been used to represent these functional groups, the chosen compounds give a general indication of the type of complexation between Fe and organic matter. Structures of the chosen references are shown in Figure A.1. The following organic compounds were tested, but were insufficiently soluble or oxidized Fe(II): dodecyl sulfate, benzoate, deferrioxamine B (DFO-B), hematin, oxalate, pyrazole, and dibenzothiophene.

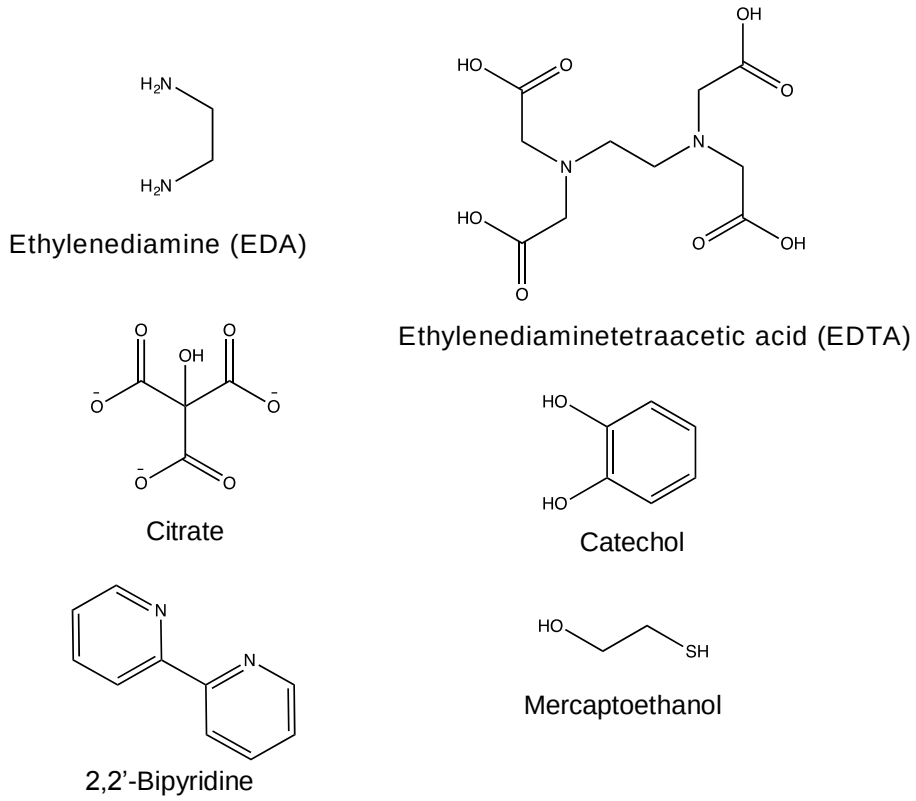

Figure A.1. Chemical structures of organic standards used in Fe EXAFS experiments.

Table A.1 Details of organic reference solutions

Organic compound	Concentration (M)	Concentration Fe(II) or Fe(III) (M)	pH
Citrate	1.08	0.002 Fe(II)	6.7-7.0
Citrate	0.969	0.002 Fe(III)	6.7-7.0
Pyrocatechol	2.54	0.002 Fe(II)	6.7-7.0
Pyrocatechol	1.818	0.002 Fe(II), oxidized to Fe(III)	6.7-7.0
2,2'-bipyridine	0.045	0.015 Fe(II)	6.7-7.0
Ethylenediamine (EDA)	3.62	0.014 Fe(II)	unadjusted
EDTA	0.96	0.002 Fe(II)	6.7-7.0
Mercaptoethanol	3.46	0.014 Fe(II)	unadjusted

Table A.2. pH of NOM samples

Sample	pH
LHA_{red} + Fe(II)	6.7
LHA + Fe(II)	6.9
LHA+ Fe(III)	6.9
LHA_{red}	6.7 – 7.0
$SRFA_{red}$ + Fe(II)	6.7 – 7.0
SRFA + Fe(II)	6.9
$SRHA_{red}$ + Fe(II)	6.8
$SRNOM_{red}$ + Fe(II)	6.7
$SRNOM_{red}$ + Fe(II)	4.0

A.2 Beam damage of solution-phase Fe(II) citrate samples

During X-ray absorption spectroscopy analysis, multiple scans of a solution-phase Fe(II) citrate sample showed changes in the shape of the white line over the course of the analysis (Figure A.2). Due to these observed changes, I decided to lyophilize the samples and mount them in a liquid nitrogen cryostat during analysis to prevent beam-induced changes. The lower energy of the white line in the lyophilized sample spectrum also suggests that this sample is more reduced than even the first scan of the solution-phase sample.

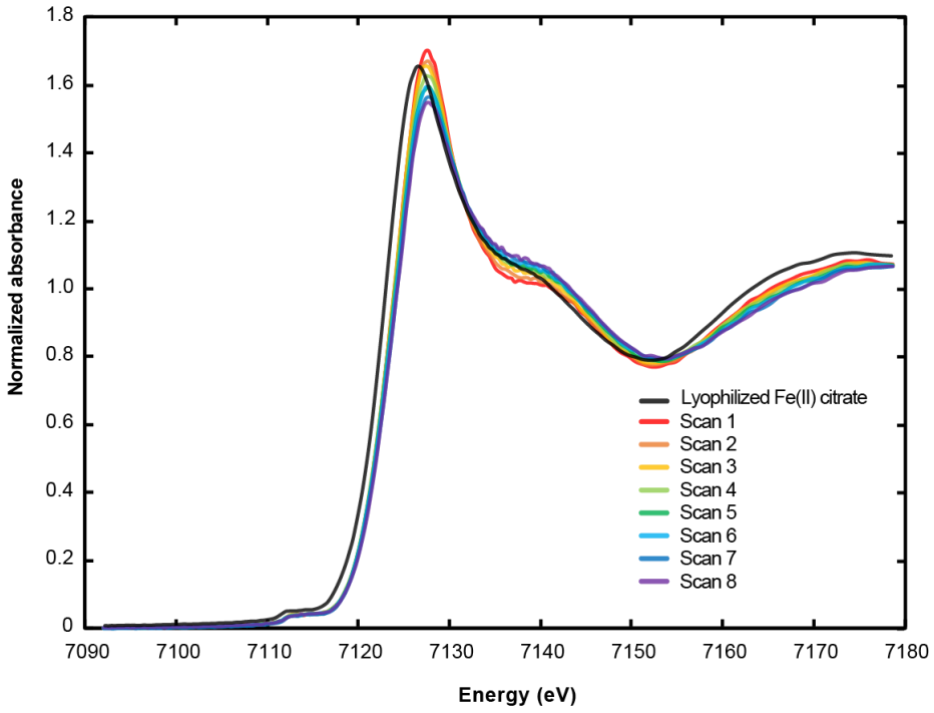

Figure A.2. Normalized Fe K-edge XANES spectra of solution-phase Fe(II) citrate (colored lines) showing reduced peak height (beam effects) with subsequent scans, and lyophilized Fe(II) citrate (black line).

A.3 Electron paramagnetic resonance spectroscopy (EPR)

To determine the amount and polymerization of Fe(III) present in the Fe-NOM samples, continuous wave electron paramagnetic resonance (cw-EPR) spectra were collected. I used a Bruker ELEXSYS E 500 spectrometer with Bruker Xepr software for operation and data analysis at the Environmental Molecular Sciences Laboratory (EMSL) at Pacific Northwest National Lab (PNNL), in Richland, WA, USA. Samples were packed in glass tubes in an anaerobic glove box to prevent oxidation. Spectra were collected at room temperature and operation parameters were optimized for the Fe(III) signal. Modulation frequency was 100 kHz, receiver gain was 60 dB, and modulation amplitude was 10 Gauss. The magnetic field was swept from 0 – 6000 G in 83.89 seconds, and 4 scans were collected and averaged. The spectrum of an empty glass tube was used for background subtraction.

Two prominent signals were identified in the EPR spectra, one at a *g*-factor of ~2.005, corresponding to organic radical species (Paul et al., 2006), and another at ~4.3, typical of mononuclear high-spin Fe(III) with low symmetry (Bou-Abdallah and Chasteen, 2008).

A.4 Oxidation of Fe(II) upon addition to LHA

Several lines of evidence point to oxidation of Fe(II) upon addition to LHA. First, the Fe K-edge spectrum for LHA + Fe(II) is nearly identical to that of LHA + Fe(III) (Figure A.3). Wavelet transforms of LHA + Fe(II) and LHA + Fe(III) are also nearly identical. The 50-fold increase in signal from LHA_{red} + Fe(II) to LHA + Fe(II) at g = 4.28 (1625 Gauss) illustrates the much higher quantity of Fe(III) in the as-received samples (Figure A.3, C). Collectively, these analyses demonstrate the oxidation of Fe(II) in the presence of LHA and the equivalent, mononuclear complexation of added Fe(III) and added Fe(II) with as-received LHA.

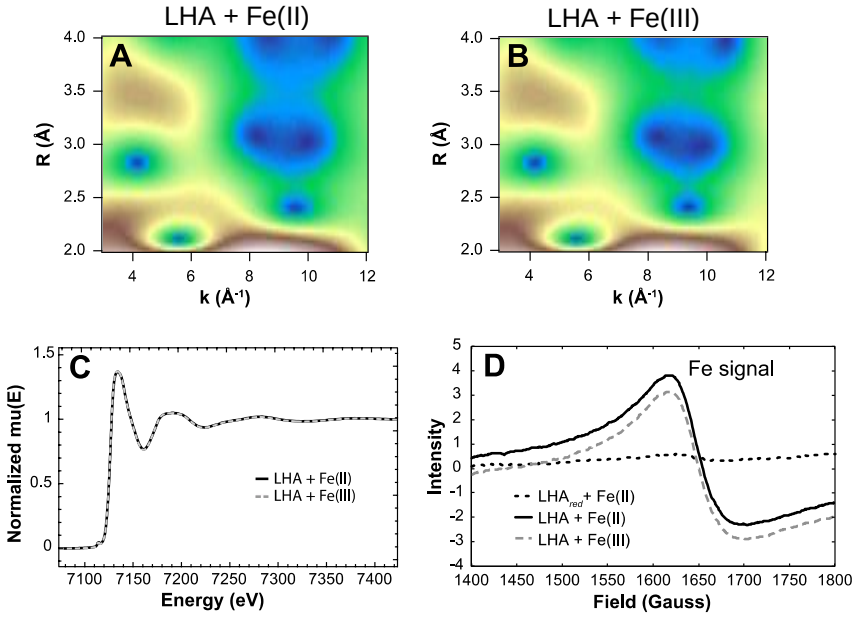

Figure A.3. Oxidation of Fe(II) by LHA: Wavelet transforms of (A) LHA + Fe(II) and (B) LHA + Fe(III); (C) Fe K-edge normalized μ(E) spectrum of LHA + Fe(II) and LHA + Fe(III); and (D) EPR spectra selectively showing the Fe(III) signal region for LHA_{red} + Fe(II), LHA + Fe(II), and LHA + Fe(III).

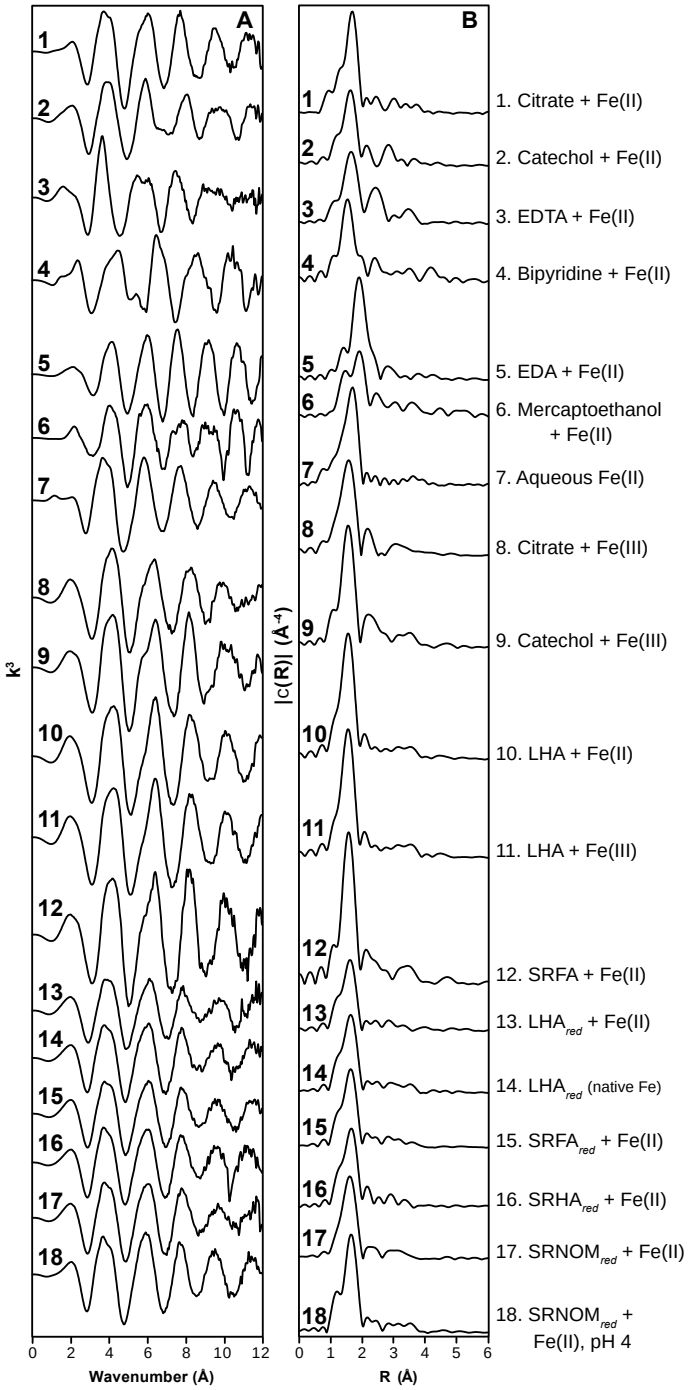

Figure A.4. (A) K^3-weighted $\chi(k)$ EXAFS spectra and (B) Fourier transform spectra of Fe-NOM samples and Fe–organic compound references at pH ~7 (unless indicated otherwise).

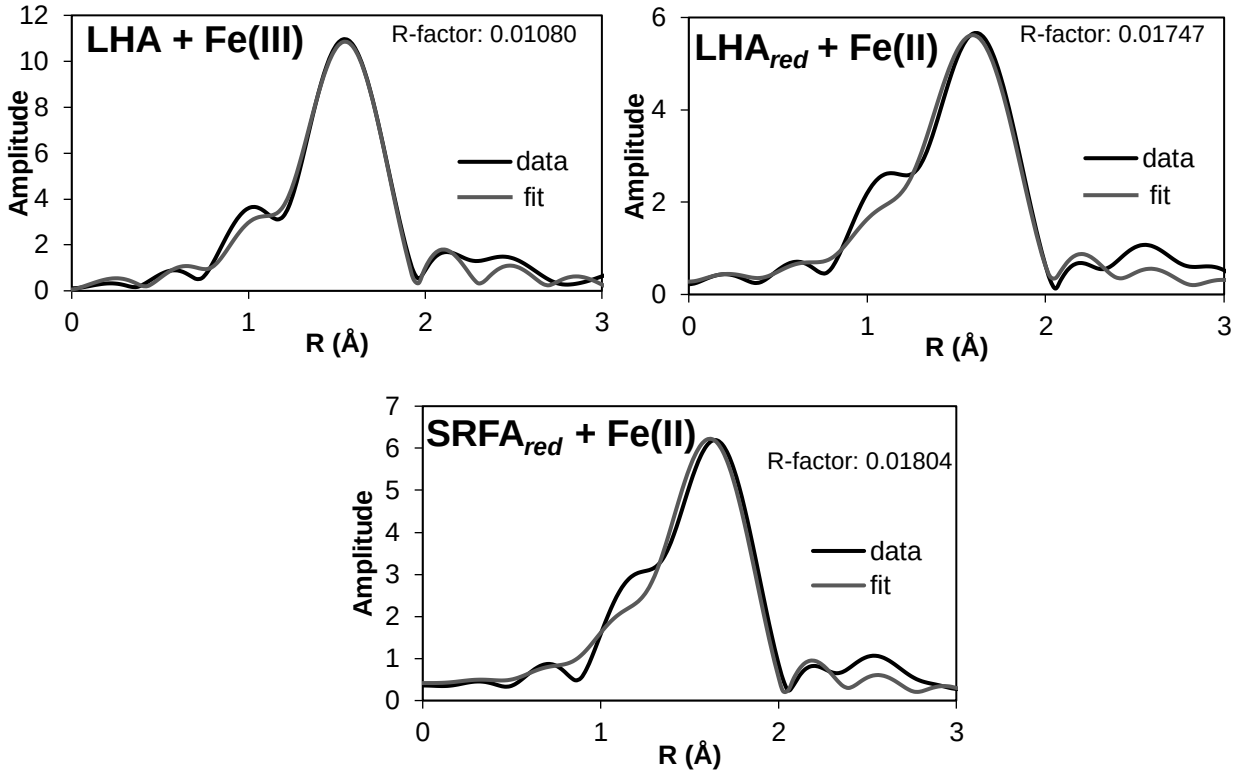

Figure A.5. Examples of first shell fits of the Fourier transforms of Fe EXAFS. The ferrihydrite single-scattering Fe-O path was used to fit this region.

A.5 Linear combination fitting

Combinatorial linear combination fitting analyses were performed using Athena software (Ravel and Newville, 2005) on k^3-weighted Fe EXAFS spectra from 3-11.5 k. Sums were floated and all components were limited between 0 and 1. Number of standards was limited to 8 and no minimum contribution of standard was required. Representative fits of three samples are shown in Figure A.6. Many of the top combinatorial fits were statistically indistinguishable by the Hamilton test (Downward et al., 2007), so the top 10 fits for each sample were averaged, and the reported standard deviations represent either the average of the standard deviation of the values used to compute the average, or the average of the reported errors from the top 10 fits, whichever was larger. The top 10 combinatorial fits and their average for LHA$_{red}$ + Fe(II) are shown in Figure A.7.

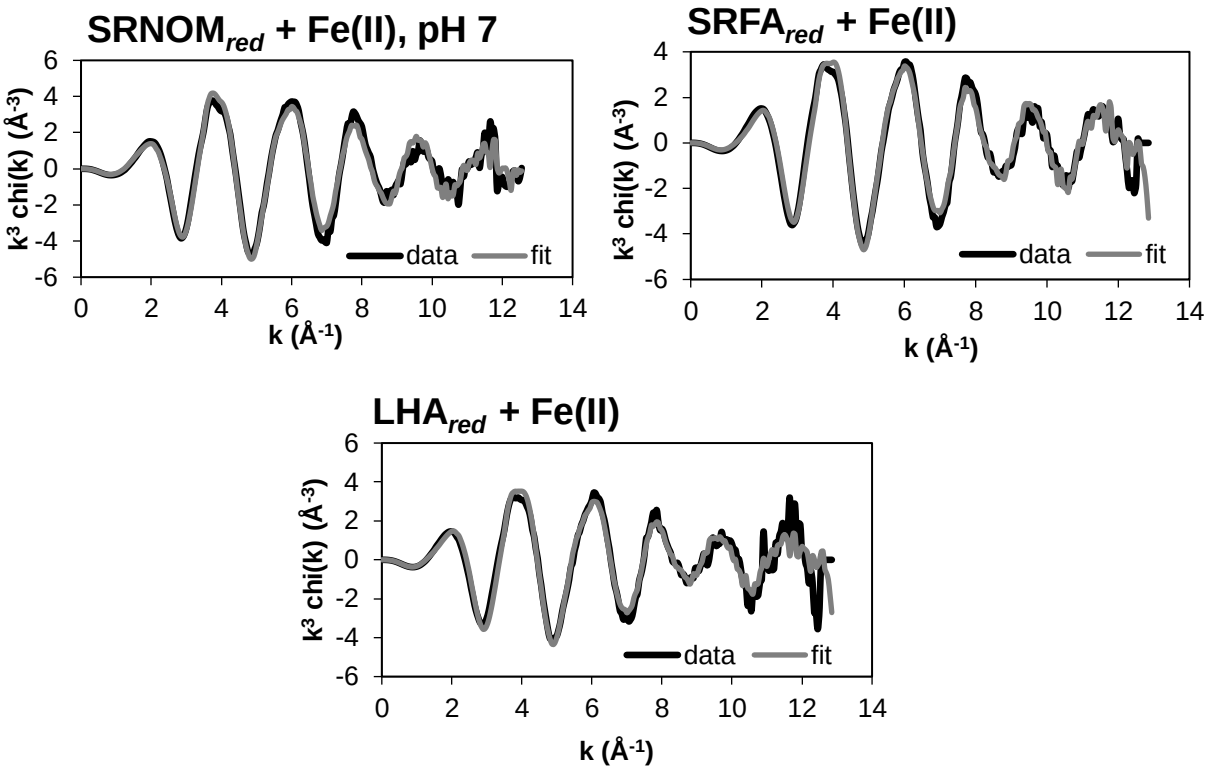

Figure A.6. Examples of linear combination fits of k^3-weighted Fe K-edge EXAFS spectra for Fe in reduced OM complexes. Fitting range was from 3 - 11.5 k.

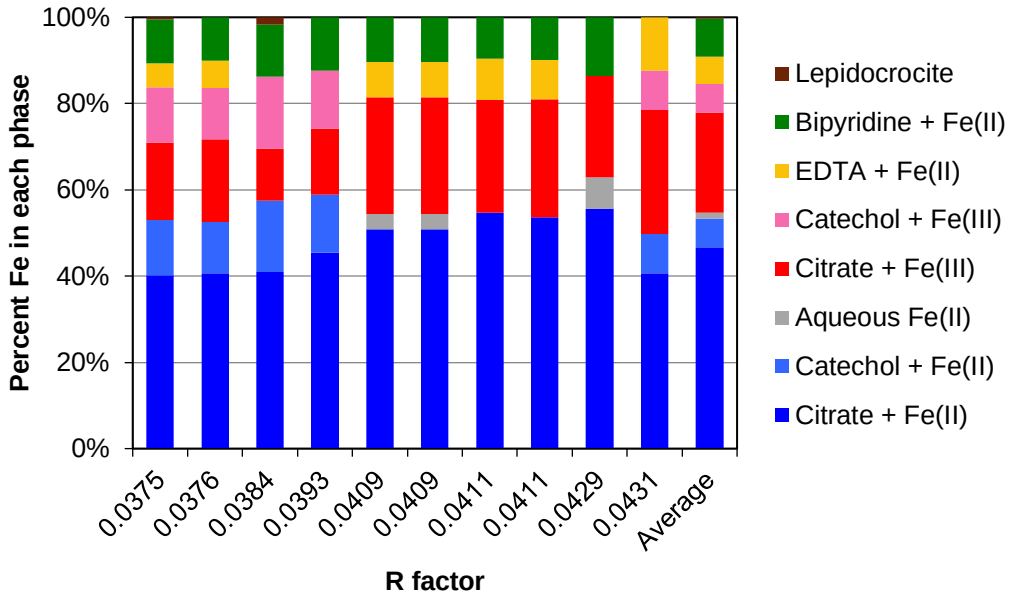

Figure A.7. Top 10 combinatorial linear combination fits and their average for LHA_{red} + Fe(II).

A.6 Fe(II) oxidation experiments and buffer interference

Good's buffers are known to cause interferences in oxidation experiments (Grady et al., 1988; Baker et al., 2007). To test whether PIPES affected the Fe(II) oxidation rate, we studied the kinetics of Fe(II) oxidation at 4.1 mM and 41 μM PIPES concentrations (i.e., a 100x difference) in the absence of LHA. At the lower PIPES concentration, pH could be maintained within 6.8–7.1 by 10-μL additions of 1-M NaOH. The solutions were stirred continuously and kept in the dark except when aliquots were taken. For 4.1 mM PIPES the pH varied between 6.87–6.99 and the fitted pseudo-first-order rate constant was 2.2 ± 0.3 x 10^{-4} s^{-1}, which is consistent with previously published values (Santana-Casiano et al., 2005; Pham and Waite, 2008). For 41 μM PIPES the pH varied between 6.80–7.1 due to manual additions of 0.1M NaOH and the fitted rate constant was 3.7 ± 0.5 x 10^{-4} s^{-1} (Figure A.8). In each case, the errors are one standard deviation from the fit to a single kinetics measurement.

As shown in Figure A.8, there is a difference in the oxidation rates at the two PIPES concentrations. Although I cannot rule out PIPES participation in the redox reactions, I believe it is

likely that the addition of concentrated base is the principal explanation. These additions made it possible to maintain the overall pH within 0.3 pH units, each addition caused a transient and localized increase in pH until it was mixed into the stirred solution. The faster rate is likely due to the additional Fe(II) oxidation at pH > 7 caused by each addition. The change in reaction rate as a result of increasing the concentration of PIPES is also far smaller than the effect of adding reduced organic matter.

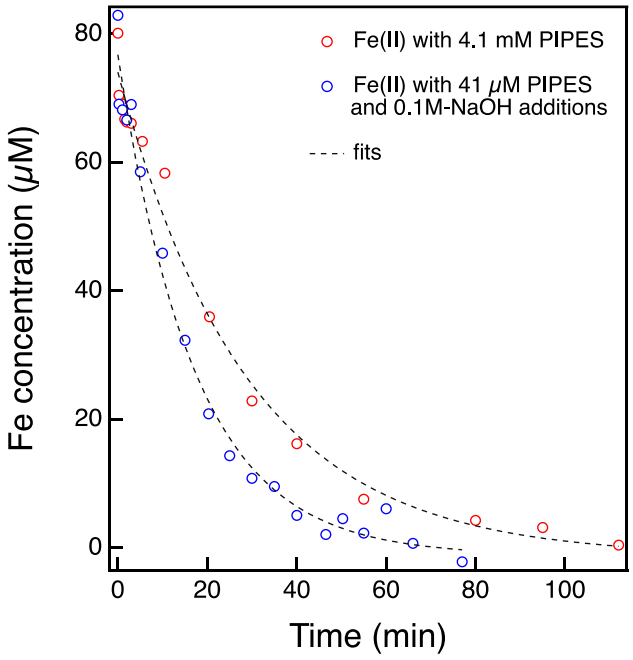

Figure A.8. Comparison of Fe(II) oxidation in the presence of 4.1 mM PIPES (red circles) and 41 μM PIPES (blue circles) along with corresponding fits (k' = 2.2 ± 0.3 x 10^{-4} s^{-1} (4.1 mM PIPES), and k' = 3.7 ± 0.5 x 10^{-4} s^{-1} (41 μM PIPES)).

A.7 Hydrogen peroxide generation

Generation of hydrogen peroxide (H_2O_2) during oxidation of 2 mg/mL LHA_{red} with and without 0.08 mM Fe(II) was monitored using the Amplex red assay (A-22188, Molecular Probes, Invitrogen), which utilizes the Amplex Red reagent (10-acetyl-3,7-dihydroxyphenoxazine) in combination with horseradish peroxidase to form resorufin, a colored and red-fluorescent product. Linear calibration curves were obtained in water confirming that H_2O_2 concentrations could be measured spectrophotometrically at 560 nm according to manufacturer guidelines. However, the assay

response was significantly higher than expected when LHA_{red} was present. As a result, reliable H_2O_2 concentrations could not be obtained in the presence of organic matter, but the assay did confirm the generation of this species. Although the Amplex red data do not provide reliable quantification of H_2O_2, they do show that this species is generated when LHA_{red} is oxidized by O_2, and further demonstrate that the presence of iron reduces the amount or lifetime of H_2O_2 (Figure A.9).

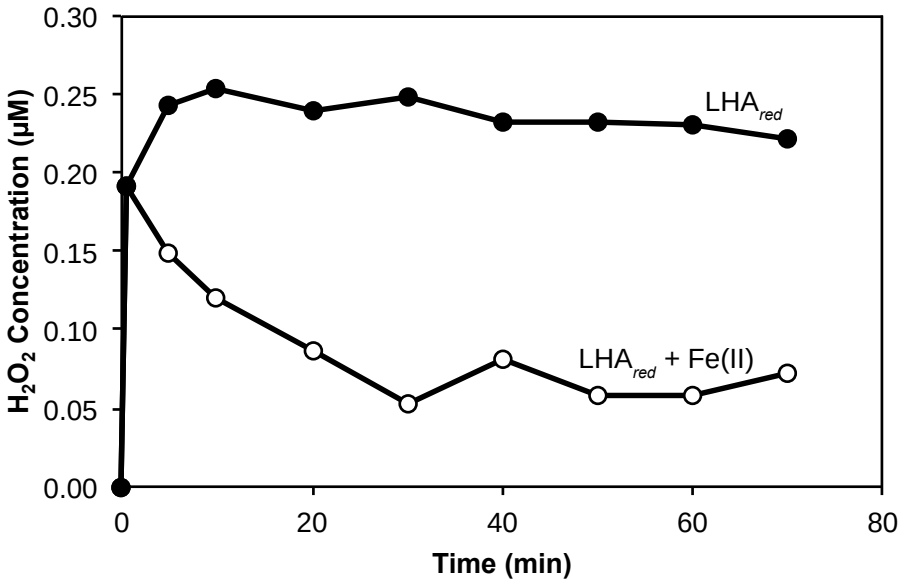

Figure A.9. H_2O_2 production during oxidation of 2 mg/mL LHA_{red} with and without 0.08 mM Fe(II). Addition of Fe(II) decreases the amount or lifetime of H_2O_2

A.8 Fe oxidizing and reducing capacity

A third experiment measured the Fe oxidizing capacity of as-received LHA and the Fe reducing capacity of chemically reduced LHA (Figure A.10). As-received LHA (2 mg/mL) oxidized almost 40% of the 1 mM Fe(II) added. Reduced LHA (2 mg/mL) reduced over 60% of 2 mM Fe(III) (as $FeCl_3$) added.

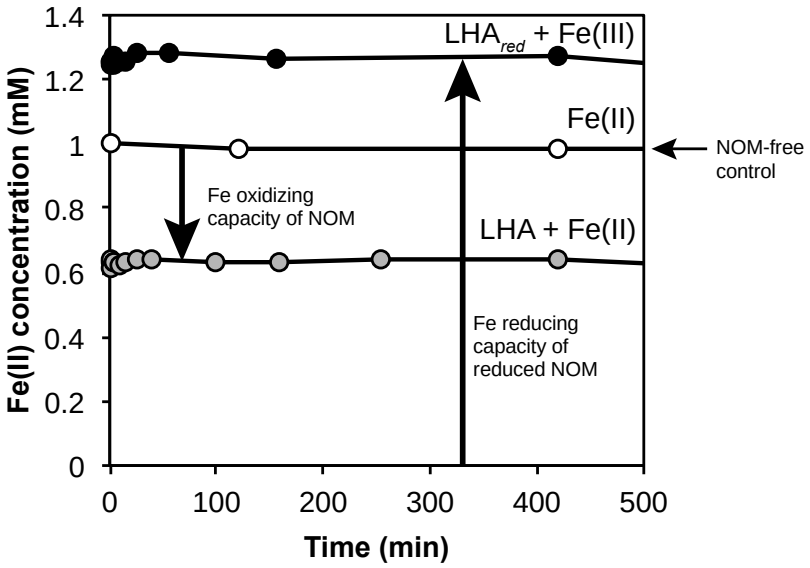

Figure A.10. Fe oxidizing and reducing capacity of as-received and reduced DOM (respectively). Fe oxidizing capacity measured with mixture of 1 mM of Fe(II) and 2 mg/mL LHA; Fe reducing capacity measured with mixture of 2 mM Fe(III) and 2 mg/mL LHA$_{red}$

REFERENCES

Baker C. J., Mock N. M., Roberts D. P., Deahl K. L., Hapeman C. J., Schmidt W. F. and Kochansky J. (2007) Interference by Mes [2-(4-morpholino)ethanesulfonic acid] and related buffers with phenolic oxidation by peroxidase. *Free Radic. Biol. Med.* **43**, 1322–1327.

Bou-Abdallah F. and Chasteen N. D. (2008) Spin concentration measurements of high-spin (g' = 4.3) rhombic iron(III) ions in biological samples: theory and application. *J. Biol. Inorg. Chem.* **13**, 15–24.

Downward L., Booth C. H., Lukens W. W. and Bridges F. (2007) A variation of the F-test for determining statistical relevance of particular parameters in EXAFS fits. *AIP Conf. Proc.* **882**, 129–131.

Grady J. K., Chasteen N. D. and Harris D. C. (1988) Radicals from "Good's" buffers. *Anal. Biochem.* **173**, 111–115.

Paul A., Stösser R., Zehl A., Zwirnmann E., Vogt R. D. and Steinberg C. E. W. (2006) Nature and abundance of organic radicals in natural organic matter: Effect of pH and irradiation. *Environ. Sci. Technol.* **40**, 5897–903.

Pham A. N. and Waite T. D. (2008) Modeling the kinetics of Fe(II) oxidation in the presence of citrate and salicylate in aqueous solutions at pH 6.0-8.0 and 25 degrees C. *J. Phys. Chem. A* **112**, 5395–405.

Ravel B. and Newville M. (2005) ATHENA, ARTEMIS, HEPHAESTUS: data analysis for X-ray absorption spectroscopy using IFEFFIT. *J. Synchrotron Radiat.* **12**, 537–41.

Santana-Casiano J. M., González-Dávila M. and Millero F. J. (2005) Oxidation of nanomolar levels of Fe(II) with oxygen in natural waters. *Environ. Sci. Technol.* **39**, 2073–9.

APPENDIX B: SUPPORTING INFORMATION FOR CHAPTER 3 - TEMPERATURE EFFECTS ON SORPTION OF DISSOLVED ORGANIC MATTER ON FERRIHYDRITE UNDER DYNAMIC FLOW AND BATCH CONDITIONS

B.1 Low concentration, low C:Fe continuous flow experiments

Continuous flow studies were conducted with 10 mg/L ESHA in PIPES-buffered (pH 7.5) synthetic groundwater medium and 10 g of ferrihydrite-coated sand at 5, 23, and 45 °C and 50 μL min^{-1} flow rate.

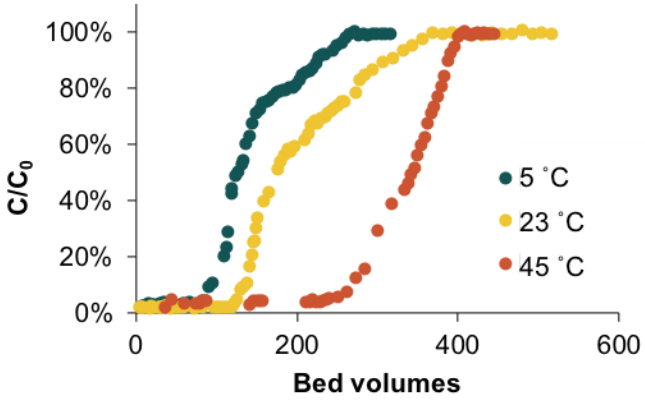

Figure B.1. Breakthrough curves of ESHA at three different temperatures—5 °C (blue), 23 °C (yellow), and 45 °C (red)—in columns of 10 g ferrihydrite-coated sand. Solution conditions: pH 7.5 (buffered with 1.35 mM PIPES), and I = 0.015 M, C_0 = 10 mg/L, and flow rate = 50 μL min^{-1}.

B.2 Flow rate studies

Continuous flow studies were performed at 10 μL min^{-1} and 250 μL min^{-1} flow rates to determine the kinetic limitations of the system. The same materials and methods were used as described in the main manuscript except for the following differences. A fresh batch of ferrihydrite-coated quartz sand (FHQ) was used in the flow rate studies. It had a surface area of 3.7140 m^2 g^{-1} as measured by BET. Solutions of SRNOM and ESHA were filtered through 0.22 μm polyethylene

sulfone (PES) filters. There was no visual difference in the amount of material trapped by the cellulose nitrate and PES filters and no meaningful difference in DOM concentrations after filtration.

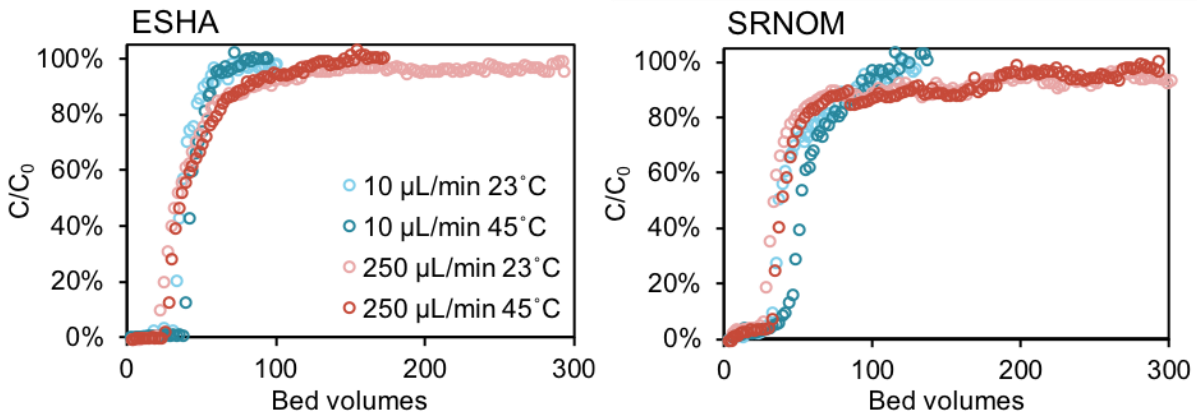

Figure B.2. Breakthrough curves of SRNOM and ESHA for experiments conducted at 10 µL min^{-1} and 250 µL min^{-1} flow rates and 23 and 45˚C. As measured by UV absorbance spectroscopy at 254 nm.

B.3 Fast shaker speed kinetic batch study

A preliminary batch experiment was carried out with 45 mL of DOM solution added to 0.5 g of FHQ (surface area = 3.714 m^2 g^{-1}) and placed on rotary shaker table at 200 rpm. By 1 hr, all sample solutions were cloudy from suspended ferrihydrite. To prevent spectroscopic interference of ferrihydrite, aliquots were centrifuged and the supernatant extracted prior to analysis by UV absorbance spectroscopy at 254 nm.

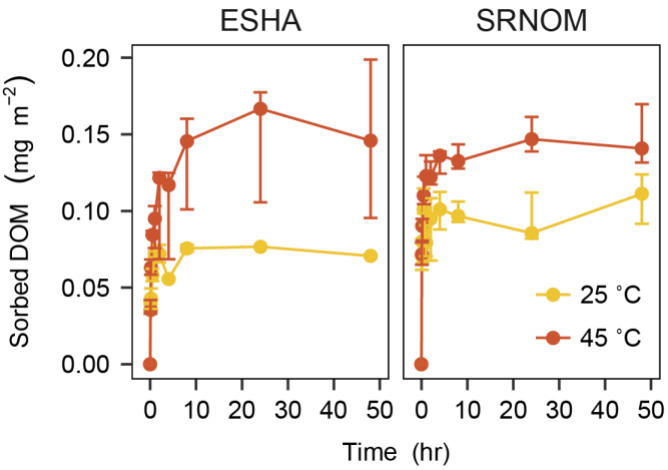

Figure B.3. Results of high shaker speed batch experiment. Amount of DOM adsorbed to ferrihydrite-coated sand by surface area at each time point. Points represent medians and error bars represent the range of values for triplicates, except for ESHA at 35 °C, which is a duplicate. 50 mL of 27 mg/L ESHA or 23 mg/L SRNOM in SGM at pH 6.9 ± 0.1 added to 1 g ferrihydrite-coated sand.

Table B.1. Mean and standard deviation of DOM adsorbed to ferrihydrite-coated sand in fast (200 rpm) and slow (80 rpm) shaker speed batch studies studies (n = 3 for all but ESHA at 25 °C and 200 rpm, where n = 2). At 80 rpm, 50 mL of DOM solution was added to 1g of ferrihydrite-coated sand. At 200 rpm, 45 mL of DOM solution was added to 0.5 g of ferrihydrite coated sand. Total amount of DOM adsorbed is normalized to the BET-measured surface area of ferrihydrite-coated sand.

		Total DOM sorbed (μg m^{-2})	
DOM	Temperature (°C)	80 rpm	200 rpm
ESHA	7	71.7 ± 5.7	--
	23/25	90.9 ± 3.0	76.70 ± 0.09
	45	117.4 ± 3.8	150 ± 21
SRNOM	7	164 ± 12	--
	23/25	192 ± 11	93.1 ± 8.8
	45	232.6 ± 1.3	149.0 ± 6.2

Table B.2. $SUVA_{254}$ values (mean ± standard deviation) for final supernatant in batch studies conducted with 50 mL of 27 mg/L ESHA or 23 mg/L SRNOM in SGM at pH 6.9 ± 0.1 added to 1 g ferrihydrite-coated sand, at 80 rpm shaker speed.

DOM	Temperature (°C)	$SUVA_{254}$ (L mg C^{-1} m^{-1})
ESHA	Stock	8.86
	7	9.44 ± 0.74
	23	9.49 ± 0.54
	45	9.64 ± 0.56
SRNOM	Stock	4.72
	7	4.81 ± 0.10
	23	5.56 ± 0.39
	45	4.76 ± 0.39

Table B.3. pH values of stock solutions and final samples from batch kinetics experiment. For sample measurements, mean and standard deviation of 3 samples are given.

	Temperature		
Sample	7 °C	23 °C	45 °C
Stock ESHA	6.80	6.98	6.90
Sample ESHA	6.17 ± 0.45	6.49 ± 0.03	6.61 ± 0.06
Stock SRNOM	6.68	6.84	6.79
Sample SRNOM	7.21 ± 0.30	6.82 ± 0.10	6.86 ± 0.01

APPENDIX C: CHEMICAL CHARACTERIZATION OF UNSORBED DISSOLVED ORGANIC MATTER FRACTIONS

A major goal for Chapter 3 was the determination of temperature effects on sorptive fractionation of dissolved organic matter (DOM) on ferrihydrite. Understanding what types of molecules preferentially sorb at different temperatures could provide insight into favored mechanisms of interaction and the relative chemical recalcitrance of microbially accessible and inaccessible organic matter pools. Due to the complex nature of DOM and the small sample quantities created from the dynamic flow experiments, standard organic analytical techniques could not be used to characterize DOM chemistry. I therefore elected to use Fourier transform ion cyclotron resonance mass spectrometry (FT-ICR-MS) and nuclear magnetic resonance (NMR) spectroscopy. Despite substantial efforts to prepare clean, salt-free samples, I was unable to obtain high enough signal to noise ratios to use data collected from either technique. Descriptions of the methods used to produce samples and some example data are provided here to document the extensive work done for these analyses. The appendix concludes with a summary of the work and recommendations for future work.

C.1 FT-ICR-MS analysis

C.1.1 Preparation of samples

Several effluent samples from continuous flow experiments (described in Chapter 3) were selected for chemical characterization via electrospray ionization (ESI) FT-ICR-MS, an ultra-high resolution mass spectrometry technique uniquely capable of distinguishing amongst tens of thousands of compound molecular weights present in DOM. Samples were collected from the low (early), middle, and high portions of the breakthrough curves of the Suwannee River reverse osmosis natural organic matter (SRNOM) and Elliott Soil humic acid (ESHA) sorption experiments at 7, 25, and 45 °C. Three to five effluent fractions were combined to increase the quantity of DOM for analysis. Solid

phase extraction (SPE) using Agilent Bond Elut PPL cartridges was performed on all samples according to the method published in Dittmar et al. (2008) to desalinate and concentrate DOM solutions. Briefly, combined samples were acidified to pH 2 with trace metal grade HCl solution to increase extraction efficiency of carboxylates and phenols. The solid phase was conditioned using liquid chromatography mass spectrometry (LCMS)-grade methanol and pH 2 solution. Samples were transferred to cartridges and allowed to infiltrate by gravity. The column was then rinsed with pH 2 solution, dried under N_2 gas, and DOM extracted with 500 μL LCMS-grade methanol. Extracts were stored at 4 °C until analysis.

ESHA, as a humic acid fraction, becomes less soluble with decreasing pH, so the Dittmar SPE method did not work well for samples containing this type of DOM. Not only did some material aggregate and pass through the cartridge, some also remained on the cartridge after methanol extraction. Several methanol extracts also flocculated when stored for several weeks at 4 °C. For these reasons, it was nearly impossible to prepare adequate ESHA samples for FT-ICR-MS analysis.

SRNOM extracts were analyzed at the High Magnetic Field Laboratory in Tallahassee, FL, using a custom-built FT-ICR-MS (Kaiser et al., 2011) equipped with a 9.4 T horizontal 200 mm bore diameter superconducting solenoid magnet (Oxford Corp., Oxford Mead, UK) operated at room temperature. During analysis the samples clogged the nano-capillary, which made dilution necessary. Depending on the data quality, 100-200 scans were collected in negative ion mode, and spectra were calibrated internally using a "walking" calibration equation based on highly abundant homologous mass series (Savory et al., 2011).

C.1.2 FT-ICR-MS data

Sample spectra were dominated by surfactant-like contaminant peaks, which prevented accurate calibration and chemical formula assignments (Figure C.1). All sample spectra were determined to be of insufficient quality for further analysis. Some continuous flow experiments were

repeated with the goal of producing clean samples for FT-ICR-MS. All glassware was combusted at 400 °C for 4+ hours, plastic materials were washed, sonicated, and rinsed with methanol, filters were rinsed with 200 mL of MilliQ water prior to filtration, and heat stable reagents were combusted at 400 °C. Unfortunately, these efforts still yielded contaminated results.

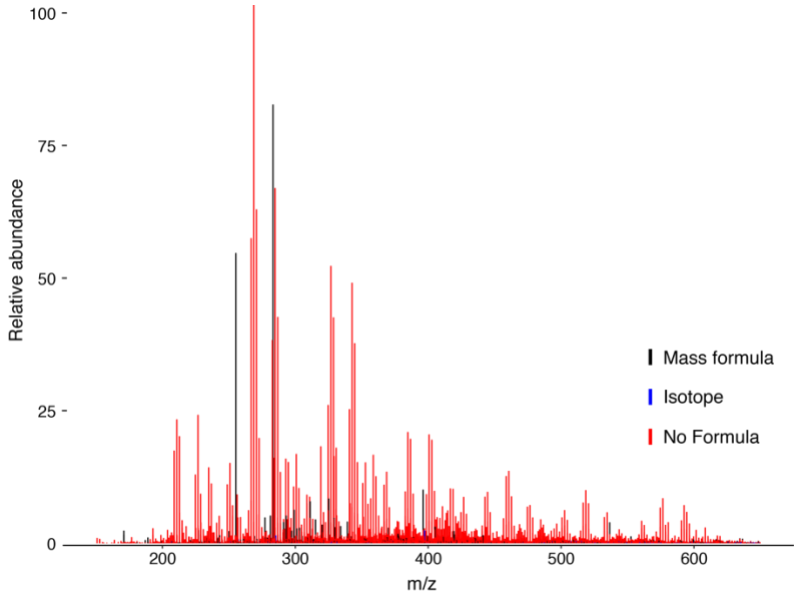

Figure C.1. Sample mass spectrum for ESHA effluent sample. Most peaks could not be assigned formulas.

C.2 NMR analysis

C.2.1 Preparation of samples

Several ESHA and SRNOM effluent and stock samples from continuous flow experiments were selected for NMR analysis. As for FT-ICR-MS, concentration of samples was required. Lyophilization led to precipitation of large amounts of salts, which prevented redissolution of OM into the small volume of D_2O necessary for NMR analysis using a microprobe. Therefore, I used the SPE method described in Section B.1.1 (with the substitution of methanol-d_4 for methanol in the final elution step) to desalinate and concentrate the samples. Extracts were then dried down under N_2 gas and redissolved in 10 μL methanol-d_4 and transferred to 1 mm NMR tubes.

C.2.2 NMR data

^{1}H-NMR analyses were performed at the Environmental NMR Laboratory at the University of Scarborough, Toronto. Spectral quality suffered from some of the same issues as the mass spectra—contaminants were apparently concentrated during the SPE process and overshadowed the small signals coming from DOM (Figure C.2). Spectra were also characterized by poor resolution and overall low signals. Comparison of freeze-dried stock DOM material dissolved in D_2O and methanol-d_4 also revealed problematic solvent effects from the methanol-d_4.

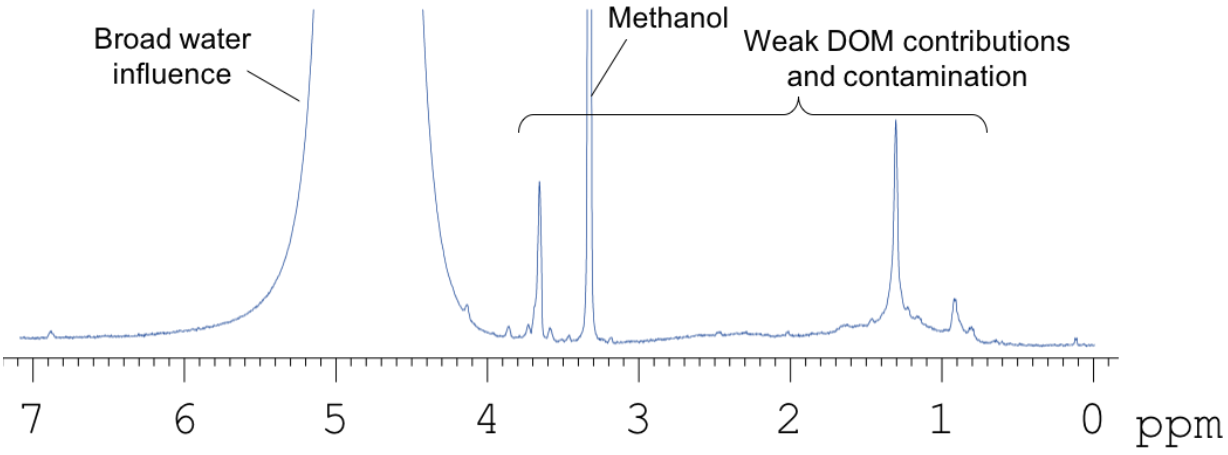

Figure C.2. Sample ^{1}H NMR spectrum for SRNOM effluent

.

C.3 Conclusions

Neither analysis method succeeded in producing useful spectra. Sample concentration using SPE increased contaminant concentrations, and lyophilization produced high salt concentrations that prevented redissolution of DOM. The SPE method commonly used for preparation of DOM samples for FT-ICR-MS analysis (Dittmar et al., 2008) performs poorly for ESHA, which aggregates at low pH. Based on these observations, I conclude that the effluent samples gathered from the continuous flow adsorption experiments were too dilute (for laboratory-prepared samples) to be successfully analyzed with high resolution mass spectrometry and NMR. Future experiments could improve

sample quality by (a) using higher concentrations of DOM, (b) using minimal salt, and (c) using all new, high purity chemicals and meticulously cleaning glass and plastic ware. For ESHA and other soil organic matter with low solubility in acidic solutions, an alternative concentration and desalination method needs to be employed for FT-ICR-MS sample preparation.

REFERENCES

Dittmar T., Koch B., Hertkorn N. and Kattner G. (2008) A simple and efficient method for the solid-phase extraction of dissolved organic matter (SPE-sDOM) from seawater. *Limnol Ocean. Methods* **6**, 230–235.

Kaiser N. K., Quinn J. P., Blakney G. T., Hendrickson C. L. and Marshall A. G. (2011) A Novel 9.4 Tesla FTICR Mass Spectrometer with Improved Sensitivity, Mass Resolution, and Mass Range. *J. Am. Soc. Mass Spectrom.* **22**, 1343–1351.

Savory J. J., Kaiser N. K., McKenna A. M., Xian F., Blakney G. T., Rodgers R. P., Hendrickson C. L. and Marshall A. G. (2011) Parts-Per-Billion Fourier Transform Ion Cyclotron Resonance Mass Measurement Accuracy with a "Walking" Calibration Equation. *Anal. Chem.* **83**, 1732–1736.

APPENDIX D: SUPPORTING INFORMATION FOR CHAPTER 4 - HYDROGEOMORPHIC CONTROLS ON SOIL CARBON QUANTITY AND COMPOSITION IN COLORADO SUBALPINE WETLANDS

D.1 Detailed site description

In Fraser Experimental Forest (FEF), average temperature ranges from -10 °C to 13 °C, and precipitation at headquarters (2725 m) is 58 cm, falling primarily as snow (Alexander et al., 1985). FEF is comprised of 8 watersheds; slope wetlands in this study were located in two of these (Retzer, 1962). One slope wetland (S1 - N 39° 54.133, W 105° 54.265) is located in the Dead Horse (DH) watershed. The other two slope wetlands (S2 - N 39° 52.946, W 105° 51.843 and S3 – N 39° 53.115 W 105° 51.811) are located in the Fool Creek (FC) watershed. The DH watershed is slightly larger than the FC watershed with approximate sizes of 925 and 714 acres, respectively. FC is primarily composed of northwest facing slopes, whereas DH is primarily southwest facing. S1 is approximately 53 m long 9 to 16 m wide at an elevation of 2867 to 2889 m. There are two tributaries connecting S1 to the surrounding forest that are located along one side, and through the wetland. There is standing water at the top for much of the year (samples from this location were not included in the study). In 1956, the wetlands of the FC watershed were mapped; in total there were 122 recorded spring (slope) wetlands in this watershed (Retzer, 1962). All wetlands are located at comparable elevation ranges (2700 – 3300 m). Of the two FC slope wetlands in this investigation, S2 (~3076-3089 m) is at higher elevation than S3 (~3037-3047 m), with both belonging to the same spring system. S2 is about 35 m long (up to downslope) and about 6 to 29 m wide. There is one main tributary that is located on the northeast side of the wetland that is generally flowing throughout the year. S3 is approximately 37 m long, and the width ranges from 31 to 13 m, becoming progressively narrower downslope. S3 is fed by two tributaries, one is located on the northeast side that has running water much of the year, and

the other smaller tributary is located through the center of the wetland. S3 has a perennial pool upslope, samples from which were not included in this study.

The depressional wetlands are located adjacent to FEF, immediately west of headquarters (39° 54' N, 105° 51' W). Eleven different depressional wetlands were located within this area, of which three were chosen for further study (D1, D2, and D3). D1 contains a large pond in its center which is perennially saturated. Immediately following spring run-off, D2 and D3 are saturated with water (May-June), and slowly dry down during the summer months. At the beginning of fall (August-September), the surface soil of D2 and D3 is generally dry and cracked.

D.2 Bulk density

Bulk density was estimated for carbon stock calculations. For organic soil depths, I used the literature value of 0.224 g/cm^3 (Rawls, 1983). For mineral soils, the bulk density of the soil in g/cm^3 was estimated using the equation:

$$\text{Soil bulk density} = \frac{100}{\frac{\%\ \text{organic matter}}{0.224} + \frac{100 - \%\ \text{organic matter}}{\text{mineral bulk density}}} \quad (1)$$

Where % organic matter is calculated using:

$$\%\ \text{organic matter} = \%\ \text{soil organic carbon} \times 1.9 \quad (2)$$

and mineral bulk density is deduced from charts of texture percents (Rawls, 1983). Results are displayed in Table D.1.

Table D.1. Bulk density in g cm^{-1} values of soils from all sites within both types of wetland, depressional (D) and slope (S), used for carbon stock calculations. Locations within D wetlands are center/low (L) and mid (M). Locations with slope wetlands are midslope (M) and lower (L).

	Sample											
Depth (cm)	D1-L	D1-M	D2-L	D2-M	D3-L	D3-M	S1-M	S1-L	S2-M	S2-L	S3-M	S3-L
0-10	0.224	0.224	0.224	0.224	0.224	0.224	0.224	0.224	0.224	0.224	0.224	0.224
10-20	0.224	0.224	0.224	0.224	0.224	0.224	0.224	0.224	0.224	0.224	0.224	1.31
20-30	0.224	0.88	0.224	0.224	0.84	0.224	0.224	0.96	0.224	0.91	0.224	1.35
30-40	0.224	0.90	0.224	0.224	0.79	0.224	0.224	1.20	0.224	0.98	0.99	1.49
40-50	0.224	0.93	0.224	0.224	0.81	0.224	0.79	1.11	0.224	1.46	1.42	1.53
50-60	0.224		0.224	0.224	1.28	0.224	1.43	1.33	1.14	1.51	1.50	1.53
60-70	0.224			0.224	1.51	0.224	1.46		1.50			
70-80						0.224	1.48		1.48			

Table D.2. Horizon delineations and colors for middle (M) and lower (L) sites in each depressional and spring wetland**.**

Horizon	Depth (cm)	Color	Horizon	Depth (cm)	Color	Horizon	Depth (cm)	Color
Depressional wetlands								
D1-M			*D2-M*			*D3-M*		
Oi	0-9		Oi	0-15		Oi	0-10	
Bg1	9-26	GL1 4/5 GY	A	15-20	10 YR 3/2	A	10-40	1 YR 3/2
Bg2	26-43	10 YR 8/1	Bg1	20-30	5 YR 6/1	Bw	40-75	10 YR 4/2
			Bg2	30-70	2.5 Y 6/1			
D1-L			*D2-L*			*D3-L*		
Oi	0-6		Oi	0-3		Oi	0-3	
Bg	6-65	10 YR 7/1	Bg1	3-41	10 YR 6/1	BA	3-16	10 YR 6/2
			Bg2	41-57	GL 1 4/10 Y	Bg1	16-37	7.5 YR 7/1
						Bg2	37-53	GL 1 4/10 Y
						2C	53-68	10 YR 8/1
Slope wetlands								
S1-M			*S2-M*			*D3-M*		
Oi	0-26		Oi	0-26		Oi	0-15	
A	26-47	10 YR 4/2	Bw	26-34	10 YR 4/1	A	15-30	10 YR 3/1
Cg	47-80	GL 1 5/10 Y	Ab	34-50	2.5 Y 3/2	Bg	30-45	GL 1 4/10 GY
			Cg	50-80	GL 1 5/10 GY	2Cg	45-54	GL 1 7/10 Y
S1-L			*S2-L*			*S3-L*		
Oi	0-10		Oi	0-10		Oi	0-8	
A	10-17	10 YR 3/2	Oe	10-22		2Cg1	8-40	GL 1 4/10 Y
Bg1	17-25	10 YR 6/1	A	22-31	2.5 Y 3/2	2Cg2	40-60	7.5 YR 6/8
Bg2	25-60	5 Y 6/2	Cg	31-58	GL 1 5/10 GY			

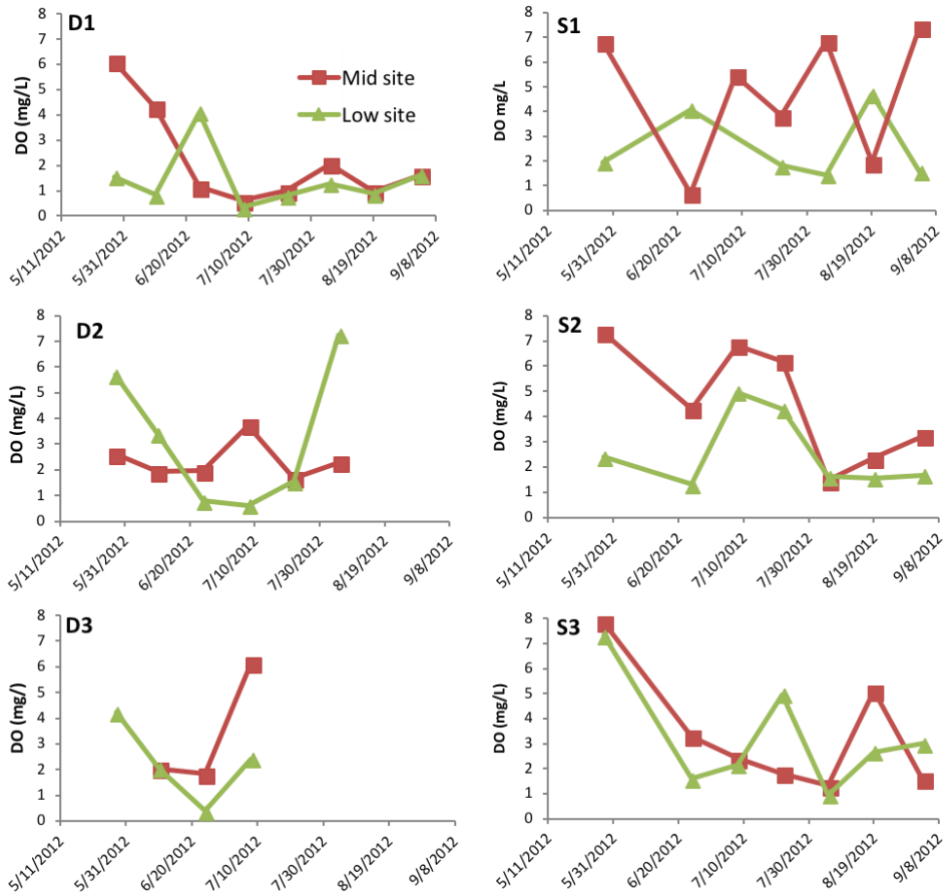

Figure D.1. Dissolved oxygen (DO) measurements from wells at middle (red squares) and lower (green triangles) sites in each wetland.

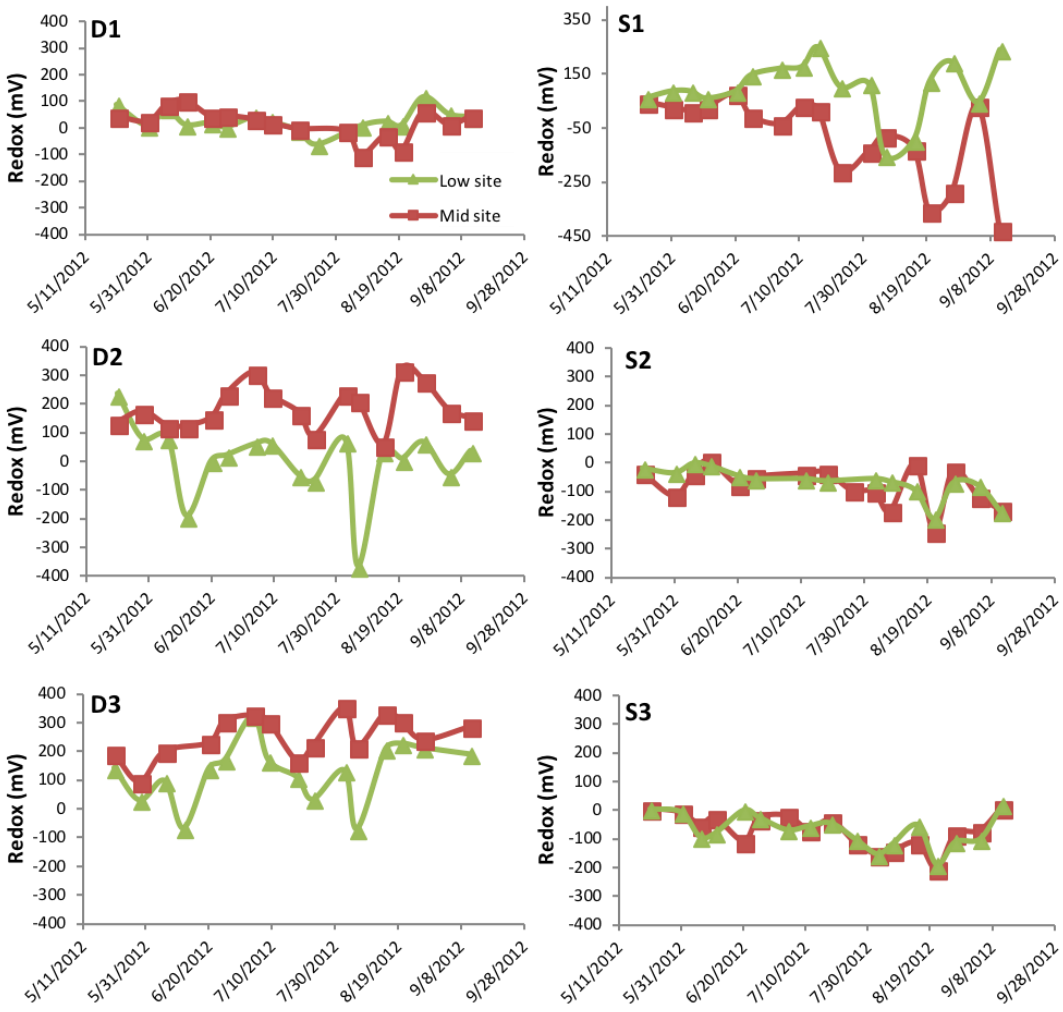

Figure D.2. Redox measurements from wells at middle (red squares) and lower (green triangles) sites in each wetland.

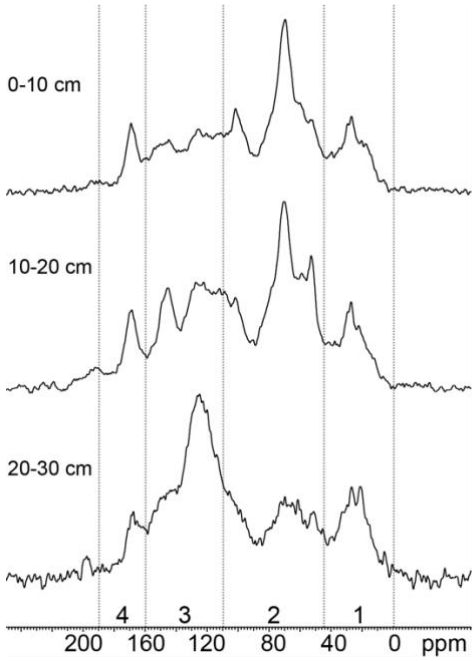

Figure D.3. Example 13-C NMR spectra from S3 showing integration regions (1) 0-45 ppm: alkyl C, (2) 45-110: O-alkyl C, (3) 110-160: aromatic C, and (4) 160-190: carbonyl C.

Figure D.4. Photographs showing vegetation in D1 and S3.

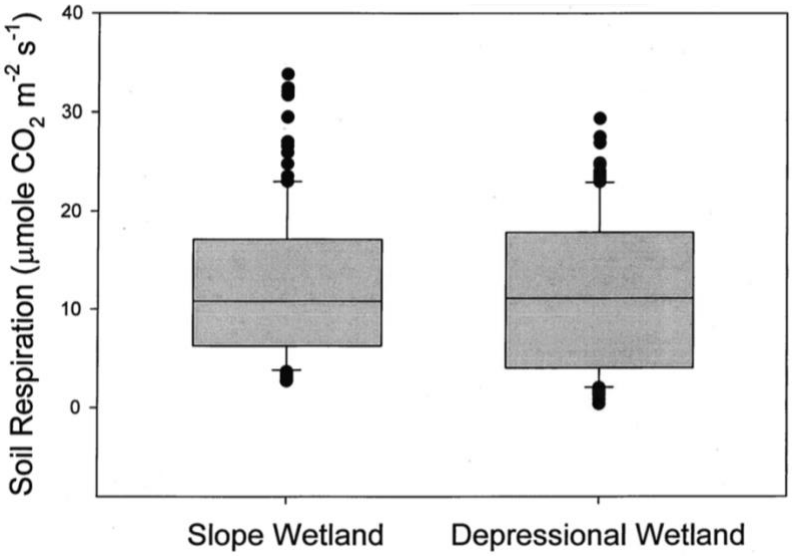

Figure D.5. Soil respiration rates from representative slope and depressional wetlands, collected from May to September, 2012.

Table D.3. C:N ratios for surface (0-20 cm) and deep (>20 cm) soils in each wetland class

	Depth	Median	Mean	Standard deviation	Range
Depressional	Surface	13.5	13.4	1.8	11.1-16.0
Depressional	Deep	15.5	15.2	2.8	8.2-21.6
Slope	Surface	18.6	18.2	3.8	12.7-24.3
Slope	Deep	15.0	16.7	6.3	8.7-38.1

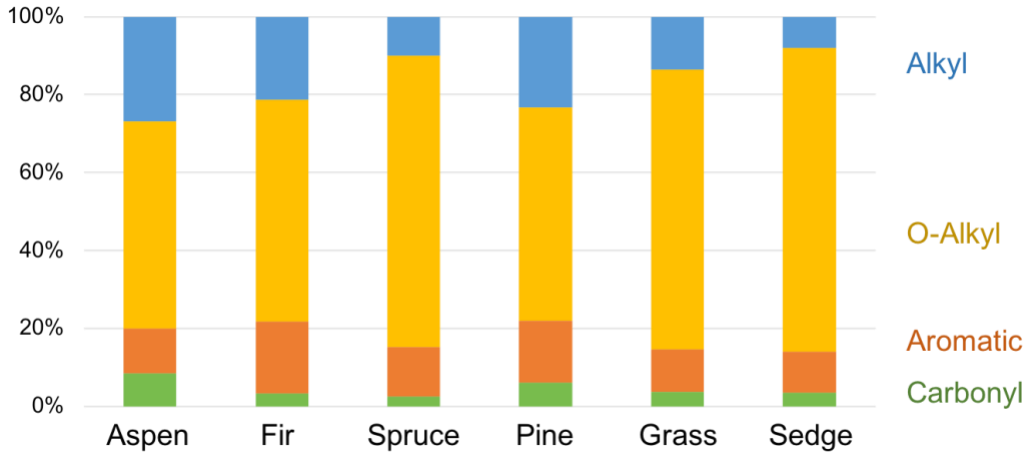

Figure D.6. NMR Integrations for dominant vegetation in and around wetlands, including aspen litter, fir litter, spruce litter, pine needles, grass leaves, and sedge leaves.

REFERENCES

Alexander R. R., Troendle C. A., Kaufmann M. R., Shepperd W. D., Crouch G. L. and Watkins R. K. (1985) *The Fraser Experimental Forest, Colorado: Research program and published research 1937-1985*., U.S. Department of Agriculture, Forest Service, Rocky Mountain Forest and Range Experiment Station, Fort Collins, CO. Available at: https://doi.org/10.2737/RM-GTR-118.

Rawls W. J. (1983) Estimating soil bulk density from particle size analysis and organic matter content. *Soil Sci.* **135**, 123–125.

Retzer J. L. (1962) *Soil Survey of Fraser Alpine Area, Colorado.*, U.S. Department of Agriculture, Washington, D.C. Available at: https://www.fs.fed.us/rm/pubs_journals/1962/rmrs_1962_retzer_j001.pdf.